group of peptides was evident. These results suggest that folding by nucleation about a defect is not confined to small systems only.

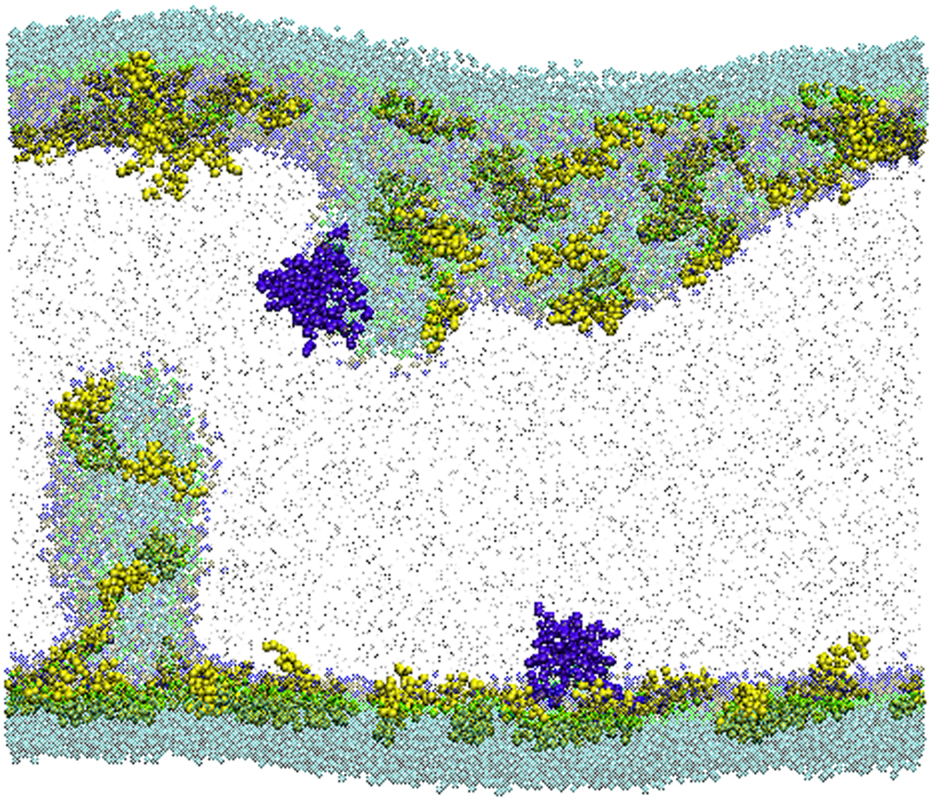

Figure 3.12: Folding in monolayers containing pre-aggregated peptides. In monolayers containing 2304 DPPC and 32 SP-B_{1-25} molecules each, 4 peptides were removed and replaced with a pre-formed peptide aggregate consisting of 4 peptides (purple), after 20ns of simulation under a small negative surface tension. This snapshot was obtained after the aggregate containing monolayers were simulated for 25ns under a small negative surface tension. Simulations were also performed where the peptide aggregate was inserted after 0ns of simulation (not shown). For both replacement times we got the same result: fold nucleation about a defect occurred in one of the monolayers and the other monolayer folded by amplification of undulations.

It has been previously proposed that variations or defects in the monolayer could act as nucleation sites for collapse. For instance, small height differences existing at domain boundaries between coexisting condensed and expanded phase domains have been suggested as nucleation sites for the formation of macroscopic folds [159, 206,

223]. Packing defects have also been suggested as inducers of pre-collapse instabilities [171, 218]. The surfactant proteins could act as impurities or defects in the monolayer, which lower the activation barrier for collapse. Hydrophobic surfactant proteins have been proposed to have a destabilizing effect on monolayers that assists collapse [189, 220]. SP-C mutants containing only 13 residues (with smaller α-helices) were also reported to act as defects in the monolayer, which were squeezed-out of the monolayer instead of more tightly packed lipids [171].

The behaviors of the surfactant peptides and their roles as nuclei in the folding process observed in our simulations are in broad agreement with inferences from several other experimental observations. Serrano and Pérez-Gil [224] suggest that SP-B associates preferentially at the monolayer interface, binding to surfactant lipids with high affinity, inducing perturbations in packing, and promoting the transfer of lipids between the interfacial film and adjacent bilayers. Krol et al. [166] suggest that SP-B localizes at the edge of bilayer protrusions, reducing line-tension and functioning like a zipper, enabling disc-like bilayers to squeeze-out of the monolayer and respread rapidly during the breathing cycle.

It has been suggested that SP-B could undergo some combination of conformational, orientational, or aggregational change induced by compression to high surface pressures [158, 160]. After observing the formation of SP-B clusters at domain boundaries in DPPC films, Cruz et al. [209] suggested that aggregation could occur after the solubility limit of the peptide in the lipid monolayer is reached. Experiments have also shown that aggregation of SP-B in phospholipid membranes leads to membrane destabilization [225], and when present at high concentration, SP-B perturbs DPPC bilayers and induces large amplitude lipid reorientation, likely leading to significant bilayer curvature [201].

We propose that the size of the protein affects its surface activity and that the aggregation of SP-B_{1-25} could be a mechanism for replicating the activity of the

full-length protein. Experimentally, SP-B_{1-25} can mimic the effects of the full-length protein, but only at higher concentrations. SP-B exists as a homo-dimer, which increases the contact area available for interaction with lipids in the monolayer and associated reservoir. One can envision how the aggregation of SP-B_{1-25} could lead to the formation of a cluster of peptides with positively charged regions facing outward toward the water sub-phase and hydrophobic regions facing in, available for lipid interaction. In fact, experimental studies have shown that fragments of SP-B show decreased fusogenic, lytic, and surface-tension-lowering abilities relative to the full-length SP-B, but that these properties are improved when the fragments are present at higher concentrations [226, 227]. Another important study suggested that homo-dimerization of SP-B is primarily related to surface tension reduction [228]. In this study, SP-B monomer restored surfactant function in SP-B deficient mice, but was not as effective as dimerized SP-B at surface tension reduction. However, a significant increase in SP-B monomer resulted in a surface tension reduction similar to that produced by lower concentrations of dimeric SP-B.

The peptide aggregation observed in our simulations occurred for SP-B_{1-25}, SP-C, and all mutant peptides tested, suggesting that the observed aggregation does not result from specific protein-protein interactions. Furthermore, peptide aggregation occurred in monolayers containing a single phase and a single lipid component, suggesting that the observed aggregation is not due to phase separation or specific lipid-peptide interactions. Instead the observed aggregation occurred by a lipid-mediated mechanism. These local lipid-mediated interactions hold the peptides together in a fold-inducing aggregate, analogous to the way local interactions hold peptides together to form a pore. The undulatory modes of the monolayer, which produce curvature in the surface, act as sinks for monolayer impurities. Our observations are in agreement with a universal mode of curvature-induced aggregation proposed by Reynwar et al. [229]. Utilizing CG-MD simulations, Reynwar et al. [229] modeled

curvature-inducing proteins as caps in a bilayer membrane, with a hydrophilic attraction to the lipid headgroups of the bilayer, but no attraction to other caps. The overlap of the bilayer deformations formed by curvature-inducing proteins leads to an indirect attractive force between the proteins, since overlap helps to minimize the elastic energy of the membrane. This attraction results in aggregation of the caps and subsequent vesiculation of the cap rich region. The peptides in our simulations are relatively small and are not associated with sizeable curvature induction; however the undulations that arise from the compression of the monolayer provide substantial curvature to drive the aggregation of peptides.

3.4.4 Mutants

Ryan and co-workers [224, 227] used synthetic peptides to map the fusogenic and lytic domains of SP-B and determine how these fusogenic and lytic capabilities influence surface activity. They determined that the N-terminal half of the protein (residues 1-37) was mostly responsible for the fusogenic, lytic and surface-active properties of the full-length protein, with helix 1 (residues 7-22) being highly lytic and mainly responsible for perturbing lipid packing [224, 227]. Moreover, amino acid substitutions that impaired fusogenic or lytic activities of SP-B also impaired surface tension reduction, which suggests that SP-B fusion and lysis likely play an important role in the formation and maintenance of the alveolar surface film [227].

Ryan and co-workers further concluded that the N-terminal tail (residues 1-9) is required to insert into and perturb compressed interfacial films [224, 227] and appears to have a crucial role in surface tension reduction [227]. An amino acid substitution of alanines for prolines at positions 2,4, and 6 (resulting in the extension of helix 1 and elimination of the tail motif, but no significant change in hydrophobicity) restricts the ability of the peptide to perturb the packing in the interfacial film and promote lipid insertion [224]. Paired substitution of hydrophobic residues on the nonpolar face

of helix 1 or substitution of multiple positively charges residues lead to an increase in minimum surface tension [227]. In accord with these results, atomistic molecular dynamics simulations have suggested that the N-terminal tail motif is important for anchoring SP-B_{1-25} to the monolayer and charged amino acids are important for positioning the peptide in the monolayer [35].

The results of our mutant peptide simulations can be compared with those of Ryan and co-workers only qualitatively. In the MARTINI model, the secondary structure of the peptides is held fixed by the angle and dihedral potentials, so any change in the secondary structure of the peptides is not captured. Although the secondary structure is not altered in our simulations, removal of the highly hydrophobic insertion sequence has a similar effect as the substitutions made by Ryan and coworkers to the N-terminal tail motif, namely it causes the peptides to penetrate less deeply into in the monolayer resulting in less perturbation. In general, we find that altering the hydrophobicity of the peptides affects the perturbation of the monolayer and thus the propensity for collapse.

A BLAST alignment for SP-B in human, pig, sheep, dog, mouse, rat, and xenopus species reveals some modest variation in the amino acid sequence with some key elements that are conserved [51]. Most notably the 7 cysteine residues that form dimers (three intramolecular and one intermolecular) are strictly conserved across all species for which the sequence is known. The conservation of the cysteine residues suggests that the dimerized structure of SP-B has physiological significance. As mentioned previously, SP-B_{1-25}, dSP-B_{1-25} and monomeric SP-B are capable of mimicking the effects of the full-length protein, but are less effective and require higher concentrations. In addition, the hydrophobic insertion sequence is well conserved across species with tryptophan (residue 9) perfectly conserved. The highly hydrophobic insertion sequence (especially tryptophan) is thought to be important for rapid adsorption to the interface.

The alignment of SP-C in several species also reveals modest variation in the amino acid sequence with some key features that are well preserved.Key features include a valine-rich stretch of hydrophobic residues proceeded by two positively charged residues, and near the N-terminus the presence of either two side-by-side palmitoylated cysteine residues or a palmitoylated cysteine beside a phenylalanine residue [51]. These features provide the correct placement of SP-C in the monolayer, with the N-terminal region displaying an affinity for membrane interfaces and the highly hydrophobic valine-rich stretch forming a transmembrane α-helix. Current evidence suggests that the secondary structure of SP-C is more important than the exact amino acid sequence, see [51] for review. Unfortunately the MARTINI model does not account for changes in the secondary structure, preventing the assessment of structural determinants and limiting analysis regarding amino acid substitution.

Although current peptide mimics have shown some success, they are less than optimal. For example KL4, the first SP-B-inspired synthetic peptide to reach clinical trials, has shown some success in removing lung inactivation and treating patients with ARDS, but disproportionately large amounts of palmitic acid are required to allow the surfactant preparation to reach low surface tensions [51]. Our simulations show that small peptides can destabilize the monolayer leading to the formation of collapse structures. The addition of PA appears to stabilize the monolayer against the formation of these collapse structures, and likely alters the mode of collapse. The dimeric structure of SP-B could be important for stabilizing collapse, thereby allowing LS to reach near-zero surface tensions.

3.4.5 Squeeze-out and Supercompression

At pressures above π_e, the disordered LE phase collapses at rates that are finite, in contrast to condensed phases that have been shown to sustain surface pressures well above π_e [186]. At physiological temperature (37°C) DPPC is the only component

that can form a condensed phase at surface pressures below π_e [186]. This observation led to classical squeeze out theory, which holds that in order to reach a near-zero surface tension the monolayer must be refined by the selective squeeze-out of non-DPPC components from the interface, leaving behind a monolayer that is highly enriched in DPPC.

There are recent experimental findings that suggest that the collapse structures formed from model surfactant mixtures are enriched in non-DPPC components. However, enrichment does not necessarily imply that the monolayer left behind is almost pure DPPC as held by classical squeeze-out theory. Mao et al. [230] studied the collapse of perdeuterated DPPC (DPPC-d62)/DPPG/SP-C/cholesterol films at 20°C. They determined that all three components with identifiable IR signatures (DPPC-d62, DPPG, and SP-C) were present in the multilayers, but fluorescence and IR data suggested that both SP-C and DPPG were enriched in the multilayer phase [230]. Several other experimental studies have reported protein enrichment in collapse structures, in model surfactant mixtures containing SP-B or SP-C [166–169, 172, 175]. Additionally, the atomistic simulations of Rose et al. [27] show that the addition of unsaturated phospholipids influences the response of DPPC monolayers to compression, resulting in some of the unsaturated lipids begin ejected from or partially forced out of the monolayer. Rose et al. suggest that this constitutes evidence for the selective squeeze-out of POPG. However, they admit that their simulations are limited both by system size and simulation time, which could affect the observed collapse behavior. In contrast, some experimental studies report little or no difference in composition between the monolayer and the collapse phase. For example, Yu and Possmayer [184] found no significant differences in lipid composition between the multilayer and the adsorbed interfacial monolayer, in films spread from dispersions containing BLES.

It has been suggested that since the monolayer flows continuously into the col-

lapsed phase, the collapse structure should have the same composition as the phase from which it is formed [164]. The coexistence of DPPC-rich LC phase and non-DPPC rich LE phase could therefore lead to enrichment of collapse structure (formed from the LE phase) in non-DPPC components. However, in extracted surfactant at 37°C the LC phase occupies only 4-6% of the interface when collapse from the LE phase begins [188]. Therefore compositional refinement by selective exclusion is thought to be limited [164]. Moreover, to attain a film of only LC phase would require an unphysiologically large area reduction [188, 192], providing a strong argument against classical squeeze-out.

An alternate hypothesis to explain the ability of lung surfactant to maintain stability at near zero surface tensions has been proposed by Hall and co-workers. According to this hypothesis, when compressed quickly enough, fluid monolayers can transform into metastable films capable of maintaining high surface pressures. This supercompression likely results in amorphous solids that exhibit resistance to flow [186, 188, 192], and references therein. Supercompression has been demonstrated in CLSE and in monolayers composed entirely of the unsaturated phospholipid POPC, verifying that the observed metastability does not result from a change in composition [186]. As collapse occurs material is removed from the interface thereby lowering the surface pressure; therefore to attain high surface pressures the monolayer must be compressed faster than the rate of collapse [188, 192]. Although the compression rate during normal breathing exceeds the rate required for supercompression, in excised lungs much slower compressions produce functional films [188, 192]. This stability is unexplained by supercompression.

In agreement with recent experimental results suggesting no differences in lipid composition between the monolayer and surfactant reservoir [184], no significant differences in lipid composition between the monolayer and fold are observed in our collapsed LE-phase monolayers. Our simulations do however suggest that the col-

lapse structures can be enriched in surfactant peptides, when folding occurs by nucleation around a peptide aggregate. Our simulations do not display any evidence of supercompression.

3.4.6 Reversibility and Bicelle Formation

Our results suggest that the peptides promote the formation of the collapse phase, and show that the folds can be reversibly reincorporated upon expansion, if the connectivity between the fold and the monolayer remains. Our simulations provide no evidence suggesting the peptides are required to provide reversibility. Lung surfactant proteins SP-B and SP-C could, however, have an anchoring effect, which would attach the collapse phase to the monolayer interface providing reversibility. In one of our DPPC monolayers containing SP-C, with the α-helix of the SP-C molecules placed initially embedded in the tail region, we do observe the anchoring of a bicelle fold to the interface by a SP-C aggregate that remains partially embedded in the monolayer interface (Figure 3.4).

It has been suggested that SP-C stabilizes the collapse structures by anchoring the multilayer collapse structure to the surface monolayer, with its palmitoyl chains inserted into one layer and its α-helix inserted into the adjacent layer [30, 168–172, 174]. It has also been proposed that portions of SP-B may remain associated with the interface at high surface pressures, facilitating lipid transfer to and from the interface [224, 226, 227]. Additionally, films containing dSP-B_{1-25} exhibit better respreadability than films containing SP-B_{1-25}, possibly because dimerization in native SP-B or in dSP-B_{1-25} could maintain the lipid reservoir by creating a bridge with one monomer attached the reservoir and the other attached to the interface [226]. The role of SP-B in maintaining the collapse structure could be similar to the proposed role of SP-B in the crosslinking of vesicles [231], in which charged regions of SP-B interact with the head-groups of the two vesicles and the central parts of SP-B present a nonpolar

surface across which lipid transfer occurs.

The molecular dynamics simulations of Baoukina et al. [29], which used the MARTINI CG model to simulate 4:1 and 1:1 DPPC:POPG monolayers, report the transformation of the folds into "flat circular bilayers" and in some cases into vesicles. The fold-to-vesicle transition was favorable for larger and softer aggregates (having a lower bending modulus) and was driven by the line tension at the edge of the bilayer fold. Low line tension (resulting in a longer monolayer-bilayer connection) at the monolayer-fold junction is important to the reversibility of collapse, because the line tension regulates the connectivity, which is necessary for the transfer of lipids to and from the collapse structure [29]. Our folds take on the shape of flat circular bilayers, but we did not observe vesicle or semi-vesicle formation as seen in the simulations of Baoukina et al. [29], which employed constant interfacial area to investigate the evolution of the collapse structures. Instead, our simulations employ continuous compression, under which the folds continue to grow and the connection between the folds and the monolayer is reduced, making the folds more circular in shape, and at last, in most cases, they desorb from the monolayers, becoming bicelles.

3.4.7 Fusion and Surface Refining

The fusogenic and lytic properties of SP-B may be important to a number of processes occurring within the lung surfactant life cycle including the transfer of lipids to and from the interface, processing of the SP-C proprotein in the multivesicular body, the organization of lamellar bodies, and the formation of tubular myelin [224, 226, 227]. In our simulations, the ability of the surfactant peptides to destabilize (especially after aggregation) the monolayer, promoting collapse, reflects the lytic capabilities of the peptides. We further observed the interaction of peptides (SP-B_{1-25} and mutant) from two separate monolayer folds, leading to the fusion of the folds and the formation of a lipid bridge. Ultimately this process was observed to result in sur-

face refining (a change in the interfacial composition by the addition and/or removal of surfactant material to or from the interface). The observed peptide-mediated fusion, is in good agreement with recent experimental findings [220] that suggest protein-protein interactions could be important to facilitate membrane-membrane apposition during fusion. Several experimental studies [232–235] have proposed that the ability of surfactant proteins to promote adsorption may be attributed to the fluidization of the monolayer and the destabilization of the adsorbing vesicles by the surfactant proteins. The proteins may also act as docking sites [232] or stabilize a structural intermediate formed during the adsorption process [234]. However, a systematic study of fusion and adsorption is beyond the scope of this work and would require a different set up allowing for more consistency between simulations (the fusion between folds seen here can only occur if the folds from each monolayer come close to each other).

3.4.8 Effects of System Size and Time-Scale

When comparing simulation results to experimental or physiological systems, it is important to take account of the limits of the simulations, which could lead to artifacts or inherent differences in behavior between the simulated membranes and their experimental counterparts.

Due to the use of periodic boundary conditions, imposing a small box size leads to artificial membrane rigidity and suppressed undulations [7, 58, 80, 84, 92, 147]. Previous coarse-grained molecular dynamics simulations of DPPC monolayers have shown a decrease in area compressibility modulus (i.e., an increase in compressibility) as system size is increased, due to the ability of the larger system to undulate [28, 58]. Both CG and atomistic simulations of lipid monolayers or bilayers yield compressibility moduli that are significantly larger than experimental estimates [28, 29, 58, 146]. Applying a surface tension will also decrease undulations and thereby reduce the undulatory contribution to the compressibility and the magnitude of finite-size effects

[147]. Size differences between our simulated folds and experimental collapse structures could result in differences in line tension at the monolayer fold connection (λ_c) and at the fold perimeter. For instance, the experimental line tensions at the edge of a bilayer fold are smaller than those calculated from a CG bilayer slab in water (5-30pN vs. 50pN) [29]. As the fluidity of the monolayer is increased, the line tension at the monolayer-fold connection (λ_c) is decreased, favoring the formation of collapse structures. For instance, an increase in unsaturated phospholipids decreases the energetic penalty for lipid deformations at the monolayer-fold parameter and results in a decrease in λ_c [29]. Imposing a small box size leads to artificial membrane rigidity, and therefore increases λ_c . Consequently, the simulated line tension at the monolayer-fold connection (λ_c) is likely larger than that which exists experimentally. To the best of our knowledge no experimental values of λ_c are available for comparison.

The system size affects the magnitude of the energy barrier that must be overcome for buckling to occur [32]. The system size restriction also affects collapse by reducing the probability of monolayer defects. Although 1:1 DPPC:POPG monolayers do not exhibit folding at the smallest system size simulated, even under a small negative surface tension, when we increase the system size by a factor of 4 or 9, folding is observed. In contrast, the pure DPPC monolayers do not display folding even at the largest system size and lowest surface tension tested. By decreasing the surface tension, simulated monolayers can be induced to buckle, but this occurs at lower surface tensions than for real monolayers due to the smaller system size [29]. In agreement with the observations of Baoukina et al. [29], our simulations display an increase in undulations with decreasing surface tension, with buckling occurring at negative or near-zero surface tensions, for all system sizes studied.

Simulated compression occurs much faster than experimental compression rates. Previous simulations [29] utilized intermittent compressions separated by constant area simulations, performed at selected surface densities, to allow time for equilibra-

tion. However, the results of these simulations differ from those of our constant-pressure simulations only in that in the former, vesicles form when the compression is halted and the interfacial area is held fixed. Although an increase in compression rate was associated with larger buckling amplitudes and lower surface tensions obtained before folding, the collapse pathway was independent of compression rate and method [29]. However, the compression rate is likely to affect whether folding occurs by amplification of undulations or by nucleation about a defect.

3.5 Summary

Utilizing coarse-grained molecular dynamics simulations of model surfactant mixtures, we have identified two mechanisms by which monolayer folding can occur, namely (1) through the growth of undulations and (2) by nucleation around a defect. The occurrence of folding depends on monolayer fluidity and can be correlated directly with the carbon deuterium order parameter of the lipid tails. We find in our simulations, under small negative surface tension, that folding occurs when the average order parameter is less than 0.331. Unsaturated phospholipids (POPG) and surfactant proteins (SP-B and SP-C) fluidize the monolayer, while palmitic acid (PA) displays a charge-dependent condensing affect. The extent to which the peptides fluidize the monolayer, and thus enable folding, depends on the hydrophobic character of the peptides. The peptides appear to provide a larger driving force for folding than does POPG, allowing fold formation to occur for peptide containing monolayers under conditions for which it does not occur in the presence of POPG alone. The formation of a lipid bridge by peptide-mediated fusion and the ensuing redistribution between monolayers upon re-expansion demonstrate the fusogenic abilities of the peptides and their role in surface refining. Despite limitations resulting from potential system-size and time-scale effects, CG simulation is a valuable tool for studying the structural transitions of lipid/peptide films and can be used to identify pertinent

interactions that may act as driving forces for these transitions. Our results show that the MARTINI model can capture qualitatively the effects of lipid and protein components on the fluidity and collapse behavior of the monolayer in good agreement with experimental observations.

CHAPTER IV

Preliminary Study of LC-LE Phase Transitions in Lipid and Lipid-Peptide Monolayers.

4.1 Introduction

Lung surfactant (LS) is a mixture of phospholipids, fatty acids, neutral lipids, and surfactant proteins that forms the surface-active lining in the lungs and decreases the work of breathing by reducing and regulating the surface tension in the alveoli. Lung surfactant consists of approximately 90% lipids and 10% proteins by weight [45]. Of the surfactant lipids, about 80% are phosphatidylcholines, about half of which is dipalmitoylphosphatidylcholine (DPPC) [45]. Infants born prematurely lack functional lung surfactant and develop respiratory distress syndrome (RDS). Surfactant replacements have greatly reduced the mortality rate of RDS, but are not optimal [46]. Another form of RDS known as acute respiratory distress syndrome (ARDS) can develop in adults and has proven difficult to treat due to complications associated with underlying lung injury [47]. ARDS is often associated with the leakage of plasma proteins and other molecules into the lungs, resulting in inhibited lung surfactant function, which can be attributed to a variety of factors such as competitive adsorption. It is well known that in order to be effective, lung surfactant must display rapid adsorption, the ability to compress to near-zero surface tension upon end-expiration, and rapid respreading upon film expansion [53]. However, further research is needed to understand the mechanisms involved and the roles of individual

surfactant components in the respiratory process, in order to aid the development of more efficient surfactant replacements to treat both neonatal and adult RDS.

The surfactant film undergoes constant changes in surface pressure under the dynamic cycling occurring with each breath. Maintaining proper surfactant functionality under these demanding conditions requires a number of components. The primary component, dipalmitoylphosphatidylcholine (DPPC) has a high transformation temperature of 41°C [48], and therefore exists in the liquid condensed (LC) phase at body temperature. In the condensed phase DPPC is tightly packed and can be compressed to surface pressures well above the equilibrium spreading pressure (π_e) without collapse. For this reason DPPC is thought to be primarily responsible for the ability of lung surfactant to reach near-zero surface tension (high surface pressure). However, due to its rigidity at physiological temperature, DPPC exhibits poor respreadibility [152]. Additional surfactant components enhance the surface activity of LS. Unsaturated phospholipids, such as palmitoyloleoylphosphatidylcholine (POPC), fluidize lung surfactant surface films increasing adsorption to the interface and are thought to enhance respreading [45]. Neutral lipids and fatty acids are also present, such as cholesterol (5-10wt% of native surfactant); an important component of lung surfactant, which is systematically removed from most surfactant replacements [54]. Lung surfactant also contains surface-associated surfactant proteins SP-B and SP-C, which are essential to modulate the physical properties of the surface film and to promote the rapid formation of surface films capable of reaching near-zero surface tensions under repetitive cycling [156]. Both peptides are highly hydrophobic and amphipathic. SP-B contains seven cysteines, which form three intramolecular disulfide bridges and an intermolecular one leading to the formation of a homodimer [154]. SP-B contains more polar and hydrophilic residues than SP-C and is therefore less hydrophobic. SP-C contains palmitoyl chains on cysteine residues 5 and 6 [155]. The tertiary structure of SP-B is unknown; however the structure is known for the

25-residue N-terminal fragment (SP-B_{1-25}), which is thought to retain most of the functionality of the full-length protein.

As the monolayer is compressed from a high molecular area to a low molecular area (low surface pressure to high surface pressure) it passes through distinct regions of the pressure area isotherm (see Figure 2.1(a)) : G, LE+G, LE, LC+LE, LC. In the gas (G) phase the lipids are very sparse and behave like a 2D gas [88]. The liquid-expanded (LE) phase is characterized by a fluid-like structure, where the molecules are in close contact with one another, but the lipid tails are conformationally disordered and contain a significant number of gauche configurations [88]. The liquid-condensed (LC) phase is a 2D semi-crystalline phase, which is characterized by hexagonal packing, lipid tails in the all-trans conformation with a substantial drop in the number of gauche defects, and decreased lateral mobility [88]. Upon compression the monolayer passes through two regions of phase coexistence (LE-G and LC-LE). In this chapter we will focus on LC-LE phase transitions. Several experimental studies have provided clear microscopic evidence of the coexistence of LC and LE phase in model surfactant monolayers, proving the existence of both micro-scale and nano-scale domains [53, 176, 177, 208, 209, 236].

It is not fully understood how monolayers respond to the large changes in surface area, which occur during breathing [44]. Neither the structural transitions involved nor the roles of each surfactant component are entirely clear. For example, the mechanism by which lung surfactant is able to avoid irreversible collapse under near-zero surface tensions remains a matter of great debate. The ability of lung surfactant to be rigid enough to sustain near-zero surface tension and yet fluid enough to respread rapidly, seems contradictory, This dichotomy, has lead to classical "squeeze-out" theory [119, 179, 180], which suggests that as the monolayer undergoes compression the surface is refined by the selective squeeze-out of non-DPPC components leaving behind a monolayer highly enriched in DPPC. Recently, alternative theories have been

proposed, such as the theory of supercompression [186, 188, 189, 237].

To reach the near-zero surface tensions existing in the lungs the alveolar lining must compress past the equilibrium spreading pressure, and is thus by definition meta-stable. The effective viscosity of the alveolar film controls the rate at which the film flows into the bulk phase in response to the thermodynamic driving force [237]. It is therefore thought that to avoid collapse the monolayer must undergo a transition to become a highly viscous material. According to Hall and coworkers [186, 188, 189, 237] this can be achieved by the transformation of the monolayer into either a solid-like LC phase, as suggested by classical "squeeze-out" theory, or into a super-compressed fluid phase. Hall and co-workers have shown that both CLSE and the unsaturated phospholipid POPC can reach near-zero surface tensions if compressed quickly enough (super-compression) [186, 188, 189, 237]. Such a super-compressed fluid maintains the high disorder of the fluid phase, but attains the resistance to flow that characterizes a solid.

In order to begin to address these fundamental uncertainties, an understanding of the interfacial structure of model surfactant mixtures is necessary. It is important to understand the phase transitions occurring in lipid and lipid-peptide monolayers, because the phase state of a surfactant monolayer will determine its surface-active properties. As discussed in chapter 3, the mechanism of collapse depends on the phase morphology, which is determined by the temperature, surface pressure, composition, and compression rate. For example, Gopal and Lee [206] showed that for a 7:3 DPPC/POPG monolayer at low temperatures (below 28°C) the monolayer is biphasic and collapses by forming reversible large-scale folds (up to millimeters in length), while at high temperatures (above 33.5°C) the monolayer is homogenous and collapses by forming micron-scale vesicular structures, and at intermediate temperatures (28-33.5°C) collapse occurs by forming both folds and vesicles. Lee and co-workers [158, 163, 190] suggest that coexistence of LC and LE phase is an essential feature required

for reversible collapse via the macroscopic folding transition. They propose that the coexistence of LC and LE phases provides the monolayer enough flexibility to bend and enough cohesiveness to prevent loss of material to the subphase.

Because the phase (or phase coexistence) of the monolayer determines the properties of the monolayer such as minimum surface tension, collapse mechanism, rate of collapse, and reversibility of collapse, an understanding of how lung surfactant components affect phase behavior at high surface pressures is important to the rational design of surfactant replacements. To this end, here we study LC-LE phase transitions for DPPC monolayers and monolayers of DPPC with additional LS components.

Historically, lipid phase transitions have proven difficult to simulate, requiring length and time scales not attainable by atomistic simulation. However, recent papers [23, 34] have shown that it is possible to simulate the formation of small LC nuclei via atomistic simulation. However, such simulations are computational expensive. Therefore, these simulations have been limited to pure DPPC monolayers and to relatively short time scales, preventing the study of the phase transformation process in much detail. In recent years, the development of coarse-grained models has allowed the simulation of longer length and time scale events. Utilizing an early version of their MARTINI force field [58], Marrink et al. [7] applied CG-MD to the study of gel-liquid crystalline phase transformations in DPPC bilayers. This work showed that the MARTINI model could be successfully applied to the study of lipid phase transformations. To the best of our knowledge, MD simulation has yet to be applied to the study of phase transitions in multicomponent lipid monolayers. Here we apply the MARTINI coarse-grained model [56, 57] to the study of LE-LC phase transitions in DPPC monolayers, and phase transitions in mixed monolayers containing DPPC with additional lipid and peptide components.

In the LC phase DPPC molecules tilt at an angle of 25° with respect to the normal [88]. This tilt is due to a mismatch between the minimum cross-sectional area of 50Å^2

for the head group and 38Å^2 total for both of the phospholipid tails [88]. For this reason the term tilted condensed (TC) is often used to describe the liquid condensed phase of monolayers containing DPPC. Although the tilted condensed phase is often discussed experimentally, all results reported here are for the untilted condensed phase. Because the MARTINI model implicitly incorporates some of the tail entropy of the lipid tails into the volume of the CG interaction sites, the DPPC molecules do not form the tilted condensed phase [7]. However, the formation of the tilted condensed phase can be simulated by decreasing the size of the tail beads by 10% [7]. Furthermore, the terminology phase transition is typically used in the experimental literature regarding lung surfactant. Therefore, we will keep this terminology. However, it is important to note that the phase transitions observed here are distinctly non-equilibrium.

4.2 Simulation Methods

The MARTINI CG model [56, 57] was used in all simulations reported here. The CG mapping of DPPC, cholesterol, sodium ions, chloride ions, and water molecules is the same as that provided in the topology files on the MARTINI website [79]. The Perl script seq2cgtop_martini_v2.1tryout.pl [79] was used to generate the topology for coarse-grained SP-B$_{1-25}$ and SP-C. The structure files for SP-B$_{1-25}$ and SP-C were created by coarse-graining structure files for SP-B$_{1-25}$ [197] and SP-C [198] that were obtained by FTIR and NMR spectroscopy. The MARTINI model is parameterized based on thermodynamic data, and has successfully reproduced membrane properties such as area per lipid [56, 58], pressure-area isotherms [28], gel - liquid-crystalline phase transitions in bilayers [7], phase transitions between lamellar and non-lamellar phases [199, 200], self assembly of bilayers, and structural and dynamic features of protein-lipid interactions [57]. Furthermore, the MARTINI model yields profiles of lateral pressure versus vertical position in the monolayer that are qualitatively similar

to those obtained from atomistic simulations, suggesting that the MARTINI model captures the essential lipid/solvent properties [24].

Each configuration was constructed from two disordered lipid monolayers (each composed of 256 DPPC molecules) placed with heads facing each other across a layer of water, and tails separated by vacuum, in a periodic box, as described previously (chapter 1 and [28]). The z-dimension, normal to the layers, was adjusted to 100nm, which allows more than enough space to prevent the tail regions of the two monolayers interacting. The SP-B_{1-25} molecules were then placed in each monolayer, oriented normal to the interface with the insertion sequence, which is the last eight residues on the N-terminus side, placed close to the head group region. Four peptides were inserted into each monolayer in three initial configurations: 1) with the peptides clustered together (not in contact, but with each peptide 1.7nm from the center of the box), 2) in a line (separated by 3.3nm), and 3) in a square (with each peptide placed 4.5nm from the center of the box). CG chloride ions were then added to make the system electroneutral. The system was then energy minimized. SP-C was placed in the monolayer in the same manner as SP-B_{1-25} in the line configuration as described above, but with the α-helix placed initially embedded in the lipid tail region and tilted with respect to the interface. The SP-C molecules were initially placed differently that the SP-B_{1-25} molecules to account for differences in the experimental orientation of the two peptides in DPPC monolayers. SP-B is thought to reside near the headgroup region with its α-helix parallel to the interface [203]. However, SP-C is highly hydrophobic and infrared reflection-adsorption spectroscopy has revealed that SP-C adopts a tilted orientation, embedded within DPPC monolayers [204]. Although the simulated peptide concentrations are larger that the average physiological concentrations, as noted previously [201], local concentrations of physiological lung surfactant components could be much higher than the physiological average, particularly if interactions between components result in non-uniform distributions.

The CG topology and structure files for POPC were adapted from the lipid topology file and a palmitoyloleoylphosphatidylethanolamine (POPE) bilayer CG structure file taken from the MARTINI website [79], by replacing the ethanolamine head group bead (Qd) with a choline head group bead (Q0). A system containing two POPC monolayers was constructed in the same way as described for the DPPC monolayers. To create 1:1 DPPC:POPC monolayers, POPC molecules were randomly replaced with DPPC molecules to obtain a 1:1 mixture and the system was then energy minimized. In the DPPC/cholesterol monolayers, 50 cholesterol molecules were randomly inserted into each DPPC monolayer and the system was then energy minimized. The topology used for cholesterol is the same as that reported on the MARTINI website[79]. The structure file for cholesterol was created by coarse-graining the first of eight atomistic structures for cholesterol (molecule A) reported by Shieh et al. [238], which were obtained by x-ray diffraction.

For all simulations, temperature was maintained by coupling to a Berendsen thermostat [67] with a 1ps time constant. Berendsen pressure coupling was used with a 1ps time constant and all compressibilities set to 5E-6bar^{-1}. Pressure was coupled anisotropically to 0bar in all directions (zero surface tension). The surface tension is calculated from Equation 3.1. As mention in chapter 3, due to pressure fluctuations the actual time-average surface tension differs slightly from this set point. For more details on each coupling mechanism the reader is referred to the GROMACS User Manual [70] and relevant simulation papers [41, 43, 75, 76, 78]. For all simulations, a timestep of 0.02ps was used, and periodic boundary conditions employed. All simulations were performed using GROMACS simulation software [68, 69, 202]. The following parameters were taken from the MARTINI website [79] and have been optimized for the coarse grained model: short-range electrostatic and van der Waals cutoffs of 1.2nm, with van der Waals interaction shifting smoothly to Lennard Jones interaction at 0.9nm, and with the Lennard Jones cutoff set to 1.2nm. The neighbor

list was updated every 10 steps using a grid with a 1.2nm cutoff distance. In addition to the large computational speed-up, the molecular diffusivities of CG water and lipid molecules are around four times higher than for atomistic ones. As a result, the effective time of a simulation is roughly four times longer than the physical time [56]. However, all times reported here are physical times, as reported by the simulation.

After energy minimization the initial configurations (described above) were equilibrated for 1μs at high temperature (338K for all peptide-free monolayers, and 333K for peptide-containing monolayers). The final configurations from these runs were used as starting states for runs at low temperature (283K for all systems), to allow each monolayer to order. The final configurations of the high and low temperature runs were used as initially disordered and initially ordered starting configurations for subsequent runs, which were performed between 283K and 338K in 5K increments. The trajectories of these runs were saved for packing analysis every 1ns. Shorter (100ns) runs are also reported for DPPC monolayers to assess artifacts attributed to simulation time. To allow more data points for packing analysis, the trajectories of these runs were saved for packing analysis every 0.2ns. The percentage of hexagonal packing was averaged between 500ns and 1μs for the 1μs runs and between 50 and 100ns for the shorter runs. For the longer time-scale runs there are a couple of cases where the transition from disordered to ordered phase or vice-versa occurs late in the simulation (after 500ns), for these runs the hexagonal packing was averaged after the transition was complete, between 900ns and 1μs. The error bars reported on the hysteresis loops represent the standard deviation.

The simulations of DPPC monolayers yielded a large hysteresis loop with respect to temperature. In order to estimate the true transition temperature and study the growth of the ordered and disordered phases, the final configurations resulting from 1μs simulations of initially ordered and initially disordered DPPC monolayers at 308K were merged together. As the monolayers condense the lateral dimensions

of the monolayer decrease and the thickness increases. This transformation results in a thicker (larger in the z-dimension) water subphase in the system containing ordered monolayers. Therefore, to allow the ordered and disordered monolayer to align the disordered system was spliced and a small water box containing 993 CG water molecules was inserted between the top monolayer and the original water subphase. The disordered and ordered boxes were then placed side by side in the x-dimension. A small 0.7nm mismatch between the monolayers in the y-dimension remained. To account for this mismatch two different systems were constructed, which we will call Merge1 and Merge2. In Merge1 the dimensions of the disordered box were shrunk by 0.7nm, effectively compressing the disordered box slightly. Another configuration (Merge2) was generated where the larger y-dimension was kept, effectively disrupting the packing in the ordered system along the edge of the box where 0.7nm of empty space is added. These systems containing side by side ordered and disordered regions were energy minimized and run at temperatures falling within the region of hysteresis (between 303K and 323K) for 100ns. The coordinates were output to the trajectory every 10ps to allow the growth or disappearance of the condensed phase to be captured in greater detail.

A program called Triangle was used to perform a Delaunay refinement on the simulation trajectories [239]. From the Triangle output files condensed phase lipids can be identified. The output files from Triangle were converted into an index file containing only the C2 tail sites that are considered to be in the liquid condensed phase. Marrink et al. developed the following criteria: in order to be in the condensed phase (gel phase for bilayers) the C2 tail sites of a lipid must be six coordinated, corresponding to hexagonal packing, and must have five of its six neighboring C2 sites less than 0.75nm away [7]. The second criterion is used to eliminate lipids that are six coordinated, but deviate considerably from hexagonal packing [7]. We used the same criteria in our analysis, except we tightened the second restraint to require that all

six C2 sites be within 0.75nm. This was done to eliminate noise in our data, which appeared as a few isolated C2 sites. In monolayers containing DPPC and POPC, the C2 sites of both phospholipids were used in the calculation of the percentage of hexagonally packing. In monolayers containing cholesterol, the R3 beads of the cholesterol molecules are treated as neighboring C2 sites in order to determine the the extent of hexagonal packing for DPPC. However, the reported percentage of hexagonal packing is only calculated for the C2 sites of the phospholipids. The R3 beads of cholesterol were chosen as neighboring sites for the hexagonal packing analysis, because they lie in the roughly the same xy-plane as the C2 sites of DPPC.

4.3 Results and Discussion

4.3.1 LC-LE Phase Transitions in Pure DPPC Monolayers

To obtain disordered monolayers of DPPC, the system containing two DPPC monolayers separated by vacuum (described in the simulation methods section) was equilibrated at 338K for 1μs. The final configuration from this simulation was then used as the starting state for a 1μs simulation at 283K. The ordered (LC) and disordered (LE) configurations resulting from the simulations at 283K and 333K were used as the starting states for subsequent runs. It should be noted that within the simulation time the monolayer does not become fully ordered. There are small defects in the packing (disclinations) even after 1μs at 283K (Figure 4.1(a)). Likewise, even the most disordered monolayer (338K) contains a few isolated sites and small patches (<20 C2 sites), which meet the criteria of being hexagonally packed (Figure 4.1(b)).

Simulations were then run between 283K and 338K in increments of 5K from both disordered and ordered starting configurations. As the temperature is decreased from 338K to 313K (Figure 4.2(a)) the monolayer remains disordered but small patches of LC phase are evident. As the temperature is further decreased to 303K (Fig-

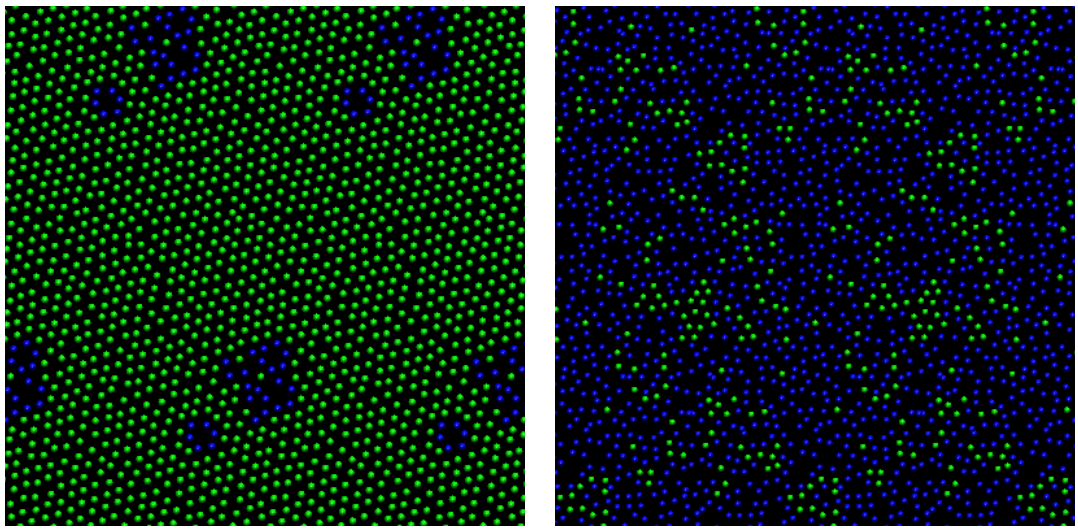

(a) (b)

Figure 4.1: Ordered and disordered initial configurations. (a) The ordered initial configuration obtained after a 1μs simulation at 283K. (b) The disordered initial configuration obtained after a 1μs simulation at 338K. In this and subsequent figures only the C2 sites from a single monolayer are shown for clarity. Within a given simulation, the top and bottom monolayer monolayers tend to show the same behavior. Some periodicity is also shown for clarity. The same color scheme is used throughout this chapter. The green C2 sites are in the liquid condensed (LC) phase and the blue C2 sites are in the liquid expanded (LE) phase.

ure 4.2(b)), the monolayer undergoes a transition to the LC phase, and only small patches of LE phase remain. As the temperature is increased from 283K to 318K (Figure 4.2(c)) the monolayer remains ordered but small patches of LE phase are evident. As the temperature is further increased to 323K (Figure 4.2(d)), the monolayer undergoes a transition to the LE phase, and only small patches of LC phase remain. Hysteresis is evident from these snapshots; an initially disordered monolayer remains disordered after a 1μs simulation at 313K (Figure 4.2(a)), however an initially ordered monolayer remains ordered after a 1μs simulation at 318K (Figure 4.2(c)). We will further investigate this hysteresis later in this chapter.

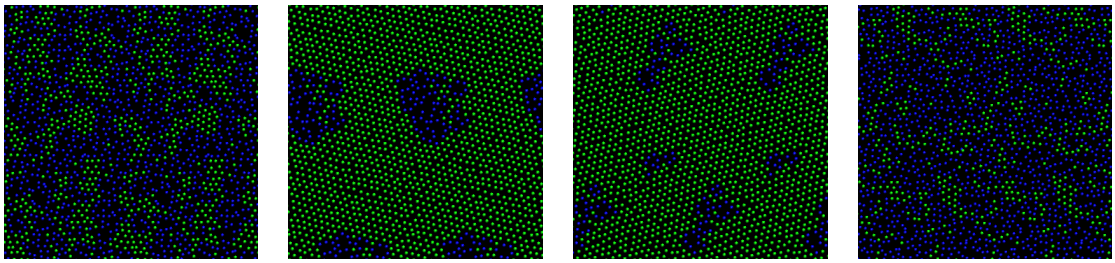

(a) (b) (c) (d)

Figure 4.2: LC-LE phase transitions in DPPC monolayers. An initially disordered monolayer (338K) is quenched to (a) 313K and (b) 303K. An initially ordered monolayer (283K) is heated to (c) 318K and (d) 323K. The snapshots were taken after 1μs of simulation time.

4.3.2 LC-LE Phase Transitions in DPPC Monolayers Containing Peptides

To study the effect of surfactant peptides on the phase behavior of DPPC monolayers 4 SP-B_{1-25} molecules were added to each DPPC monolayer. The peptides were initially placed perpendicular to the interface, however they quickly reorient (with the first few nanoseconds) and adopt an orientation that is roughly parallel with the interface and embedded superficially into the monolayer, in agreement with the experimental observations [203]. The system was then equilibrated at 333K for 1μs. The final configuration from the 1μs run at 333K was used as the starting state for a 1μs simulation at 283K. The ordered and disordered configurations resulting form the simulations at 283K and 333K were used as the starting states for runs between 283K and 333K in increments of 5K . In Figure 4.3, snapshots are shown for DPPC monolayers containing SP-B_{1-25} after being quenched from 333K to (a) 308K and (b) 303K and after being heated from 283K to (c) 303K and (d) 308K. Regardless of starting state (initially ordered or disordered) the monolayers are ordered at 303K and disordered at 308K. The disordered monolayers at 308K contain small patches of LC phase lipids. At 303K the peptides loosely aggregate and localize within a single LE phase domain, while away from the peptides the monolayer is in the LC phase

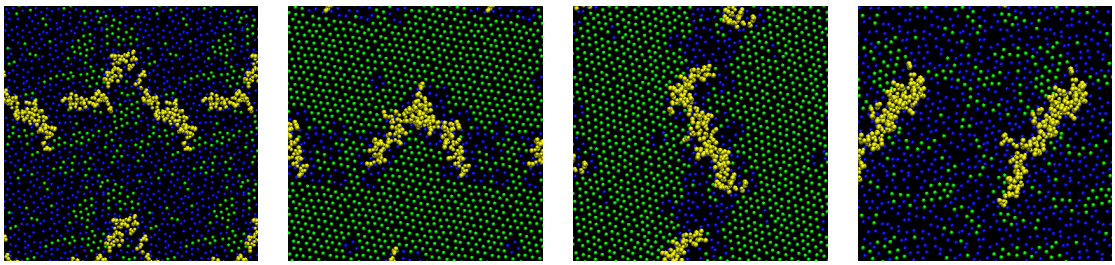

(a) (b) (c) (d)

Figure 4.3: LC-LE phase transitions in DPPC monolayers containing SP-B_{1-25}. An initially disordered monolayer (333K) is quenched to (a) 308K and (b) 303K. An initially ordered monolayer (283K) is heated to (c) 303K and (d) 308K. All snapshots correspond to the line initial configuration. The snapshots were taken after 1μs of simulation time, and show a single monolayer. In this figure and subsequent figures the peptides are shown in yellow.

with a few small defects.

Our observations agree well with experimental observations of the influence of surfactant peptides on lipid packing. SP-B, SP-B_{1-25} and SP-C are known to localize within the fluid phase [158, 160, 161, 163, 166–170, 172, 173, 208, 209]. and have been found to perturb monolayers of DPPC, DPPC/DPPG, and PA, increasing the overall fluidity of the monolayers and producing smaller and more numerous condensed phase domains [158–160, 166, 167, 208, 209]. Fluorescence and scanning force microscopy report that SP-B affected the distribution of LE and LC regions of DPPC at both the microscopic and nanoscopic level causing and overall reduction in the total amount of LC phase present and an increase in the LC-LE interface [209]. It has therefore been hypothesized that SP-B promotes the formation of a fine nanoscopic framework of lipid and lipid-protein nano-domains that lends the film a substantial mechanical resistance to deformation and rupture. SP-B has also been observed to segregate and form clusters at phase boundaries [209]. Our simulations show that SP-B_{1-25} perturbs the packing of the neighboring lipids. Also, the peptides tend to localize within a single LE phase domain. This localization could lead to the aggregation of the peptides.

To further evaluate the affect of the peptides on the monolayer, a larger system was generated from the disordered starting state by copying the box laterally to create a system containing four times as many molecules as the original system. After 1μs of simulation at 303K, these larger monolayers show a large amount of LC phase with some LE phase centered around the peptides. The peptides disrupt the crystallinity of the ordered phase and act as defects in the monolayer. In order to propagate the LC phase must grow into peptide-free regions of the monolayer, this growth essentially pushes the peptides together uniting them within the small fraction of disordered phase (Figure 4.4). This type of behavior may explain why SP-B has been observed to aggregate experimentally. Furthermore, the fact that the peptide impedes the spread of ordered domain may explain, at least in part why the peptides have been observed at domain boundaries. Simulations containing larger LE domains in coexistence with the LC phase, would help to provide more definitive results regarding the localization of the peptides at domain boundaries. However, such simulations would be computationally expensive and are not yet practical. From Figure 4.4, it is apparent that the peptide filled LE phase breaks up the condensed phase. This behavior is in consensus with the proposed role of SP-B_{1-25} in the formation of a fine nanoscopic framework.

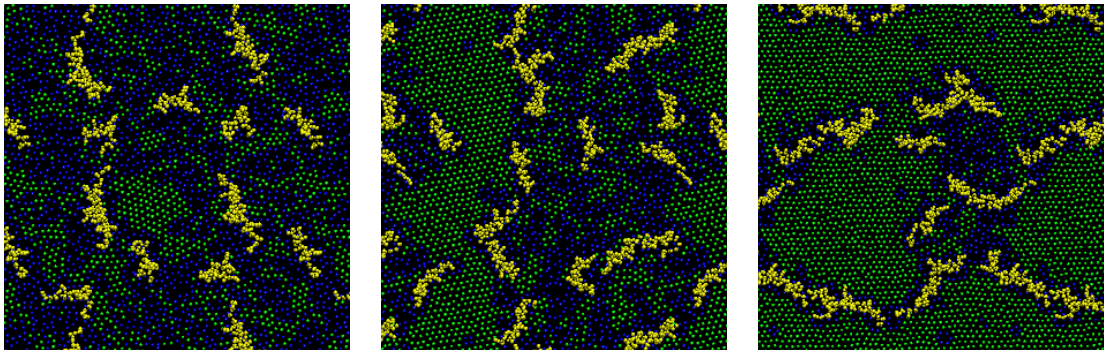

(a) (b) (c)

Figure 4.4: Packing in larger monolayers composed of DPPC with SP-B_{1-25}. An initially disordered monolayer (333K) is quenched to 303K. The snapshots shown were taken after (a) 10ns, (b) 100ns, and (c) 1μs of simulation time.

To test the dependence of the domain formation on the initial position of the peptides three different initial configurations were used. As described in the simulation methods section four peptides were placed partially inserted in each monolayer so that they formed a square, a line, and a cluster, with respect to each other. All snapshots in Figures 4.3 and 4.4 correspond to the line initial configuration. In Figure 4.5 the monolayers with the line (left) initial configuration are reproduced alongside corresponding simulations with the square (center) and cluster (right) initial configurations. The snapshots shown were taken after 1μs of simulation for the line and square initial configurations and after 100ns of simulation time for the cluster initial configuration. Note that the simulations involving the cluster initial configuration were limited to 100ns due to the onset of fold nucleation around the peptide aggregate (as discussed in chapter 3) limiting access to longer simulation times. The snapshots shown were taken at 303K after quenching from a disordered state (top) and heating from an ordered state (bottom). The simulations with the square initial configuration result in similar amounts of LC and LE phase lipids as the line initial configuration. However, the amount of LC phase is slightly greater in the monolayer were the peptides were initially clustered together. These simulations show that condensed phase formation is perturbed by the insertion of peptides, and the extent of perturbation depends on the position of the peptides relative to one another. The peptides perturb the surrounding lipids, and therefore if the peptides are clustered together, the LC phase is only perturbed in the immediate vicinity of the peptide cluster and most of the LC phase is left unaffected. In fact the total amount of LE phase lipids at 303K, is roughly the same in the cluster configuration (Figures 4.5(c) and 4.5(f)) as for the pure lipid system (Figure 4.2(b)). However, if the peptides are spread-out (as is the case for the line and square starting states), the LE phase surrounds the peptides, covering more area and decreasing the total amount of LC phase present in the monolayer. Therefore, the growth of the LC phase favors the

aggregation of the peptides.

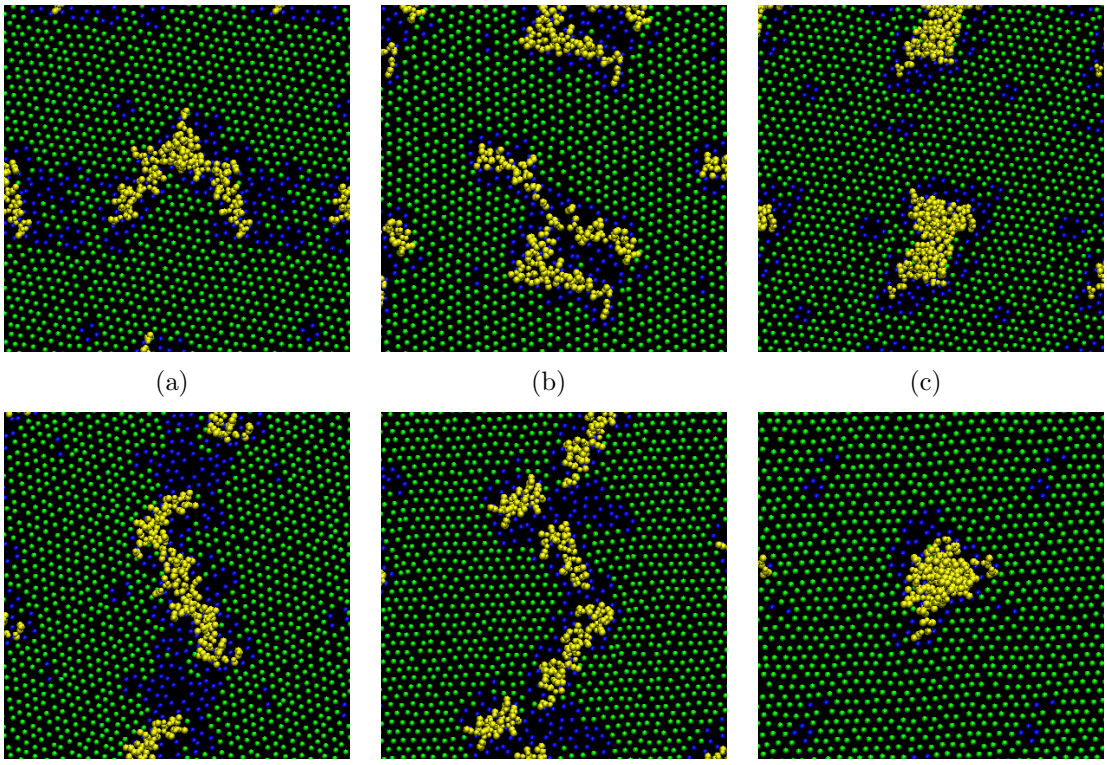

Figure 4.5: The influence of peptide orientation on the LC-LE phase coexistence. Three peptide initial orientations were studied: Line (left), square (center), and cluster (right). The snapshots were taken after 1μs of simulation at 303K, with the exception of cluster, which was taken after 100ns of simulation time. The monolayers on the top were quenched from a disordered state and the monolayers on bottom were heated from an ordered state.

A limited number of simulations were also performed for monolayers containing SP-C. To correspond with experimental observations, SP-C was placed initially tilted and embedded in the DPPC monolayer [204]. Using the "line" initial configuration, disordered and ordered starting states for DPPC/SP-C monolayers were generated in the same manner as the starting states for the DPPC/SP-B_{1-25} monolayers. Simulations were performed at 303K and 308K using both starting states. Both the initially ordered and initially disordered monolayers are ordered after a 1μs simulation at 303K (not shown). However, hysteresis is evident at 308K. After 1μs at 308K, the initially disordered monolayer remains disordered (Figure 4.6(a)) and the initially

ordered monolayer remains ordered (Figure 4.6(b)).

It is unclear why at 308K, initially ordered DPPC/SP-C (Figure 4.6(b)) monolayers remain ordered, but initially ordered DPPC/SP-B_{1-25} (Figure 4.3(b)) monolayers disorder. To further elucidate this difference in phase behavior at 308K, the DPPC/SP-C (Figure 4.6(c)) and DPPC/SP-B_{1-25} (Figure 4.6(d)) monolayers are visualized from the side. Here SP-C penetrates deeper into the monolayer than SP-B_{1-25}. However, the SP-B_{1-25} containing monolayer shows substantial deformation around the SP-B_{1-25} aggregate, resembling a pre-collapse instability. These results suggest that the observed phase behavior in the peptide containing monolayers may be linked to the curvature of the monolayer near the peptide, and require further investigation. It is also interesting to note that in Figure 4.6(d), the palmitoyl chains of SP-C (shown in red) remain firmly embedded within the monolayer. It has been proposed that at high surface pressures (low surface tension) SP-C is partially squeezed-out of the monolayer with associated lipids, but remains anchored to the monolayer interface by it's palmitoyl chains, which remain embedded within the monolayer [30, 168–172, 174].

4.3.3 LC-LE Phase Transitions in Binary Lipid Monolayers Containing DPPC

In addition to DPPC, lung surfactant contains many other important lipid components including unsaturated phospholipids and cholesterol. Due to chain unsaturation, phospholipids such as POPC have low transition temperatures and are thus in the LE phase at physiological temperature. To study the effects of POPC on the LC-LE phase transition, monolayers were constructed containing a 1:1 mixture of DPPC and POPC. The majority of the 1:1 DPPC:POPC simulations contained 256 lipids per monolayer. A simulation was also performed on monolayers four times larger, to study the system size effects on the phase distribution.

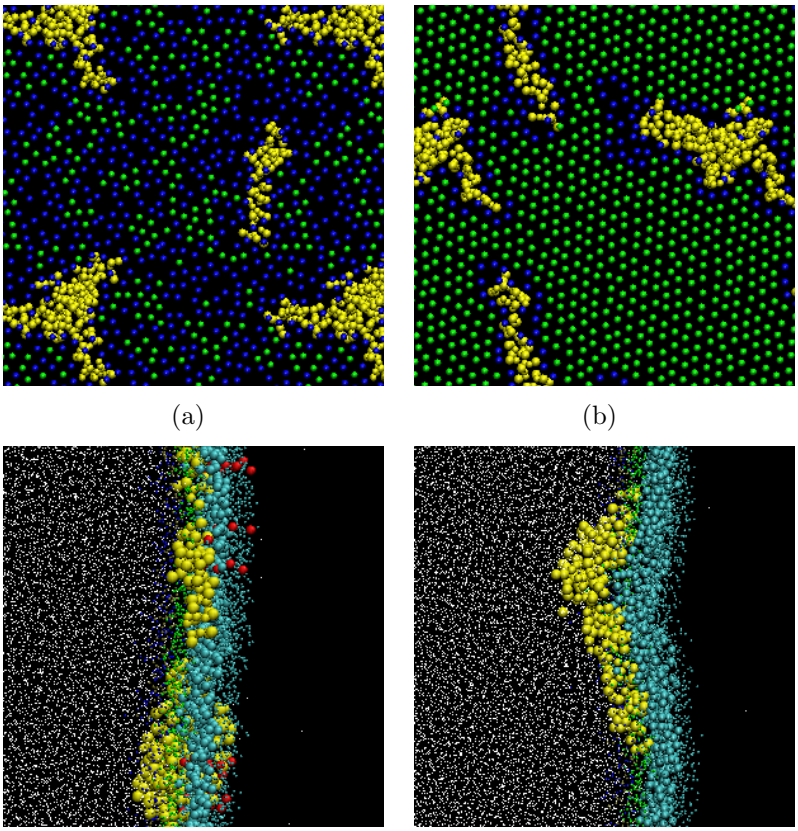

Figure 4.6: The phase behavior of monolayers containing SP-C. After 1μs of simulation at 308K, the initially disordered DPPC/SP-C monolayers remain disordered (a) and the initially ordered DPPC/SP-C monolayers remain ordered (b). In contrast to the DPPC/SP-C monolayers (b), initially ordered DPPC/SP-B_{1-25} monolayers disorder at 308K (Figure 4.3(b)). To elucidate this difference, side views of the DPPC/SP-C (c) and DPPC/SP-B_{1-25} (d) monolayers are given. All snapshot were taken after 1μs of simulation at 308K. In (c) and (d) the peptides are shown in yellow, the palmitoyl chains of SP-C are shown in red, and the CG water molecules are shown as small white dots. The DPPC tails, headgroups, and glycerol linkages are shown in turquoise, dark blue, and green, respectively. The C2 sites of the phospholipid tails are enlarged with respect to the rest of the phospholipid sites.

Cholesterol is another important component of lung surfactant composing about 5-10 wt% of natural surfactant [54]. The effect of cholesterol of lipid bilayers has been studied extensively. Studies of monolayers containing cholesterol are much less prevalent. It has been suggested that cholesterol modulates the phase behavior of

surfactant membranes by disordering phospholipids in the LC phase and ordering phospholipids in the LE phase, resulting in the formation of the liquid-ordered (Lo) and liquid-disordered (Ld) phases, respectively [54]. To study the effects of cholesterol on the LC-LE phase transition, cholesterols were added to each DPPC monolayer to create a system containing 256 DPPC and 50 cholesterol molecules per monolayer.

Both the cholesterol and POPC containing monolayers were run at 338K for 1μs to obtain initially disordered starting states and the final configurations of these runs were than used as the initial configurations for 1μs runs at 283K to obtain initially disordered starting states.

4.3.3.1 Monolayers Containing Cholesterol

The DPPC/Cholesterol monolayers are quenched and heated from the disordered and ordered starting states to temperatures between 338K and 283K, in 5K intervals. In Figure 4.7 snapshots are shown at selected temperatures with corresponding radial distribution functions (RDFs) showing the distribution between cholesterol molecules and disordered C2 sites (blue), ordered C2 sites (green), and other cholesterol molecules (red). After the monolayer is quenched to 323K (Figure 4.7(a) and 4.7(b)) the monolayer remains mostly disordered, with small patches on LC phase. If the temperature is reduced to 303K (Figure 4.7(c) and 4.7(d)) the monolayer orders, but small patches of LE phase remain. After the monolayer is heated from an ordered starting state to 303K (Figure 4.7(e) and 4.7(f)) the monolayer remains mostly ordered with only a small patch of LE phase and some scattered disordered sites. At 328K (Figure 4.7(g) and 4.7(h)) the monolayer disorders, but patches of LC phase remain. Our simulations show that cholesterol packs well within the LC phase, and does not perturb the packing of the surrounding lipids (Figure 4.7(c) and 4.7(e)). Cholesterol also prefers to reside either in the LC phase, or at the interface between the LC and LE phase. Even when there is a larger amount of LE phase present, cholesterol is rarely surrounded entirely by disordered lipids, but instead tends to

reside at the interface between ordered and disordered lipids. Cholesterol's apparent preference for the ordered phase could be an artifact of the instantaneous cooling and the short time-scale of simulation, which could cause cholesterol to become trapped in the ordered phase. However, cholesterol shows a clear preference for the interface over the disordered phase.

The RDFs reinforce the observed preference of cholesterol to reside at the interface. The RDFs obtained from the disordered monolayers (Figure 4.7(b) and 4.7(h)) demonstrate a stronger association of cholesterol with the ordered sites than with the disordered sites, as evident from the magnitude of the first peaks in the radial distribution functions. In contrast the RDFs corresponding to ordered monolayers (Figure 4.7(d) and 4.7(f)) demonstrate a stronger association of cholesterol with the disordered sites than with the ordered sites, as evident from the magnitude of the first peaks. The stronger association of cholesterol with disordered sites in a mostly ordered monolayer and with ordered sites in a mostly disordered monolayer reflects cholesterol's preference for the interface. In the disordered monolayers (Figure 4.7(b) and 4.7(h)) the first peak in the cholesterol-cholesterol distribution is very weak, showing that cholesterol does not associate strongly with itself. In the ordered monolayers (Figure 4.7(d) and 4.7(f)) the self-association increases, but remains relatively weak. The RDFs also show little structural difference between the two disordered monolayers (Figure 4.7(b) and 4.7(h)). Likewise, little structural difference is seen between the order monolayers (Figure 4.7(d) and 4.7(f)). The RDFs of the ordered monolayers show long-range order. The RDFs for the disordered monolayers show a few well-defined peaks indicating some short-range order resulting from small patches of condensed phase.

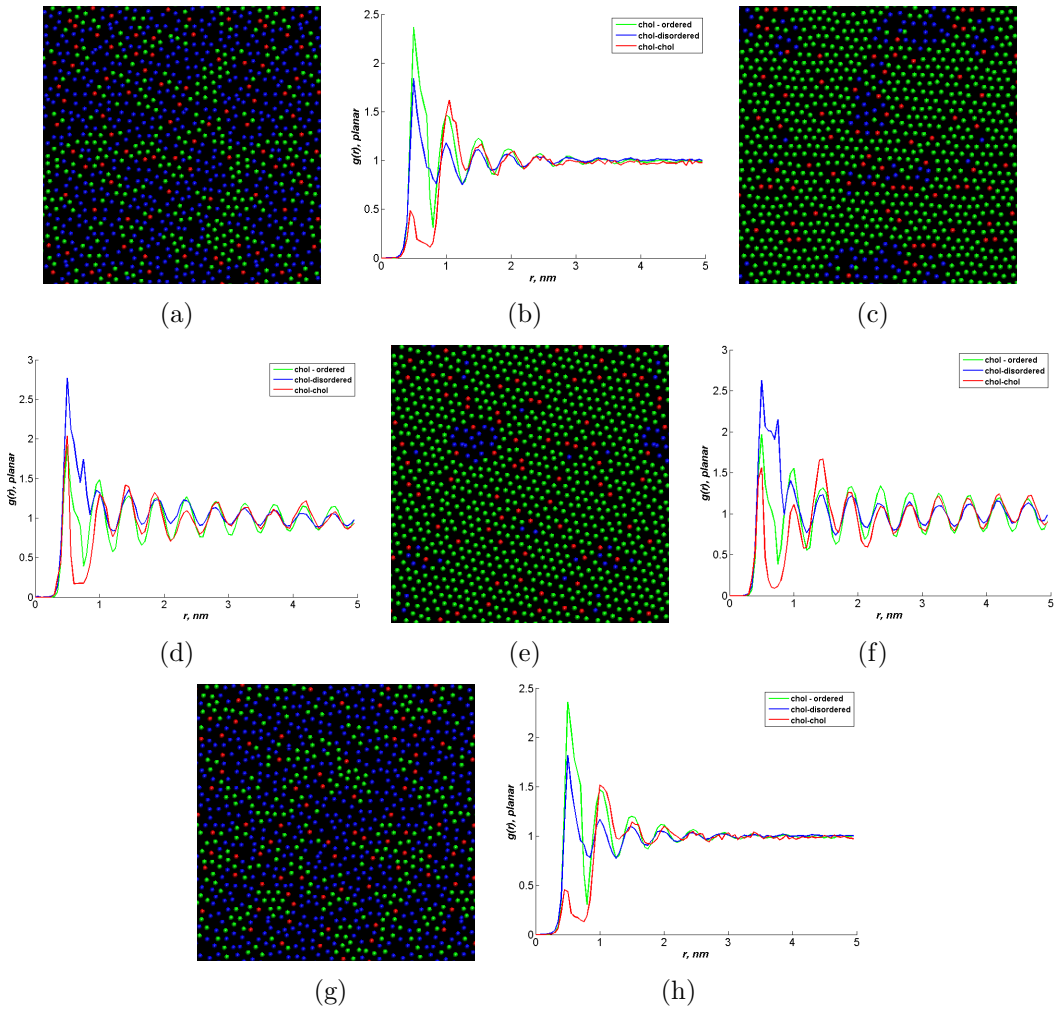

Figure 4.7: LC-LE phase transitions in DPPC monolayers containing cholesterol. An initially disordered monolayer (338K) is quenched to 323K (a and b) and 303K (c and d) . An initially ordered monolayer (288K) is heated to 303K (e and f) and 328K (g and h). In the snapshots (a,c,e,g) ordered sites are green, disordered sites are blue, and cholesterol is red. In the radial distribution functions (b,d,f,h) the cholesterol-ordered, cholesterol-disordered, and cholesterol-cholesterol distributions are shown in green, blue, and red, respectively.

4.3.3.2 Monolayers Containing POPC

The LC-LE phase transition was also studied for 1:1 DPPC:POPC monolayers. Each C2 site (from either DPPC or POPC) was included in the packing analysis. The 1:1 DPPC:POPC monolayers are quenched and heated from the disordered and ordered starting states to temperatures between 338K and 283K, in 5K intervals.

After the initially disordered monolayer is quenched from 338K to 293K (Figure 4.8(a)), the monolayer remains mostly disordered with small patches on LC phase. When the ordered monolayer is quenched further to 288K (Figure 4.8(b)), the monolayer orders and only a single patch of LE phase remains. The LC phase consists of both DPPC and POPC, in similar proportions. We do not observe substantial enrichment of either component in the LE (or conversely LC) phase. After the initially ordered monolayer is heated from 283K to 293K (Figure 4.8(c)), the monolayer remains mostly ordered there are still substantial patches of LE phase present. If the temperature is increased to 298K (Figure 4.8(d)), the monolayer disorders and only small patches of LC phase (containing both DPPC and POPC) remain.

From the snapshots in Figure 4.8 it is clear that the 1:1DPPC-POPC monolayers undergo the LC-LE phase transition at much lower temperatures than the pure DPPC monolayers, with the monolayer remaining disordered at temperatures as low as 293K. We did not observe any segregation of the DPPC and POPC within the LE phase. It appears that in monolayers of 1:1 DPPC:POPC there are too many POPC molecules spread evenly throughout the monolayer to allow the DPPC molecules to nucleate a condensed phase region at temperatures above the point where POPC is also able to form a condensed phase.

Within the LC phase some separation between the two components is evident, the saturated (green) and unsaturated (red) components cluster together, but do not completely demix (Figures 4.8(b) and 4.8(c)). In contrast the LE always remains well mixed (not shown). In Figure 4.8(e-g) RDFs are given for an initially ordered monolayer quenched to 283K (corresponding to the system shown in Figure 4.8(b)). The DPPC-DPPC (e), POPC-POPC (f), and DPPC-POPC (g) RDFs are presented. The height of the first peak is bigger in the DPPC-DPPC and POPC-POPC RDFs then in the DPPC-POPC RDF, indicating a closer association of DPPC and POPC with themselves than with each other. The RDFs are averaged over five time intervals:

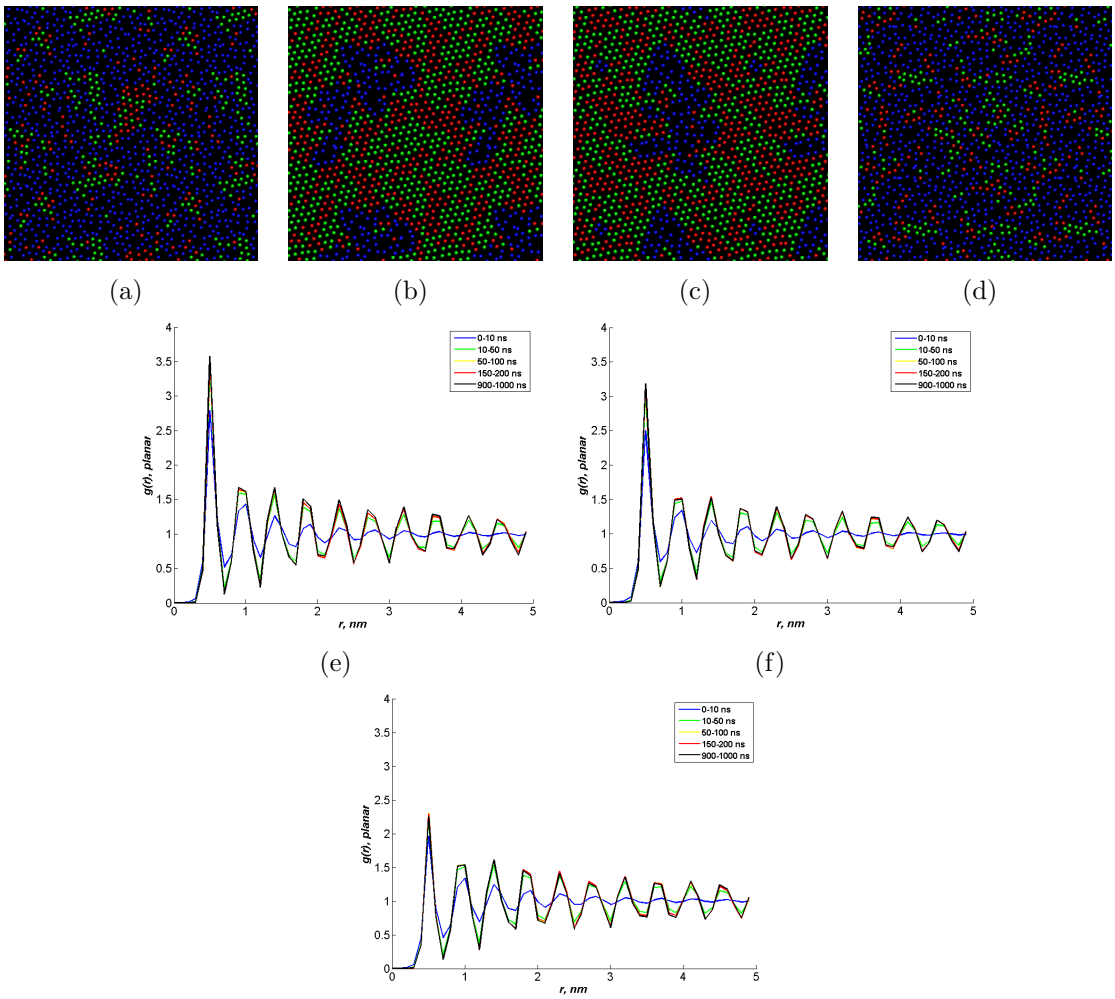

Figure 4.8: LC-LE phase transitions in 1:1 DPPC:POPC monolayers. An initially disordered monolayer (338K) is quenched to (a) 293K and (b) 283K. An initially ordered monolayer (283K) is heated to (c) 293K and (d) 298K. In the LC phase the C2 sites of DPPC molecules are shown in green, and the C2 sites of the POPC molecules are shown in red. The entire (both POPC and DPPC) LE phase is shown in blue. Radial distribution functions are also shown for DPPC-DPPC (e), POPC-POPC (f), and DPPC-POPC (g). The RDFs are averaged from 0-10ns (blue), 10-50ns (green), 50-100ns (yellow), 150-200ns (red), and 900-1000ns (black).

0-10ns (blue), 10-50ns (green), 50-100ns (yellow), 150-200ns (red), and 900-1000ns (black). In all of the RDFs, there is a clear increase in order and in the height of the first peak at later times compared to the first time interval (0-10ns). However, there is a negligible difference between the RDFs at later times. Therefore after the

first 10ns, the DPPC and POPC domains do not show significant coarsening over the length of the simulation.

A larger system size simulation containing 1024 lipids per monolayer was run at 283K to see if coarsening can be seen in segregated DPPC and POPC domains within the LC phase. However, after 1μs of simulation significant coarsening is not evident. Longer simulation times will be required to see if coarsening can be observed. However, once the condense phase forms the lipids are relatively immobile; it is therefore unclear if coarsening will be seen.

4.3.4 Hysteresis Loops

For each simulation, the percentage of hexagonal packing was averaged between 500ns and 1μs and graphed versus temperature in order to obtain hysteresis loops. The hysteresis loop obtained for the DPPC monolayer is compared to the hysteresis loops obtained for DPPC/cholesterol (a), DPPC/POPC (b), and DPPC/SP-B_{1-25} (c) monolayers.

In the pure DPPC monolayers we observe phase transitons between 303K and 323K. This range of temperatures, which agrees well with the experimental main phase transition temperature for DPPC bilayers of 314K [48]. In the pure DPPC monolayers the originally disordered system orders between 308-303K and the originally ordered system becomes disordered between 318-323K. This hysteresis is not surprising since the formation of liquid condensed domains is very similar to crystallization, and involves a nucleation process [7]. Furthermore the kinetics of the order-disorder phase transition are known to have strong dependence on cooling and heating rates. Marrink et al. also observed significant hysteresis between melting and freezing transition temperatures for coarse-grained DPPC bilayers [7]. They suggest that the condensed phase can remain stable well past its transition temperature due to kinetic trapping.

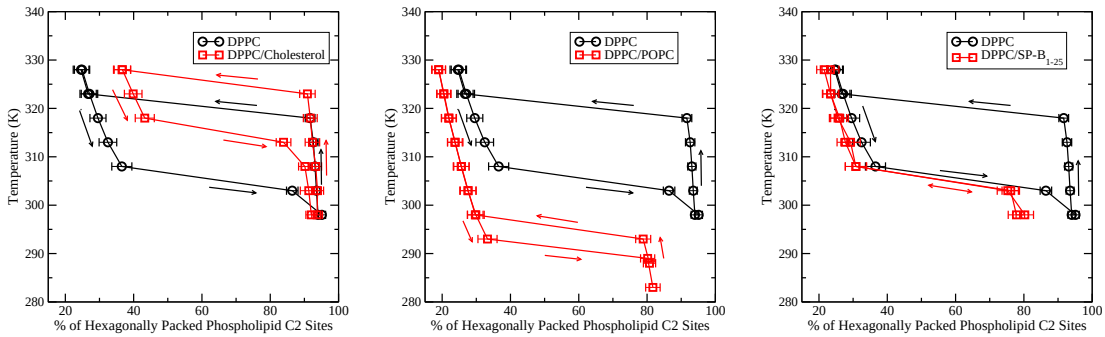

(a) (b) (c)

Figure 4.9: Hysteresis loops. Hysteresis loops showing the change in the percentage of hexagonally packed phospholipid C2 tail sites versus temperature for monolayers composed of DPPC (black circles) and monolayers composed binary mixtures of DPPC with another lipid or peptide component (red squares). The binary mixtures consist of: DPPC/cholesterol (a), DPPC/POPC (b), and DPPC/SP-B_{1-25} (c).The error bars shown represent the standard deviation in the percentage of hexagonal packing at each point.

In Figure 4.9(a) the disordered region of the hysteresis loop becomes more ordered upon the addition of cholesterol, leading to a shift in the disordered side of the hysteresis loop. This suggests that the DPPC-cholesterol mixture is displaying a phase of intermediate order, which could be the liquid-disordered (Ld) phase. There is no significant difference between the ordered side of the hysteresis loops for DPPC and DPPC/cholesterol. In addition, the hysteresis loop has shifted up slightly, suggesting that the addition of cholesterol has resulted in an increase in the transition temperature, and stabilization of the ordered phase.

In Figure 4.9(b) the addition of POPC to DPPC monolayers to create a randomly mixed 1:1 monolayer, leads to a substantial drop in the hysteresis loop to lower temperatures. This is to be expected, because unsaturated phospholipids have low transition temperatures in comparison to saturated phospholipids. The presence of POPC spread throughout the monolayer prohibits the DPPC condensed phase domains from nucleating at higher temperatures on the length and time scales of the simulations reported here. Also, once the ordered phase forms, there is a larger

amount of LE phase remaining in the 1:1 DPPC:POPC monolayers than in the pure DPPC monolayers as evident by the shift in the ordered side of the hysteresis loop to lower percentages of hexagonal packing. Yet, the disordered phase was not observed to be substantially enriched in either component.

From Figure 4.9(b), it is evident that the DPPC monolayers display a substantial amount of hysteresis, which is decreased by the addition of a second component. While the addition of cholesterol or POPC decreases the hysteresis loop, the addition of SP-B_{1-25} abolishes the hysteresis loop altogether. SP-B_{1-25} nucleates disorder causing the disappearance of the ordered side of the hysteresis loop (Figure 4.9(c)).

4.3.5 Nucleation and Growth and Fluctuations in Packing

The 1μs simulations of DPPC monolayers lead to a large amount of hysteresis, with the LC-LE phase transition occurring between 303K and 323K. To obtain a better approximation of the true transition temperature of our DPPC monolayers, several simulations were run where ordered and disordered monolayers were merged together as described in the discussion methods section. In short, two systems were constructed, Merge1 and Merge2. To attain the proper alignment between the ordered and disordered systems, the disordered monolayer was condensed by 0.7nm in the y-direction in Merge1 and in Merge2 the width of ordered box was increased by 0.7nm in the y-direction. The starting configuration for Merge2 is shown in Figure 4.10(a). The starting configuration for Merge1 (not shown) is visually similar to the configuration shown for Merge2. The extra space along the edge of the box in Merge2 leads to the disordering of the lipids along the edge of the box, which causes the size of the LC domain to shrink, (see Figure 4.10(b)).

The construction of Merge1 and Merge2 established two systems with a well-defined front between the ordered and disordered phases, making them ideal systems for the study of the nucleation and growth of LC phase and also the melting of the

LC phase. Our simulations show a nucleation and growth mechanism similar to that reported by Marrink and co-workers in their simulations of DPPC bilayers [7]. The LC phase domains are observed to fluctuate, shrinking and growing in size. At some point a critical nucleus is obtained and the ordered phase continues to spread. After the ordered phase propagates some disordered lipids become entrapped. Further ordering is slow and defects are long lived. Defect free monolayers are not observed over the coarse of our 1μs simulations.

For example, the simulation of Merge2 at 310K is shown in Figure 4.10 (a-f). Once the simulation is started, the size of the LC phase domain quickly shrinks (Figure 4.10(b)) due to disordering of the lipids along the edge of the box where extra space was introduced. The ordered phase then begins to re-grow, and after 40ns (Figure 4.10(d)) the ordered box has reordered and the ordered phase begins to spread into the initially disordered box. After 60ns (Figure 4.10(e)) the ordered phase has propagated across the entire box and an LE phase domain becomes entrapped. After 100ns (Figure 4.10(f)) of simulation a small LE phase domain is still entrapped within the condensed phase and additional defects are also present in the LC phase packing.

Simulations were also run at 308K, 313K, and 318K for both Merge1 and Merge2 monolayers and at 315K for Merge1 monolayers. At 308K the monolayers in both Merge1 and Merge2 order, at 318K the monolayers in both Merge1 and Merge2 disorder, and at 313K the monolayers in Merge1 order but the monolayers in Merge2 disorder. The fact that Merge1 orders at 313K and Merge2 does not suggests that the critical nucleus is attained in Merge1 and not in Merge2. The disruption of the packing along the edge of the box in Merge2 likely causes the LC domain size to shrink below the critical nucleus size.

At 315K the ordered region of Merge1 began to grow into the disordered box (Figure 4.10(g)), but then shifted so that roughly half of the disordered box became

ordered and roughly half of the ordered box disordered (Figure 4.10(h)). Packing fluctuations were evident, but the relative amount of LE and LC phase did not change significantly for the remainder of the simulation (Figure 4.10(i)) suggesting that the coexistence of the condensed and expanded phase is stable on the time-scale of this simulation. These results suggest that the true transition temperature lies between 310K and 318K. Furthermore, the behavior observed at 313K and 315K suggests that these simulations are in close proximity to the actual transition temperature.

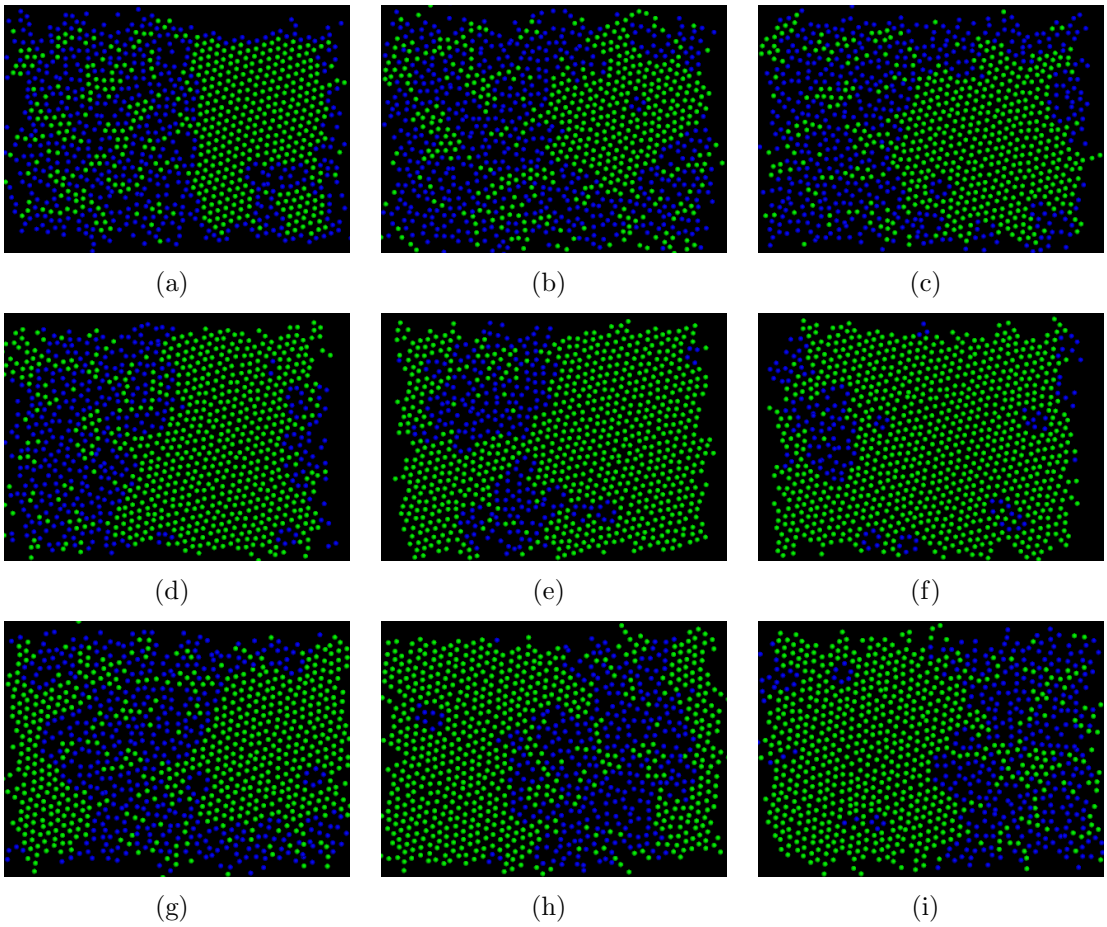

Figure 4.10: Nucleation and growth of the LC phase. The C2 tail beads of the ordered lipids are shown in green and the C2 tail beads of the disordered lipids are shown in blue. The starting configuration for Merge2 simulations is shown (a). Snapshots from the simulation of Merge2 at 310K are shown after 0ns (a), 2ns (b), 20ns (c), 40ns (d), 60ns (e), and 100ns (f) of simulation time. Snapshots from the simulation of Merge1 at 315K are shown after 14ns (g), 60ns (h), and 100ns (i) of simulation time.

In the reverse process disorder originates from a defect in the monolayer such as a disordered patch of lipids around a peptide or near the edge of the box, where extra space was inserted into Merge2. The LE phase grows at the cost of the LC phase domain, which shrinks and eventually disappears. As shown in Figure 4.9(c), the SP-B_{1-25} molecules are observed to nucleate disorder in the monolayer leading to the collapse of the hysteresis onto the disordered side of the hysteresis loop. This behavior may result from the high concentration of SP-B_{1-25} in our simulations, which could prevent the formation of a critical nucleus.

To quantify the persistent changes in packing caused by instantaneous domain patterns, we graphed the percentage of hexagonally packed sites versus simulation time (Figure 4.11). Both the top (red) and bottom (black) monolayers are shown. The fluctuations in hexagonal packing typically fall in the range of ±2-5%. The error bars reported in Figure 4.9 give the standard deviation in the percentage of hexagonal packing for DPPC, DPPC/cholesterol, DPPC/POPC, and DPPC/SP-B_{1-25} monolayers. These error bars thus reflect the magnitude of the fluctuations. From the size of the error bars and from Figure 4.11 it is apparent that the fluctuations are a little bit larger in the disordered monolayers than in the ordered monolayers. Also, the fluctuations seen in the monolayers of pure DPPC do not differ greatly from those seen in monolayers composed of DPPC with cholesterol, POPC, or SP-B_{1-25}. However, the addition of a second component does result in slightly larger fluctuations in the LC phase monolayers. The magnitude of the fluctuations also increases slightly as the temperatures approach the transition temperature on either side of the hysteresis loop.

In most of our simulations, phase transitions occur within the first 500ns of simulation. However, the monolayers are meta-stable, and long simulation times increase the probability of the development of a critical nucleus. Therefore, the size of the hysteresis loop is a function of simulation time. For DPPC monolayers at 323K the

transition from LC to LE phase occurs after 700ns of simulation time, as shown in Figure 4.11. Both the top and bottom monolayers undergo the transition at the same time.

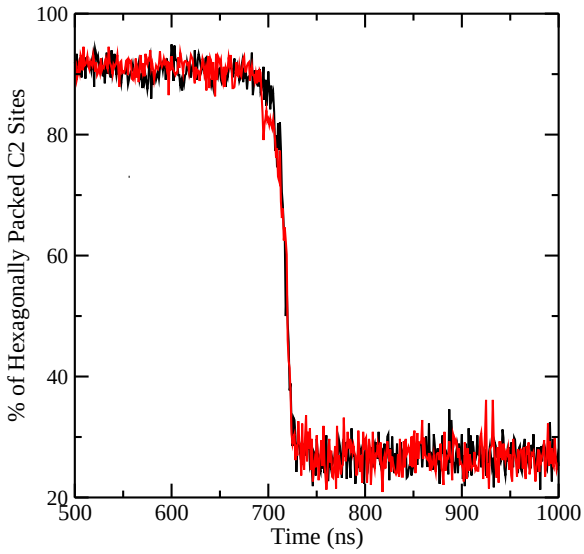

Figure 4.11: Packing fluctuations. Characteristic packing fluctuations are shown here for pure DPPC monolayers heated from an initially ordered state (283K) to 323K. Both the top (red) and bottom (black) monolayers are shown. The fluctuations shown here are similar to those seen in all of our simulations, which vary slightly in magnitude. Most of our simulations, which are observed to undergo a phase transition, undergo the transition before 500ns of simulation time. However, phase transitions can occur at later times as shown here.

The fluctuations observed in our simulations are analogous to hetero-phase fluctuations in lipid bilayers near the main transition temperature, which are discussed elsewhere [7]. Using multi-state computer models, Mouritsen et al. [5, 240] found that thermally induced density fluctuations led to inhomogeneous micro-states and instantaneous lipid domain patterns in monolayers. Mouritsen et al. [240] attribute the slow relaxation process to stabilization of the domain interfaces by intermediate conformational states, which lower the interfacial tension, analogous to softening observed in lipid bilayers.

4.3.6 System Size Effects and Simulation Time

As discussed in chapters 1 and 2, system size and simulation time artifacts should be carefully considered. This is especially true when phase transitions are involved. Simulating a biphasic system raises additional concerns about artifacts. When the box is split between phases each domain is further limited in size. Also short simulation time-scales will be associated with kinetic effects. Kinetic effects are also present in experiment (although to a lesser degree) as discussed in chapter 1 and the appendix. When simulating dynamic events the results are subject to kinetic factors. It is unclear what effect system size and simulation time may have on the evolution of the phase distribution. For instance, given long enough simulation times domain coarsening may occur with in LC phase of the CG 1:1 DPPC:POPC monolayer. Hysteresis is expected to decrease substantially given much longer simulation times or a much larger system size. Previous CG-MD simulations of the gel to liquid-crystalline phase transitions in DPPC bilayers have shown that the hysteresis observed in the freezing and melting transitions depends on both system size and time-scale [7]. In chapter 1, we have shown that increasing the system size decreases the hysteresis loop slightly. Furthermore, a comparison of hysteresis loops obtained from 1μs and 100ns simulations of DPPC monolayers reveal a substantial change in the amount of hysteresis.

The system size and time scales required to attain an equilibrium distribution of LC and LE phase are much larger than that currently accessible by molecular simulation. Although CG simulation is still limited by system size and simulation time effects, it allows observation of dynamic phase transitions on time and length scales not accessible by atomistic simulation.

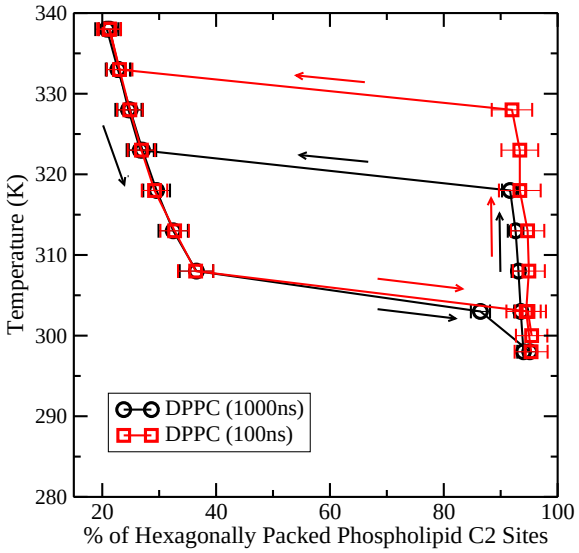

Figure 4.12: Longer simulation times lead to decreased hysteresis in pure DPPC monolayers.

4.4 Summary

Using the MARTINI model, we were able to successfully simulate LC-LE phase transitions in monolayers containing DPPC and additional lipid or peptide components. Our analysis of DPPC monolayers suggests that the LC phase forms via a nucleation and growth mechanism analogous to that observed in lipid bilayers. In the reverse process, the melting of the LC phase is observed to originate at defects in the monolayer. In addition, our snapshots of the phase distributions, hysteresis loops, and radial distribution functions have lead to a number of interesting observations about the phase behavior of binary mixtures containing DPPC. Both POPC and SP-B_{1-25} are found to fluidize the monolayer. In correlation with experiment observations SP-B_{1-25} is found to reside in the LE phase of the monolayer. SP-B_{1-25} is also observed to perturb the packing of the surrounding lipids leading to local fluidization of the monolayer. The presence of POPC spread throughout the monolayer prohibits the DPPC condensed phase domains from nucleating at higher temperatures. At low temperatures both POPC and DPPC condense. The segrega-

tion of the two lipids is observed in the condensed phase, but not in the expanded phase. The DPPC-cholesterol monolayers are found to displaying a phase of intermediate order, which could be the liquid-disordered (Ld) phase. The hysteresis loop for DPPC-cholesterol monolayers is shifted up slightly compared to the hysteresis loop for pure DPPC, suggesting that the addition of cholesterol has resulted in an increase in the transition temperature and stabilization of the condensed phase. Cholesterol is also observed to show a preference for the interface between the ordered and disordered lipids, in agreement with experimental observations. It is evident that DPPC displays a substantial amount of hysteresis, which is decreased by the addition of a second component. While the addition of cholesterol or POPC decreases the hysteresis loop, the addition of SP-B_{1-25} abolishes the hysteresis loop altogether. SP-B_{1-25} nucleates disorder causing the disappearance of the ordered side of the hysteresis loop. These results suggest that the presence of impurities in the monolayer (such as SP-B_{1-25}) may prevent the formation of a critical nucleus. These results illustrate that coarse-grained molecular dynamics simulation is a powerful tool for making qualitative observations of the dynamic phase behavior of lipid and lipid-peptide monolayers on a length-scales not accessible by experimental methods or atomistic simulation.

CHAPTER V

Summary and Future Work

In this doctoral work we have applied CG-MD simulation to the study of model lung surfactant mixtures consisting of DPPC and other lipid and peptide components. We utilize the MARTINI coarse-grained force field to simulate monolayers containing pure dipalmitoylphosphatidylcholine (DPPC) and DPPC mixed with palmitoyloleoylphosphatidylglycerol (POPG), palmitoyloleoylphosphatidylcholine (POPC) palmitic acid (PA), cholesterol, or peptides. The peptides considered include the 25-residue N-terminal fragment of SP-B (SP-B_{1-25}), SP-C, and several SP-B_{1-25} mutants.

The study of experimental and simulated pure DPPC pressure-area isotherms revealed a large amount of variability between experimental isotherms, and a reasonable reproduction of basic features of experimental isotherms by molecular dynamics simulation. Both coarse grained (CG) and an atomistic models yield results that are in rough agreement with some of the experimental isotherms, but with a steeper slope in the liquid-condensed (LC) region than seen experimentally and shifted to larger areas. The use of the MARTINI CG lipid model leads to a great increase in computational efficency and predicts pressure-area isotherm that are impressively close to those of atomistic simulations. There is much more variation among experimental isotherms than between isotherms obtained from CG simulations and from

the most refined simulation available. Both atomistic and CG simulations yield LC and liquid-expanded (LE) phase area compressibility moduli that are significantly larger than those typically measured experimentally, but compare well with some experimental values obtained under rapid compression. We find that the dynamic area compressibility modulus increases as the compression rate increases. PO4-PO4, PO4-NC3, and NC3-NC3 radial distribution functions (RDFs) show little difference between the LC and LE phases, while C2-C2 distributions show a significant decrease in tail order as the monolayer is expanded, indicating that the structure of the DPPC headgroups is affected much less by the phase transition than is the structure of the DPPC tails. Furthermore, P-N tilt angle distributions obtained from our atomistic and coarse grained simulations give an average P-N orientation that is parallel to the interface and is not significantly affected by the LC-LE phase transition. In accord with experimental observations, this provides further evidence that the DPPC headgroup region is not strongly affected by the transition from LC to LE phase.

To explore the role of lung surfactant proteins SP-B and SP-C in storing and redelivering lipid from lipid monolayers during the compression and re-expansion occurring in lungs during breathing, we simulated the folding of lipid monolayers with and without these proteins. We have identified two mechanisms by which monolayer folding can occur, namely (1) through the growth of undulations and (2) by nucleation around a defect. The first mechanism is observed in monolayers containing either POPG or peptides, while the second mechanism is observed only with peptides present, and involves the lipid-mediated aggregation of the peptides into a defect, from which the fold can nucleate. The occurrence of folding depends on monolayer fluidity and can be correlated directly with the carbon deuterium order parameter of the lipid tails. We find in our simulations, under small negative surface tension, that folding occurs when the average order parameter is less than 0.331. Unsaturated phospholipids (POPG) and surfactant proteins (SP-B and SP-C) fluidize the mono-

layer, while palmitic acid (PA) displays a charge-dependent condensing affect. The extent to which the peptides fluidize the monolayer, and thus enable folding, depends on the hydrophobic character of the peptides. The peptides appear to provide a larger driving force for folding than does POPG, allowing fold formation to occur for peptide containing monolayers under conditions for which it does not occur in the presence of POPG alone. In addition, the formation of a lipid bridge by peptide-mediated fusion and the ensuing redistribution between monolayers upon re-expansion demonstrate the fusogenic abilities of the peptides and their role in surface refining.

To explore the effects of lipid on protein components on the phase behavior of the monolayer (and thus the mechanical properties of the monolayer) we obtained hysteresis loops for monolayers composed of DPPC, DPPC/POPC, DPPC/Cholesterol, and DPPC/SP-B_{1-25}. The study of LC-LE phase transitions revealed that POPC significantly lowers the phase transition temperature. At low temperatures, 1:1 DPPC:POPC are observed to form a LC phase containing segregated domains of DPPC and POPC. However, segregation of the two components is not observed in the LE phase, which prevents the formation of LC phase domains at temperatures at or above 298K, well below the hysteresis loop (303K-323K) of our simulated DPPC monolayers. Cholesterol packs at the interface between ordered and disordered lipids and has an ordering effect on the disordered side of the hysteresis loop leading to a region of intermediate order. These observations are in agreement with experimental observations and theories regarding the phase behavior of multicomponent lipid mixtures. Unsaturated lipids such as POPC are known to have a lower transition temperature than saturated lipids such as DPPC. The addition of cholesterol to phospholipid monolayers has been proposed to lead to the formation of intermediate liquid ordered (Lo) and liquid disordered (Ld) phases. We also find that SP-B_{1-25} nucleates disorder in the monolayer leading to the disappearance of the ordered side of the hysteresis loop. This observation suggests that this peptide could act as a de-

fect in the monolayer overcoming kinetic barriers to phase and structural transitions. The formation of the LC phase was observed to occur by a nucleation and growth mechanism similar to that reported for phospholipid bilayers. The addition of SP-B_{1-25} to the monolayer could prevent the development of a critical nucleus leading to the disappearance of the ordered side of the hysteresis loop.

This work also illustrates some of the limitations associated with use of the MARTINI coarse-grained model to simulate phopholipid membranes. Although in general the MARTINI model does do an excellent job of reproducing the behavior of the molecules, it is not able to capture some details due to its coarse-grained nature. For instance some of the changes apparent in atomistic RDF functions, are not apparent in the CG counterparts. Furthermore, the MARTINI model allows long simulation times and larger system sizes to be obtained, but is still subject to system size and simulation time artifacts. For instance, values of area compressibility modulus obtained for both coarse grained and atomistic simulations overestimate those typically obtained from experiments, although the disagreement diminishes somewhat as simulation box size increases. Thus, it is conceivable that a simulation of a macroscopic system size could produce moduli within the range of typical experimental values. Furthermore, experimental isotherms tend to show higher moduli when obtained by more rapid compression, which might also help explain the relatively high moduli obtained from simulations, which are obtained under very rapid compressions compared to typical experiments. We also find that although CG and atomistic isotherms for DPPC agree very well with one another, both are shifted to higher areas/lipid than experimental ones and do not exhibit the correct shape.

Despite limitations, the MARTINI coarse-grained model can be used to answer a number of physiologically relevant questions about the behavior of lipid and lipid/peptide membranes. Simple coarse grained models, such as the MARTINI model, are powerful tools for studying such systems, on length and time scales that are difficult or

impossible to obtain using atomistic simulation. CG simulation is a valuable tool for studying the structural transitions of lipid/peptide films and can be used to identify pertinent interactions that may act as driving forces for these transitions. Our results show that the MARTINI model can capture qualitatively the effects of lipid and protein components on the fluidity and collapse behavior of the monolayer in good agreement with experimental observations. Additionally, the phase behavior observed in binary mixtures of DPPC with additional lipid and peptide components is in qualitative agreement with experimental observations and theoretical predictions. Using the MARTINI model, we were also able to quickly obtain compression and expansion isotherms for DPPC at five different temperatures and visualize the changes in packing from hexagonal to disordered as the DPPC monolayer underwent a phase change from the liquid-condensed (LC) to the liquid-expanded (LE) state. These fast and simple simulations provide a tool that can be used in conjunction with experimental observations, in order to better understand the complex mechanisms involved in lung surfactant function and other biological phenomena occurring at the membrane level.

There is a lot more that can be done to study the phase behavior of model lung surfactant mixtures. A few consideration should be taken into account in the design of future simulations. First, the model used in the current work does not account for the tilt seen in the phospholipid tails in the tilted condensed (TC) phase. Since, DPPC is observed to form the TC phase, a through analysis of the phase behavior of this system should also consider lipid tail tilt. By altering the relative head to tail group bead size, the tilted phase of DPPC can be simulated. Therefore, simulations containing this modified CG model of DPPC could address TC-LE phase behavior in mixed lipid and lipid-protein monolayers. Furthermore, as computational power increases, the simulation of larger systems becomes more cost effective. Future work should focus on larger system sizes, to reduce the system size effects. Biphasic systems are especially prone to system size artifacts. Therefore, additional measures to assess the

limitations of our CG simulations, would also add value. For example, the calculation of line tension between the LC and LE phases would help to assess the finite size effects in biphasic systems. Also, the hysteresis loops reported here show changes in packing with respect to temperature. Hysteresis loops could also be obtained with respect to pressure, which would allow more direct comparison with experimental pressure-area isotherms. Keeping this in mind, there are few particularly interesting ideas that could be addressed.

The study of ternary mixtures containing peptides is of great interest since the full functionality of lipid and fatty acid components is not realized in the absence of LS proteins, and surfactant proteins are thought to interact selectively with some lipid components. For example, electrostatic interactions between SP-B/C and anionic lipids have been suggested to dominate the association of the peptides with the lipid monolayer [241]. The effect of SP-B on phospholipids films is also more pronounced in films containing DPPG than those of pure DPPC [209]. Several experimental papers including [48] suggest that SP-B interacts preferentially with anionic phospholipids leading to the higher localized concentrations of anionic phospholipids. This has substantial consequences for monolayer collapse and the preferential interaction between SP-B and anionic phospholipids is commonly used as an argument in support of squeeze-out theory, which suggests that at high surface pressures the surface film becomes enriched in DPPC by the selective squeeze-out of other components, such as anionic phospholipids. Therefore, the simulation of anionic phospholipid/DPPC/SP-B monolayers is of particular interest. Preliminary simulations of CG DPPC/DPPG mixed monolayers containing SP-B_{1-25} accurately show stronger interaction between SP-B_{1-25} and the head groups of DPPG over those of DPPC (unpublished work). Several experimental studies including [177] have shown that the addition of calcium to the subphase, leads to electrostatic interactions, which support the phase segregation of acidic lipids. One might consider adding cations such as calcium to the

subphase in mixed lipid simulations containing neutral and anionic lipids, to promote phase separation between each component. Additionally, the study of phase behavior in tertiary mixtures containing SP-C would provide an interesting contrast to mixtures containing SP-B, and could offer some insight into the specific roles of each peptide.

Another component of particular interest is PA. Although, PA is not a significant fraction of natural lung surfactant and is commonly added to lung surfactant replacements to enhance stability. Palmitic acid and DPPC form stable crystalline monolayer phases a lower temperatures than pure DPPC monolayers [176]. Additionally, mixtures of SP-B and PA display interesting phase behavior. A low line tension between fluid and condensed phases in PA/SP-B mixtures results in the formation of stripe phases. The formation of stripe phases is suspected to involve protein conformational changes induced by pressure and lipid environment [158].

The concentration dependence of the phase behavior should be tested. For example, our 1:1 DPPC:POPC monolayers do not show the independent nucleation of DPPC LC domains, however such behavior is conceivable for lower concentrations of POPC. Binary mixtures containing cholesterol are also known to display concentration dependent phase behavior. Additionally, our simulations suggest that peptide may preventing the formation of the critical nucleus. Therefore, it would be interesting to see if a critical nucleus can form at lower peptide concentrations. Furthermore, a more detailed study of the nucleation and growth of the condensed phase would be of great value. In particular the temperature dependence of the critical nucleus can be examined to determine the line tension, as done previously for CG DPPC bilayers [7].

Packing analysis and visual observation of mixed lipid and lipid/peptide monolayers provide great qualitative insight, however additional modes of comparison add value to the study of the component effects in the LC-LE coexistence region. For in-

stance, SP-B and SP-C have also been found to reduce the mobility of phospholipids chains especially in the fluid phase [156]. Measurements of lateral mobility could show whether CG simulations reproduce this experimental trend. Measurements of viscosity could also provide further insight. Alonso et al. [176] discuss the calculation of critical solid phase fraction (A_c). The critical solid phase fraction is the fraction of condensed domains at which solid domains jam into each other and viscosity diverges. Near A_c small changes in fluid/solid ratio can lead to large changes in viscosity [176]. It is unclear of such a critical solid phase fractions can be identified through CG-MD simulations, especially because of kinetic artifacts attributed largely to system size limitations.

In addition to the above-mentioned ideas for further study of phase behavior, collapse transitions are compelling and remain ill understood. Further work in the simulation of these transitions could provide better insight into the mechanics of these transitions. Collapse transitions are a multi-scale phenomena, and therefore a multi-scale simulation approach would be ideal. Our work on the study of collapse transitions has been largely qualitative. A look at more of the nitty-gritty details involved would certainly add depth. For example, radial distribution functions could reveal favored associations between lipid and peptide components and between the peptides themselves, during the folding process.

APPENDIX

APPENDIX A

A Review of the Factors Leading to Variability Among Experimental Pressure-Area Isotherms.

A.1 Overview

It is evident that the phase behavior of DPPC (dipalmitoylphoshatidylcholine) is a complex matter that is not well understood and that, furthermore, interpretations of phase behavior drawn from the features of experimental isotherms vary and sometimes contradict each other. This illustrates the need for a better understanding of the factors affecting the shape of experimental isotherms. Trends in the pressure-area isotherms caused by compression rate, pH, ionic strength, spreading solvent, and geometry and type of apparatus are addressed in some detail below. First, however, a discussion of monolayer collapse is presented.

A.1.1 Monolayer Collapse

DPPC isotherms compressed to high dynamic surface pressure, but not to the point of collapse, exhibit a small degree of hysteresis, with a slight increase in hysteresis occurring with an increase in maximum surface pressure [96, 242]. This hysteresis can be attributed to a relaxation process associated with surface rearrangement and possibly partial ejection of DPPC from the monolayer. On the other hand, DPPC

isotherms compressed past collapse exhibit much greater hysteresis due to the poor respreadibility of DPPC [96, 133, 242]. The irreversible loss of material from the surface film causes subsequent isotherms to be displaced to the left (lower areas) due to substantial material loss upon collapse, with DPPC respreading more poorly at body temp (310.15K) than at room temp (296.15K) [243]. Gladston and Shah [133] observed an increase in hysteresis for DPPC monolayers compressed beyond their limiting area, due to material loss from the film and possible entrance of the subphase solution into gaps in the monolayer left by the ejection of lipids into the collapse phase. Taneva and Keough [242] found that films spread from low initial concentrations exhibited a greater degree of respreadibilty than those spread from surface excess conditions. The reason for this is unknown; however they have proposed that the different initial conditions could result in differences in the three dimensional collapse phase structures.

X-ray diffraction studies have indicated that in a crystalline state 18.5Å^2 is the minimum area that a single palmitoyl tail can occupy, giving a limiting area of 37Å^2/molecule for the two-tailed DPPC lipid [244]. However, the limiting area of a monolayer film is expected to be larger than that of the crystalline state [245], and the results of Hauser [89] suggest a limiting area of 39Å^2/molecule. Furthermore, the space required by the head group of phosphatidylcholine (50Å^2) is substantially larger than that required by the acyl chains [86] so that in the lamellar gel phase, the chains tilt to accommodate the larger head group area and in crystals the headgroups are displaced in an overlapping fashion to accommodate even lower areas [86, 89].

According to Keough [246] in DPPC monolayers no solid states can be formed above the main transition temperature for DPPC bilayers (314.15-315.15K). Monolayers below this temperature can be compressed into meta-stable high-pressure states. However, for monolayers above this temperature the highest surface pressure that can be reached is around 60mN/m. Therefore the main phase transition temperature for

the bilayer is taken to be the critical temperature above which no solid state can be formed [247].

In their x-ray diffraction and fluorescence microscopy study, Kjaer et al. [248] report decoupling of translational and orientational ordering in phospholipid monolayers, and the appearance of a kink in the isotherm, representing the transition from the liquid-condensed phase to the solid phase. Watkins [119] observed an inflection point at around 46Å^2/molecule in the pressure-area isotherm of DPPC at 298.15K. They suggested that this inflection point corresponds to a conformational change of the polar head group from a co-planer form to a fully extended co-axial form, which is neutralized by the penetration of subphase counter-ions (Na+ and Cl-) into the zwitterionic head group region. In contrast, many other authors interpret the observed inflection at high surface pressures not as a phase transition from a condensed to a solid phase, but as the onset of partial film collapse [111, 115, 133, 236, 249]. Using a Wilhelmy surface balance, Gladston and Shah [133] obtained an isotherm with an inflection point at 44mN/m, with a corresponding area of 42.5Å^2/molecule. They suggest that the inflection point represents the point of monomolecular collapse, and that DPPC films compressed past surface pressures of 44mN/m have been compressed beyond their limiting area, and are therefore not monomolecular. Instead these films are unstable and collapsing, with some molecules displaced from the surface film.

Clements and Tierney [250] observed a small collapse area, with a collapse plateau at 65mN/m and 35 Å^2/molecule. They observed no inflection point, and the plateau at 65mN/m was considered the true point of collapse. In addition to the inflection point at 44mN/m, Gladston and Shah [133] observed a plateau at 67mN/m and 30Å^2/molecule. They suggested that such a small area indicates that DPPC films cant be monomolecular at high surface pressures. However, the minimum areas, before a collapse plateau, of most dynamic DPPC isotherms are greater than limiting molecular area of DPPC, suggesting that the meta-stable high-pressure states are in fact

monomolecular. The findings of Gladston and Shah [133] and of Clements and Tierney [250] are open to question, because they reported minimum areas of 30Å^2/molecule and 35Å^2/molecule, respectively, which are lower than the crystallographic areas. Such small areas could be experimental artifacts caused by film leakage, which could lead to misinterpretation of the actual point of collapse and the film stability.

The results of Wüstneck et al. [121] also exhibit a collapse plateau at areas significantly less than the limiting geometrical surface area of the alkyl chains. They suggest that in order to reach the highest surface pressure (near-zero surface tension), the monolayer undergoes over-compression (area $<$ limiting area). They propose that under normal collapse the surface pressure remains constant; however under over-compression a drastic change in slope is not observed, but instead the monolayer undergoes rearrangement that starts before the limiting area is reached, with part of the monolayer remaining intact. The structures formed under over-compression are thought to be complex and are not well characterized. Wüstneck et al. [121] propose monolayer folding as a possible mechanism of over-compression, and also propose monolayer folding as the precursor to the formation of lamellar bodies. In contrast to collapsed domains, folding could lead to gradual changes in surface pressure, and thus explain the absence of a horizontal collapse plateau upon over-compression. Wüstneck et al. [121] further suggest that over-compressed monolayers can also be further compressed to the point of full collapse, leading some monolayer folds to pinch off and form lamellar structures. Wüstneck et al. [121] also suggest that a clicking sound reported by several authors using the captive bubble apparatus could be explained by a sudden folding and refolding of the lipid layer leading to an abrupt change in surface pressure. Keough [246] has also referred to high-pressure DPPC states as over-compressed, and attributed the ability of DPPC films to reach near-zero surface tension to the existence of such states.

A.2 Kinetics

Domain formation is a kinetic nucleation process and therefore the domain density and size, and thus the shape of the pressure-area isotherm, depend not only on temperature but also on the rate of compression and expansion [251]. The LC-LE (liquid-condensed/liquid-expanded) phase transition is believed to be pseudo-critical and long-lived due to the kinetic stabilization of domain interfaces by intermediate conformational states at domain boundaries. These intermediate states lower interfacial tension. The consequence of this softening is an apparent continuous phase transition [240], in which ordering appears as a continuous process with decreasing temperature and increasing domain size [252]. Using multi-state computer models, Mouritsen et al. [240] found that thermally induced density fluctuations led to inhomogeneous microstates and instantaneous lipid domain patterns in monolayers. These domain patterns are subject to persistent changes in size and distribution [5, 240]. Fluctuation effects at the phase transition have not fully been explored theoretically or experimentally [44]. There are varying explanations for these effects. Using Brewster Angle Microscopy to visualize DPPC monolayers, Li et al. [109] have found that domain structure depends significantly on compression rate. Using fluorescence microscopy, Klopfer and Vanderlick [120] and Nag et al. [99] have shown that domain shape and size distribution varies with the rate of monolayer compression. The average domain size displays a clear time dependency, although the total amount of solid and fluid lipid remains essentially constant [99].

DPPC is responsible for the ability of lung surfactant to reach near zero surface tensions during dynamic cycling of interfacial area [96]. The rigidity of DPPC enables the monolayer to compress to very low surface tensions ($<$1mN/m) in the lungs. This rigidity also results in long relaxation times and a significant reduction of the physiological surface tension, relative to the equilibrium value [111]. Equilibrium pressure-area studies do not have direct physiological relevance, because respiration

is dynamic, but equilibrium properties do allow the effects of individual components of a surfactant mixture to be compared in a well-defined way [59]. In addition, some conventional methods of isotherm measurement, such as those using a Langmuir trough, have difficulty measuring dynamic isotherms accurately, leading early studies to focus on quasi-static isotherms [97].

Many studies have evaluated the surface pressure relaxation rates of DPPC monolayers [98, 107, 108, 115, 119, 236, 243, 247, 249, 253–257]. Several experiments performed by Notter, Tabak and others, using a modified Wilhelmy balance, with a ribbon barrier to eliminate film leakage, show large differences between dynamic and equilibrium surface pressures as well as long relaxation times [98, 107, 108, 243, 257]. Tabak et al. [98] measured the time required for the dynamic pressure-area isotherm to relax to the static surface pressures found from equilibrium spreading in a beaker. They found that at 68, 49, 44, and 40Å^2/molecule, relaxation took 50s, 100s, 300s, and 850s respectively. At areas lower than 40Å^2/molecule (post-collapse) only a few mN/m of pressure relaxation were observed after 12,000s. Other studies have also shown similar differences between dynamic and equilibrium surface pressures and similar relaxation times [107, 243]. Watkins [119] also observed very slow relaxation rates, with a rate of change of only 0.1-0.3 mN/m/h, at a maximum surface pressure of 71mN/m. Schürch et al. [108] found that the extent of monolayer metastability at low surface tensions was dependent on the compression-expansion history and initial surface tension, with increasing stability for surface tensions further from equilibrium. In contrast to results mentioned above, which found moderately long relaxation times for DPPC films compressed to large surface pressures (70-72mN/m), Cruz et al. [236] found the attainment of an equilibrium value within only 15min. Cruz et al. suggest this difference in relaxation time could be attributed to differences in compression rates, extent of compression, or experimental apparatus.

There are varying explanations for the large relaxation times observed at near-zero

surface tensions (large surface pressures). Film relaxation could involve reorganization in two dimensions, or more likely, the formation of a three-dimensional collapse phase [246]. According to Tabak et al. [98], relatively small pre-collapse relaxation times are likely associated with the rearrangement of molecular structure and orientation inside the monolayer, whereas large post-collapse relaxation times can be attributed to either the inhibited ejection of molecules from the monolayer due to the crowded multilayer structure or the gradual recruitment of molecules from the collapsed multilayered reservoir structure. After collapse, molecular movement is constrained between the collapse phase and the remaining monolayer, leading to poor respreading and very long post-collapse relaxation times [59, 243]. Despite uncertainty over the exact mechanism, these results show that formation of multilayers imparts even greater film stability as evident from the large increase in post-collapse relaxation times [98]. In contrast to the inferences of Tabak et al. [98], Goerke and Gonzales [115] suggest that the monolayer collapse rate is dependent on the physical state of the monolayer, and a small kink present in the DPPC pressure-area isotherm that they observed at around 12mN/m indicates a phase transition, which would cause an increase in compressibility thereby facilitating more rapid monolayer collapse. Goerke and Gonzales [115] also found the collapse rate to be dependent on temperature, with collapse rates becoming much faster at temperatures above the bulk lipid-water phase transition temperature of 314.55K.

Using the pendant drop technique and a Langmuir trough Wüstneck et al. [247] performed relaxation experiments on DPPC monolayers. They argue that that the irregular relaxation curves obtained in their experiments at 293.15K for pressures >25mN/m result from the formation of rupturing, brittle structures in DPPC monolayers at surface pressures greater than 25mN/m DPPC. However, at higher temperatures the monolayer appeared to be more fluid. According to Wüstneck et al. [247], the observed long time dependence of the surface pressure is likely the result of a

molecular rearrangement process that begins in the LC-LE coexistence region of the isotherm, well below the equilibrium spreading pressure. Wüstneck et al. [247] also suggest that the irregular relaxation of the DPPC isotherm at 293.15K involves both a short (50-100ns) and a long (>2h) relaxation process. Furthermore, Wüstneck et al. [247] suggest that experiments that were not carried out slowly enough to encompass this longer relaxation time might have led other authors to observe the absence of a pronounced LC-LE coexistence plateau and also to conclude that isotherms are independent of compression rate.

Bangham et al. [178, 180] and Gaines [258] have suggested that the force at the interface is comprised of both thermodynamic and kinetic components. In order to remain stable, the surface tension at the alveolar air-water interface must be able not only to reach low surface tensions, but also to maintain them for a sufficiently long time at fixed lung volume [259]. Using a Langmuir-Wilhelmy surface balance at 310.15K Hildebran et al. [259] found that DPPC monolayers reach minimum surface tensions of 1-2mN/m with first-order kinetic collapse rates that reflect their metastability and long relaxation times at low surface tensions. Chen et al. [249] found that the surface pressure relaxation of dynamic DPPC monolayers followed a two-stage nucleation and growth process dictated by Prout-Tompkins and second order kinetics. Using fluorescence microscopy, Chen et al. [249] found that 5min after collapse the monolayer was nearly homogenous, but that after 1h of relaxation bright domains appeared and after 2h of relaxation a network of sharp boundaries between dark and light domains appeared. According to Chen et al. this behavior signifies the continuous growth of 3D condensed DPPC structures. Other studies also suggest that monolayer relaxation is a nucleation and growth process [254, 260, 261].

Longo et al. [93] stated that differences in the experimental results can likely be attributed to kinetic effects caused by rates of compression, among other factors. Nag et al. [99] showed that although the rate of compression affected the size and

distribution of domains, no influence on the isotherm shape was evident. Thus it is thought that even though the shape and size of domains are rate dependent, the molecules arrange themselves to fit into the available space and the flexibility of domain shape, leading to an isotherm that does not vary with compression rate [97]. Although there is a notable difference between dynamic and equilibrium pressure-area isotherms, many studies suggest that varying dynamic compression rate leads to little or no change in the pressure-area isotherm. For example, Tabak et al. [98] found that dynamic compression rates in the range of 19.2-96Å^2/molecule/min gave essentially the same isotherm with negligible variation. However, the relaxation results of Wüstneck et al. [247] indicate that there is some dependence of isotherms on compression rate, at least for surface pressures above 10 to 15mN/m. Using both the pendant drop technique and the Langmuir-Wilhelmy film balance, Jyoti et al. [97] found that varying surface compression between 1.6-371Å^2/molecule/min, led to only a slight shift in the isotherms of DPPC at 293.15K and 296.15K, with no effect on the characteristic shape.

A.3 Experimental Apparatus

There are a number of inconsistencies between experimental results of cycled lung surfactant extract and the behavior of surfactant in vivo. Langmuir-Wilhelmy surface balances display large hysteresis, whereas hysteresis is substantially less in the lungs [108, 114]. Additionally, the observed relaxation rates and degree of creep (spreading of the surface film along wall-liquid interfaces) are greater in vitro, surface balances display greater sensitivity than seen physiologically, and less compression is required in the lungs (25-30% decrease in area) to decrease the surface tension to near zero values than required in a surface balance (50-80% decrease) [108, 114]. These differences between in vitro and in vivo studies may be attributed to experimental artifacts such as surface leaks and the type and geometry of the apparatus used [93, 108]. There

are a variety of common methods for measuring pressure-area isotherms, including the Wilhelmy surface balance, Langmuir-Blodgett deposition, the pendant drop technique, the pulsating bubble, and the captive bubble. The two most widely used methods for measuring dynamic surface pressure are the Wilhelmy surface balance and the oscillating bubble method (also known as the pulsating bubble method) [59].

A.3.1 Langmuir-Wilhelmy Surface Balance

A Langmuir film balance is composed of a trough filled with an aqueous subphase, upon which a surface film is spread, with one or more moveable barriers to compress and expand the surface. In a conventional Langmuir trough a floating barrier is attached to a torsion balance enabling the determination of surface pressure [262]. In the Langmuir-Wilhelmy surface balance, a Wilhelmy slide is used as a forcesensing mechanism that determines pressure from the wetting of the plate. Complete wetting is important, in order to accurately measure pressure using a Wilhelmy plate [111]. The Langmuir-Wilhelmy balance has a design advantage over the traditional Langmuir balance. At low surface tension the subphase overflows the walls of the conventional Langmuir trough and as the water level drops, film leakage occurs under the barrier [111]. A typical Wilhelmy balance avoids overflow of the subphase and has a recessed dam-type barrier; however continues ribbon barriers can also be used [111]. A Langmuir-Blodgett surface balance is similar to a Langmuir balance; however it can be used not only to compress a monolayer to obtain an isotherm, but is also used as a device to deposit monolayers on a solid substrate by immersion of a solid surface into a liquid consisting of lipids in an organic solvent.

Material loss could be a factor in the Langmuir film balance, especially at high temperatures [251]. Surface relaxation studies are extremely sensitive to leakage effects in the Wilhelmy trough, especially for DPPC films, which have very large dynamic collapse pressures [98, 118]. Two common types of Wilhelmy balance designs

are those with a submerged dam-type barrier and those with a continuous ribbon-type barrier [107]. Tabak, Notter, and co-workers [98, 107, 263] found that whereas surface balances equipped with a continuous Teflon ribbon barrier avoided the problem of film leakage, those equipped with a recessed trough type barrier did not. Significant leakage was observed under continuous compression at 310.15K [107]. Although DPPC film leakage at 298.15K was found to be negligible during continuous compression with a recessed trough, major leakage was observed during relaxation experiments especially when barrier movement was halted [98]. This leakage led to problems with reproducibility of pressure-time data. Sources of experimental error such as film leakage tend to shift isotherms to lower surface pressures [263]. Leakage effects are typically observed as a decrease in the slope of pressure-area isotherms at large surface pressures, and can be mistaken as premature monolayer collapse [107].

Teflon ribbon barriers eliminate leakage between the barrier and the trough walls, but do not prevent creep. Creep can be exacerbated by the large perimeter of the Langmuir-Wilhelmy balance, along which monolayer creep can occur. The problem of film containment is much more substantial for lung surfactant extracts and other fluid films than for DPPC, which is relatively rigid [114]. Additionally, as surface pressure decreases the contact angle on the Wilhelmy slide can decrease, leading to contact angle hysteresis and erroneous surface pressure readings [118]. Problems with contact angle can lead to erroneously low surface tension values during film compression [112]. Also, the surface compression ($\sim$80%) and cycling rates (1-3min/cycle) used in most Wilhelmy balance studies are very different than those present physiologically [95]. Furthermore, the type and geometry of the experimental apparatus are known to have an effect on the shape of pressure-area isotherms. The geometry of a Langmuir trough should be considered, because lipids near the walls may disorder, due to the excluded volume effect, thereby skewing the measurement of area per lipid [110].

The Wilhelmy balance method has several other drawbacks including the large

fluid volume 50mL used, which requires the diluting or solvation of the sample in organic solvent, tedious cleaning of balance components to ensure proper wetting and avoid contamination, a flat surface area which does not reproduce the curvature in the alveoli, and compression and expansion rates which are much slower than the rate of breathing [113].

A.3.2 Pulsating Bubble

The pulsating bubble technique involves the formation of a small air bubble, inside a small sample chamber (20μL), where the bubble volume is made to pulsate by a precision pulsator that moves liquid in and out of the sample chamber through a capillary [59, 264]. The pressure difference between the ambient air and the liquid subphase is continuously monitored with a pressure transducer, the size of the bubble is monitored through a microscope, and the surface tension is calculated from the pressure gradient across the bubble and the bubble radius, using the Laplace equation for a sphere [59, 264]. The pulsating bubble technique avoids many of the drawbacks listed for the Wilhemy balance above. In addition, for the pulsating bubble, temperature control is relatively easy, and it is straightforward to maintain experimental conditions that mimic in vivo respiration [59]. Also, the pulsating bubble surfactometer (PBS) requires only a small sample making its use in clinical studies more feasible [59]. The pulsating bubble method mimics the physical and geometric conditions present in the alveoli [264] better than the Wilhelmy balance does, because the former involves not only compression of the monolayer but also adsorption from the subphase [59].

The pulsating bubble method also has its weaknesses, including the difficulty of analysis of multi-component systems due to uncertainties about the extent of adsorption of each component to the interface [59]. Furthermore, it is cumbersome to extract complete pressure-area isotherms from the data generated during the rapid cycling

utilized by this technique [59]. Also, surface tension is measured directly with the Wilhelmy balance, but for a pulsating bubble it must be calculated using the Young-Laplace equation, and the surface tension at small bubble size will tend to be falsely high due to volume displacement in the pressure transducer [113]. Furthermore, the pulsating bubble surfactometer does not avoid the problem of film leakage, which can occur through the inlet tube connected to the bubbles and possibly along the walls of the chamber. Thus, low tensions are typically only attainable in the pulsating bubble surfactometer at high cycling rates (20cycles/min) [114]. The PBS technique also suffers problems with creep. When the surfactant film reaches a lower surface tension than the surface free energy of the plastic walls of the chamber, then the film creeps up the plastic surface [108, 114]. Because PBS also includes adsorption of surfactant to the expanding interface, the relative rates of adsorption and expansion must also be considered. If the rate of adsorption is slower than the rate of expansion, the surface tension at maximum area will be greater than the equilibrium value. The opposite will occur during compression, if the rate of desorption is slower than the compression rate.

Inaccuracies in PBS surface tension inferred from the Young-Laplace equation can result from two inherent approximations, namely a simplified spherical bubble shape and a static surface viscosity. Hall et al. [264] studied the effects of bubble deformation and surface dilatational viscosity on the surface tension measurements using the oscillating bubble method. They found that the effects of bubble deformation were limited to extremely low surface tensions and the absolute error from the spherical approximation is minimal ($<$0.5mN/m), making corrections for bubble shape unnecessary. On the other hand, the surface dilatational viscosities of lung surfactant, DPPC, and palmitic acid were large enough to give substantial errors if neglected in the pressure drop calculations. Viscous effects vanish at the maximum and minimum surface tensions, but are significant in between, even for moderate values of

surface dilatational viscosity. According to Hall et al. [264], if corrections are made for viscous effects, the maximum surface pressure shifts toward end compression and decreases substantially in magnitude.

Two modifications have been introduced into the PBS to greatly improve the ability of the pulsating bubble surfactometer to reach near-zero surface tensions [117]. The first modification keeps the capillary dry, thereby correcting continuity between the bubble and the capillary and thus improving performance by allowing a larger degree of film compression. The second modification allows more material to be adsorbed to the surface. The large surface area occupied by the film in the unmodified PBS leads to problems with the attainment of low surface tension on the first compression for some surfactant films, and slow adsorption at minimum bubble area makes achievement of near-zero surface tensions difficult for any surfactant. However, low surface tensions can be reached using the unmodified surfactometer through repetitive cycling, which however leads to changes in wetting and surface film composition.

A.3.3 Captive Bubble

The captive bubble apparatus is composed of an air-tight 10mL syringe containing a stirred suspension of surfactant, into which air is sucked, forming a bubble [265]. The bubble size is varied using a plunger while the bubble shape is captured on camera and used for the calculation of surface area and surface tension using an automated image analyzer [265]. Recall that leakage in the Wilhelmy balance often occurs at the contact area between the barrier and the side walls and at the side walls themselves [115], and in the pulsating bubble surfactometer as a result of contact between the bubble and the outside air through the air-filled wet capillary of the sample chamber [116]. Monolayer leakage prevents surfactant films from reaching near-zero surface tensions, which leads to underestimation of monolayer stability and can explain the requirement of repetitive cycling to reach near zero surface tension in

many PBS studies [116]. On the other hand, in the captive bubble (CB) method, the absence of gaps or tubes perforating the bubble surface eliminates leakage pathways, allowing films adsorbed from natural lung surfactant to readily reach near-zero surface tensions [50, 114]. Very low surface tensions (high surface pressures) can thus be easily obtained using the captive bubble method. The captive bubble method has some other advantages over the pulsating bubble method, including the ability to expand bubbles more rapidly, thus aiding the study of the effect of adsorption rates, and also the reduction of surface tension upon film compression and the minimum value of surface tension can be measured with greater accuracy using the CB method [117]. Furthermore, because it avoids film leakage, the captive bubble method is more advantageous than the pulsating bubble method and the Wilhelmy surface balance in the study of film stability and hysteresis [114]. Although calculations are more time consuming and a larger fluid volume (1ml vs. 20μl) is required for the captive bubble method than for the pulsating bubble method, near zero surface tensions can be obtained upon the first compression at quasi-static rates [108, 114]. Furthermore, according to Schürch et al. [108] the Langmuir-Wilhelmy balance and the pulsating bubble surfactometer are not able to reproduce the stability of lung surfactant films observed in the captive bubble apparatus.

However, the captive bubble method also has disadvantages such as high cost, time inefficiency and complexity [117]. Potential problems that could arise in the captive bubble apparatus that may interfere with the measurement of bubble diameter, include satellite bubble formation, bubble distortion due to asymmetry in the surface (which is more severe at high surface pressures), and poor visibility at large suspension concentrations [116]. Contamination from the experimental apparatus itself is more problematic in the captive bubble apparatus than in the Wilhelmy surface balance, because the release of surface-active agents from the parts of the captive bubble surfactometer cannot be eliminated by repeated barrier sweeps [116]. Putz et

al. [116] have identified the silicone rubber gasket and the agar gel as possible sources of contamination in their captive bubble apparatus.

If the surface tension in the captive bubble apparatus increases suddenly, the resulting mechanical vibration produces a clicking noise, which can be mistaken as a sign of film leakage, but is likely associated with the squeeze-out of non-DPPC components and does not occur in pure DPPC films [108, 114]. Using the captive bubble apparatus to study rat pulmonary surfactant, Schürch et al. [114] found that after collapse, the material displaced from the film was no longer available for film formation upon expansion.

Using the captive bubble method, Wüstneck et al. [255] found that isotherms could be reproduced with repetitive cycling. Wüstneck et al. [121] also found that DPPC could be repeatedly and reversibly compressed to low surface tensions, with only a slight hysteresis. Putz et al. [116] found that a captive bubble surfactometer and a Wilhelmy balance gave very similar pressure-area isotherms, for DPPC monolayers at 310.15K. However, the captive bubble method, utilizing adsorbed films, yielded isotherms in which the phase transition occurred at slightly higher surface pressures than using solvent-spread films in a Wilhelmy balance. Schürch et al. [108] also found that their pure DPPC isotherms at 310.15K obtained with the captive bubble method closely matched those obtained on a Wilhelmy balance.

A.3.4 Pendant Drop

The pendant drop is an image-based instrument, utilizing axisymmetrical drop shape analysis (ADSA) of a liquid droplet hanging from the end of a capillary. Then drop volume is changed through the use of a syringe connected to a step motor, while photographs of the drop profiles are taken, and the Laplace equation is used to calculate surface tension [266]. The pendant drop method is typically used for dynamic cycling, and has an accuracy that is comparable to that of the other methods [267].

The pendant drop technique is advantageous with respect to its homogeneity of temperature, surface pressure, concentration, and the symmetry of area changes [109]. Although the small sample size used in the pendant drop method is beneficial in cases where the surfactant is difficult to obtain or is expensive, the main limitation of this method is the possibility of a large relative error, due to the relatively small amount of material used [89]. As a result of the small area utilized in the pendant drop, the calculation of molecular area can be error-prone, resulting in a shift of the isotherm along the x-axis, and errors in the calculation of limiting area [89, 109]. Further limitations include the possible inequivalence between constant decrease in the drop volume and constant decrease in surface area, the effects of surface curvature, which may lead to a limiting area that is too small, and distortions or inaccuracies produced by camera imaging. On the other hand, the pendant drop provides a relatively straightforward means of environmental control involving the use of a temperature pressure cell that protects the drop from contamination from air currents [97]. The pendant drop method is also the preferred method for calculating rheological properties, because Marangoni effects are absent, allowing the lateral transport of film components to be neglected. [121, 247]. Other methods involving the analysis of drop shape can be used, such as the sessile drop, however this method requires a surface that is perfectly smooth and homogeneous, to maintain axisymmetrical growth [60].

Like the captive bubble, the pendant drop has the advantage of a small volume requirement and isolation from environmental influences, but solvent effects can be problematic. The pendant drop allows for gas exchange, whereas the captive bubble does not [121]. One notable difference between the two methods is the increase over time of the partial vapor pressure in the captive bubble, versus the constant vapor pressure in the pendant drop [121]. Even using small amounts of spreading solvent ($<1\mu$l), Wüstneck et al. found that the pendant drop and captive bubble

techniques only agreed with each other for DPPC monolayers for pressures less than 40mN/m. There are also differences between isotherms obtained with a pendant drop and those obtained using a Langmuir film balance. Wüstneck et al. [247] found that pressure-area isotherms obtained for DPPC using these methods showed significant differences that remain unresolved. In the Langmuir film balance, the plateau was more pronounced and the film pressures during compression were much higher. Difficulty in obtaining high surface pressure in the pendant drop might be attributed to the surface film creeping over the capillary. Other potential factors that might lead to differences in the isotherms obtained with each method were also considered. Wüstneck et al. [247] considered, and discounted, the possible presence of evaporated solvent as a factor and suggested that the effect of drop curvature on surface domains could be a cause. It has been further suggested that differences in the conditions inherent to each type of apparatus, such as spreading conditions and relative compression rate, could lead to the differences in domain structures, and the surface rearrangement process, thereby affecting the characteristic shape of the isotherm [247]. Jyoti et al. found significantly different characteristic shapes of DPPC isotherms obtained with the pendant drop and Langmuir-Blodgett balance, with isotherms in the Langmuir-Blodgett balance displaying a more distinct plateau representing the LC-LE phase transition [97]. In contrast, Wege et al. [268] found that the use of the pendant drop with two different deposition methods yielded isotherms for DPPC at 293.15K that were very close to those measured with a conventional film balance by Hunt et al. [100]. Li et al. [109] found good agreement in DPPC isotherms at 293.15K obtained with a pendant drop and with a Langmuir-Blodgett film balance, except in the coexistence region, which is less pronounced and shifted to higher surface pressures in the Langmuir-Blodgett balance than for the pendant drop isotherm. There are a variety of possible causes for a shift in the coexistence region, such as differences in interface curvature, higher compression rates used in the

pendant drop method, and the presence of impurities, the effect of which is amplified in the pendant drop technique due to the small volume involved. Furthermore it has been suggested that diffusion limits the aggregation process on a curved surface, which may lead to limited domain growth [269].

A.4 pH

Surface pH values, in the alveoli, have been reported to be between 6.9 and 6.4 [270]. Changes in pH and the presence of ions can induce changes in head group interactions, which can produce changes in the transition temperature on the order of 10K [110]. Using differential scanning calorimetry Liu et al. [106] found that varying pH from 2.6 to 11.5 shifts the main transition temperature of DPPC bilayers from 323.55 to 315.15K. Liu et al. [106] found that as pH was varied from 2.6 to 5.6 to 11.5 the respreading ratio (the amount of surfactant that remains in the surface film upon expansion relative to the total amount before compression) for the second cycle was changed from 0.26 to 0.37 to 0.35, and the maximum surface pressure attained was decreased from 72.0 to 71.6 to 71.1mN/m. Note that the phosphate group of DPPC is protonated (P-OH) at 2.6 and in a deprotonated oxyanionic state (P-O-) at pH 5.6 and 11.5 [271]. This leads to a net positive ionization state at pH 2.6 and a zwitterionic state at pH 5.6 and 11.5. Liu et al. [104] concluded that the net positive ionization state at pH 2.6 decreased intermolecular hydrogen bonding and was detrimental to respreading, leading to a large difference in respreadibility between pH 2.6 and pH 5.6 and only a small difference between pH 5.6 and pH 11.5. Decreased intermolecular hydrogen bonding at pH 2.6 also presumably leads to the observed small increase in the maximum surface pressure. Furthermore, an increase in alkalinity leads to a higher degree of solvation, while an acidic medium likely hinders the degree of solvation. Gong et al. [105] suggest that phophatidylcholines are not sensitive to pH over the range of 3-8. They also note that pH and ionic strength are

interrelated, and it is possible to misinterpret the influence of ionic strength as an effect of pH. The presence of ions can promote a higher degree of solvation of the PC head groups leading to head groups that are effectively bulkier and require more surface area.

A.5 Ionic Strength

Many studies have shown that the presence of ions in the subphase causes little to no shift in the pressure-area isotherms of DPPC and other phosphatidylcholines [100–103, 272]. Zaitsev et al. [102] found that varying the subphase from pure water, to 1.0M NaCl, and to 1.0M KCl caused the shape of the isotherm to change slightly in the plateau region and led to a slight increase in the average area per molecule. Shah and Schulman [272] found that the pressure-area isotherms of phosphatidylcholine were identical on 0.02M NaCl, 0.01M Na2SO4, and 0.02M NaNO3 sub-solutions. They also found that the presence of metal ions Na+, K+, Li+, Mg2+, Ca2+, Sr2+, Ba2+, Al3+ had no effect. The NMR results of Akutsu and Seelig [273] showed that the addition of metal ions led to a small structural change in DPPC bilayers, which affected the polar head group while leaving the glycerol backbone and the fatty acyl chains unmodified. They also found that the strength of interaction increased with the charge of the metal ion (i.e. Na+<Ca2+<La3+). In a study using external reflection-adsorption IR spectroscopy, Hunt et al. [100] observed changes in the phosphate vibrations of DPPC monolayers in the presence of Ca2+ ions and Pr3+ ions and suggested that the ions interact with the lipid monolayer by displacing the phosphates hydration sphere, with Pr3+ having a larger effect due to its higher charge density. This relatively weak interaction is not thought to alter the DPPC isotherm significantly. Hunt found that adding 50mM Ca2+ or 30mM Pr3+ shifted the isotherm only slightly with the most noticeable difference in the phase transition plateau region.

In contrast, other in-depth studies have shown that the subphase ions can have a significant effect on the phase behavior of DPPC. Simon et al. [274] preformed a calometric study on the effect of various ions on the main transition temperature of DPPC monolayers. The main transition temperature (T_m, the temperature at which the lipid tails undergo a transition from ordered to disordered) was found to be 315.25K on pure water. In the presence of 1M monovalent salts, T_m varied from 313.15K for KI to 316.75K for KCl, whereas In the presence of 1M divalent salts T_m varied from 311.65K for CdI2 to 330.15K for CdCl2, and in the presence of 1M trivalent salts T_m was 315.15K for LaCl3 and 321.95K FeCl2. These data suggest that 1M ions (especially divalent ions) can have a significant affect on the phase behavior of DPPC monolayers.

Aston et al. [275] studied the effect of NH4NO3 at concentrations between 0 and 8.75mol/dm^3 (70%w/v) and found that the addition of very high concentrations of NH4NO3 leads to a large shift in the isotherm to a more expanded state, the disappearance of the horizontal coexistence region and an increase in the collapse pressure by 4mN/m. However, such high ionic concentrations are not typical of those found in the subphase of most pressure-area isotherm experiments. The shift in the isotherm produced by 1%w/v NH4NO3 was smaller, yet still significant with an expansion of 8Å^2/molecule at the transition point. Aston et al. [275] suggest that anions are more surface active than cations; thus the presence of excess nitrate anions at the surface should lead to a charged surface layer that is more expanded due to ionic repulsion. Ross et al. [276] found that although the phase transition plateau was not affected, the limiting areas of the DPPC isotherms at 293.15K were shifted slightly in the presence of 0.1mM CaCl2 and 1mM EGTA. For instance, at a surface pressure of 20mN/m the area/lipid was 46Å^2 on pure water, 47Å^2 on 0.1mM CaCl2 and 48Å^2 on 1mM EGTA. These results are in accordance with the NMR results of Akutsu and Seelig [273], who found that the addition of metal ions led to a small

structural change in DPPC bilayers, which affected the polar head group while leaving the glycerol backbone and the fatty acyl chains unmodified.

Aroti et al. [277] applied pressure-area isotherm studies, Brewster-angle microscopy, grazing incidence x-ray diffraction and infrared reflection-adsorption spectroscopy to examine in detail the effect of the Hofmeister series of anions on DPPC monolayers. They found that the presence of anions can have a significant affect on the isotherm, increasing the surface pressure at a given area per molecule (most notably at higher areas), shifting the transition region to larger surface pressures and smaller molecular areas, and decreasing the plateau length, with the effects becoming more pronounced with increasing salt concentration. The effect varies in magnitude depending on the anion present, increasing in the order Cl-<Br-<NO3-<I-<BF4-<ClO4-<SCN-. Aroti et al. [277] concluded that salts in the subphase have a stabilizing effect on the LE phase. Although the exact mechanism is still in question, they concluded that the salts adsorb at the DPPC monolayer surface in some way. Although the ions penetrate into the LE phase, the LC phase appears to remain insensitive to the presence of the ions. Two possible mechanisms are proposed, one involving preferential adsorption of anions and the other the expulsion of anions from the subphase due to positive free energy gain for the subphase water. Aroti et al. [277] further propose that the convergence of pressure-area isotherms at high pressure for various ion types and concentrations, implies that the ions are squeezed out at high pressures, indicating that strong local binding of anions to the lipid head groups is unlikely. Recent all-atom molecular dynamic simulations performed by Sachs and Woolf [278] show the penetration of ions Cl- and Na+ and large anions into POPC bilayers. They found that large anions penetrated more deeply into the bilayer than do Cl- and Na+. In contrast to the mechanism proposed by Aston et al. [275], Na+ was found to penetrate more deeply than Cl- presumably due to a more loose hydration shell around Na+.

Although experimental data suggests that at rather high concentration, ions can have a significant affect on the phase behavior of DPPC monolayers, most pressure-area isotherm studies involve concentrations significantly lower than 1M. As shown by Simon [274] and Shah and Schulman [272], with a few exceptions (i.e. Simon found T_m to be shifted to 327.65K for 0.1 M CdI2), dynamic pressure-area behavior of zwitterionic lipids is not greatly affected by salt in physiologically relevant ranges ($\leq$0.1M). In many cases the presence of ions will lead little or no change in the isotherm of zwitterionic monolayers; however it should be noted that one must be careful to maintain an uncontaminated subphase and must give thoughtful consideration to how the addition of ions could potentially affect the thermodynamic properties of the monolayer. It has been shown that the presence of minerals [103] and hydrophobic ions [101] can cause significant changes in pressure-area isotherms of DPPC.

A.6 Impurities

Impurities can arise from many sources, including the experimental apparatus itself, and lead to isotherms that do not have a well defined phase transition region, are shifted, or do not reach near zero surface tensions upon end compression. Klopfer and Vanderlick [120] attributed a shift in their DPPC pressure-area isotherm to accumulation of environmental impurities, with the influence of the impurities increasing with exposure time and surface pressure. They attributed the shift to the presence of air-borne impurities, possibly from a plexiglass box incasing the surface balance. Watkins [119] found that traces of heavy metal ions and sealing substances, which arose from parts used in the trough, caused instability at high surface pressures. It has also been suggested that fluorescent probes behave like impurities [131]. Fluorescent probes have also been shown to cause a shift in the isotherm of DPPC films, increasing the molecular area by as much as 5.5Å^2/molecule [279]. Other sources

of inaccuracies can include incomplete solvation, decomposition of solutions that are left too long, and impurities in commercial samples that have not been adequately purified [64].

A.7 Spreading Agent

Munden and Swarbrick [94] found that the choice of spreading solvent had a large effect on the displacement of isotherms along the area axis. They determined that the ratio of polar and nonpolar components in the spreading solvent was of critical importance, with 3:2(v/v) mixtures of methanol-hexane and ethanol-hexane mixtures causing a displacement of the isotherm to very low areas (20Å^2/molecule), due to loss of DPPC from the interface, because of its solubility in the spreading solution. Munden and Swarbrick also presented isotherms obtained with 1:1 hexane/chloroform, 1:3 chloroform/benzene, and pure chloroform as spreading solvents, which were all shifted to areas of 33Å^2/molecule, significantly less than the limiting area. As addressed in the paper corresponding to this supplementary material, chloroform has been shown to display surface active behavior, which can greatly affect the shape of DPPC isotherms [116, 121].

Solvent effects are more substantial for the captive bubble method and for micro-film balances such as the pendant drop method than they are for the Langmuir-Wilhelmy balance. Conventional troughs have the advantage of fast solvent evaporation and the large volume of the gas phase above the trough eliminates the influence of evaporated solvent [267]. This is not so for closed systems such as micro-film balances and the captive bubble apparatus. In these systems, the presence of organic solvents in the gas phase and in the liquid phase can both lead to a substantial increase in the surface pressure. However the influence of solvent vapor is though to be eliminated through the proper atmosphere-exchange procedures [267].

BIBLIOGRAPHY

BIBLIOGRAPHY

[1] S.J. Marrink, A.H. de Vries, and D.P. Tieleman. Lipids on the move: Simulations of membrane pores, domains, stalks and curves. *Biochim. Biophys. Acta*, 1788:149–168, 2009.

[2] J. Gumbart, Y. Wang, A. Aksimentiev, E. Tajkhorshid, and K. Schulten. Molecular dynamics simulations of proteins in lipid bilayers. *Curr. Opin. Struct. Biol.*, 15:423–431, 2005.

[3] E. Lindahl and M.S. Sansom. Membrane proteins: molecular dynamics simulations. *Curr. Opin. Struct. Biol.*, 18:425–43, 2008.

[4] E. Matyus, C. Kandt, and D.P. Tieleman. Computer simulation of antimicrobial peptides. *Curr. Med. Chem.*, 14:2789–2798, 2007.

[5] O.G. Mouritsen. Theoretical-models of phospholipid phase-transitions. *Chem. Phys. Lipids*, 57:179–194, 1991.

[6] L.K. Nielsen, T. Bjørnholm, and O.G. Mouritsen. Thermodynamic and real-space structural evidence of a 2D critical point in phospholipid monolayers. *Langmuir*, 23:11684–11692, 2007.

[7] S.J. Marrink, J. Risselada, and A.E. Mark. Simulation of gel phase formation and melting in lipid bilayers using a coarse grained model. *Chem. Phys. Lipids*, 135:223–244, 2005.

[8] S. Leekumjorn and A.K. Sum. Molecular studies of the gel to liquid-crystalline phase transition for fully hydrated DPPC and DPPE bilayers. *Biochim. Biophys. Acta*, 1768:354–356, 2007.

[9] S. Leekumjorn and A.K. Sum. Molecular characterization of gel and liquid-crystalline structures of fully hydrated POPC and POPE bilayers. *J. Phys. Chem. B*, 111:6026–6033, 2007.

[10] A.H. de Vries, S. Yefimov, A.E. Mark, and S.J. Marrink. Molecular structure of the lecithin ripple phase. *Proc. Natl. Acad. Sci. U.S.A.*, 102:5392–5396, 2005.

[11] J.B. Klauda, B.R. Brooks, and R.W. Pastor. Dynamical motions of lipids and a finite size effect in simulations of bilayers. *J. Chem. Phys.*, 125:144710–144717, 2006.

[12] T. Murtola, T. Rog, E. Falck, M. Karttunen, and I. Vattulainen. Transient ordered domains in single-component phospholipid bilayers. *Phys. Rev. Lett.*, 97(238102), 2006.

[13] E. Falck, T. Rog, M. Karttunen, and I. Vattulainen. Lateral diffusion in lipid membranes through collective flows. *J. Am. Chem. Soc.*, 130:44–45, 2008.

[14] M. Kranenburg and B. Smit. Phase behavior of model lipid bilayers. *J. Phys. Chem. B*, 109:6553–6563, 2005.

[15] O. Lenz and F. Schmid. Structure of symmetric and asymmetric ripple phases in lipid bilayers. *Phys. Rev. Lett.*, 98(058104), 2007.

[16] X. Sun and J.D. Gezelter. Dipolar ordering in the ripple phase of molecular-scale models of lipid membranes. *J. Phys. Chem. B*, 112:1968–1975, 2008.

[17] S.V. Bennun, M. Longo, and R. Faller. Phase and mixing behavior in two-component lipid bilayers: a molecular dynamics study in DLPC/DSPC mixtures. *J. Phys. Chem. B*, 111:9504–9512, 2007.

[18] M.J. Stevens. Complementary matching in domain formation within lipid bilayers. *J. Am. Chem. Soc.*, 127:15330–15331, 2005.

[19] T. Murtola, E. Falck, M. Karttunen, and I. Vattulainen. Coarse-grained model for phospholipid/cholesterol bilayer employing inverse Monte Carlo with thermodynamic constraints. *J. Chem. Phys.*, 126(075101), 2007.

[20] P.S. Niemela, S. Ollila, M.T. Hyvonen, M. Karttunen, and I. Vattulainen. Assessing the nature of lipid raft membranes. *PLoS Comp. Biol.*, 3:304–312, 2007.

[21] Z. Zhang, L. Lu, and M.L. Berkowitz. Energetics of cholesterol transfer between lipid bilayers. *J. Phys. Chem. B*, 112:3807–3811, 2008.

[22] H.J. Risselada and S.J. Marrink. The molecular face of lipid rafts in model membranes. *Proc. Natl. Acad. Sci. U.S.A.*, 105:17367–17372, 2008.

[23] D. Mohammad-Aghaie, E. Macé, C.A. Sennoga, J.M. Seddon, and F. Bresme. Molecular dynamics simulations of liquid condensed to liquid expanded transitions in DPPC monolayers. *J. Phys. Chem. B*, 114:1325–1335, 2010.

[24] S. Baoukina, S.J. Marrink, and D.P. Tieleman. Lateral pressure profiles in lipid monolayers. *Faraday Discuss.*, 144:393–409, 2010.

[25] C. Laing, S. Baoukina, and D.P. Tieleman. Molecular dynamics study of the effect of cholesterol on the properties of lipid monolayers at low surface tensions. *Phys. Chem. Chem. Phys.*, 11:1916–1922, 2009.

[26] C. Xing and R. Faller. Coarse-grained simulations of supported and unsupported lipid monolayers. *Soft Matter*, 5:4526–4530, 2009.

[27] D. Rose, J. Rendell, D. Lee, K. Nag, and V. Booth. Molecular dynamics simulations of lung surfactant lipid monolayers. *Biophys. Chem.*, 138:67–77, 2008.

[28] S.L. Duncan and R.G. Larson. Comparing experimental and simulated pressure-area isotherms for DPPC. *Biophys. J.*, 94:2965–2986, 2008.

[29] S. Baoukina, L. Monticelli, H.J. Risselada, S.J. Marrink, and D.P. Tieleman. The molecular mechanism of lipid monolayer collapse. *Proc. Natl. Acad. Sci. U.S.A.*, 105:10803–10808, 2008.

[30] Z. Leonenko, S. Gill, S. Baoukina, L. Monticelli, J. Doehner, L. Gunasekara, F. Felderer, M. Rodenstein, L.M. Eng, and M. Amrein. An elevated level of cholesterol impairs self-assembly of pulmonary surfactant into a functional film. *Biophys. J.*, 93:674–683, 2007.

[31] S. Baoukina, L. Monticelli, S.J. Marrink, and D.P. Tieleman. Pressure-area isotherm of a lipid monolayer from molecular dynamics simulations. *Langmuir*, 23:12617–12623, 2007.

[32] S. Baoukina, L. Monticelli, M. Amrein, and D.P. Tieleman. The molecular mechanism of monolayer-bilayer transformations of lung surfactant from molecular dynamics simulations. *Biophys. J.*, 93:3775–3782, 2007.

[33] J.B. Klauda, X. Wu, R.W. Pastor, and B.R. Brooks. Long-range Lennard-Jones and electrostatic interactions in interfaces: application of the isotropic periodic sum method. *J. Phys. Chem. B*, 111:4393–4400, 2007.

[34] V. Knecht, M. Müller, M. Bonn, S.J. Marrink, and A.E. Mark. Simulation studies of pore and domain formation in a phospholipid monolayer. *J. Chem. Phys.*, 122(024704), 2005.

[35] S.K. Kandasamy and R.G. Larson. Molecular dynamics study of the lung surfactant peptide SP-B1-25 with DPPC monolayers: insights into interactions and peptide position and orientation. *Biophys. J.*, 88:1577–1592, 2005.

[36] A. Skibinsky, R.M. Venable, and R.W. Pastor. A molecular dynamics study of the response of lipid bilayers and monolayers to trehalose. *Biophys. J.*, 89:4111–4121, 2005.

[37] Y.K. Kaznessis, S. Kim, and R.G. Larson. Specific mode of interaction between components of model pulmonary surfactants using computer simulations. *J. Mol. Biol.*, 322:569–582, 2002.

[38] Y.N. Kaznessis, S. Kim, and R.G. Larson. Simulations of zwitterionic and anionic phospholipid monolayers. *Biophys. J.*, 82:1731–1742, 2002.

[39] F. Sun. Constant normal pressure, constant surface tension, and constant temperature molecular dynamics simulation of hydrated 1,2-dilignoceroylphosphatidylcholine monolayer. *Biophys. J.*, 82:2511–2519, 2002.

[40] H. Dominguez, M. Smondyrev, and M.L. Berkowitz. Computer simulations of phosphatidylcholine monolayers at air/water and CCl4/water interfaces. *J. Phys. Chem. B*, 103:9582–9588, 1999.

[41] S.E. Feller and R.W. Pastor. Constant surface tension simulations of lipid bilayers: the sensitivity of surface areas and compressibilities. *J. Chem. Phys.*, 111:1281–1287, 1999.

[42] A.W. Mauk, E.L. Chaikof, and P.J. Ludovice. Structural characterization of self-assembled lipid monolayers by N pi T simulation. *Langmuir*, 14:5255–5266, 1998.

[43] S.E. Feller, Y. Zhang, and R.W. Pastor. Computer simulation of liquid/liquid interfaces. II. Surface tension-area dependence of a bilayer and monolayer. *J. Chem. Phys.*, 103:10267–10276, 1995.

[44] V.M. Kaganer, H. Möhwald, and P. Dutta. Structure and phase transitions in Langmuir monolayers. *Rev. Mod. Phys.*, 71:779–819, 1999.

[45] R. Veldhuizen, K. Nag, S. Orgeig, and F. Possmayer. The role of lipids in pulmonary surfactant. *Biochim. Biophys. Acta*, 1408:90–108, 1998.

[46] Y.Y. Zuo, R.A.W. Veldhuizen, A.W. Neumann, N.O. Petersen, and F. Possmayer. Current perspectives in pulmonary surfactant: Inhibition, enhancement, and evaluation. *Biochim. Biophys. Acta*, 1778:1947–1977, 2008.

[47] A. Günther, C. Ruppert, R. Schmidt, P. Markart, F. Grimminger, D. Walmrath, and W. Seeger. Surfactant alteration and replacement in acute respiratory distress syndrome. *Respir. Res.*, 2:353–364, 2001.

[48] R.D. Hite. Surfactant deficiency in adults. *Clin. Pulm. Med.*, 9:39–45, 2002.

[49] J.M. Hohlfeld. The role of surfactant in asthma. *Respir. Res.*, 3(4), 2002.

[50] L.M.G. van Golde, J.J. Batenburg, and B. Robertson. The pulmonary surfactant system. *News Physiol. Sci.*, 9:13–20, 1994.

[51] I. Mingarro, D. Lukovic, and M. Vilar and. Synthetic pulmonary surfactant preparations: New developments and future trends. *Curr. Med. Chem.*, 15:393–403, 2008.

[52] N. J. Brown, J. Johansson, and A. E. Barron. Biomimicry of surfactant protein C. *Acc. Chem. Res.*, 41(10):1409–1417, 2008.

[53] Y.Y. Zuo, E. Keating, L. Zhao, S.M. Tadayyon, R.A.W. Veldhuizen, N.O. Petersen, and F. Possmayer. Atomic force microscopy studies of functional and dysfunctional pulmonary surfactant films. I. Micro- and nanostructures of functional pulmonary surfactant films and the effect of SP-A. *Biophys. J.*, 94:3549–3564, 2008.

[54] J. Pérez-Gil. Structure of pulmonary surfactant membranes and films: The role of proteins and lipid-protein interactions. *Biochim. Biophys. Acta*, 1778:1676–1695, 2008.

[55] R. Wüstneck, J. Pérez-Gil, N. Wüstneck, A. Cruz, V.B. Fainerman, and U. Pison. Interfacial properties of pulmonary surfactant layers. *Adv. Colloid Interface Sci.*, 117:33–58, 2005.

[56] S.J. Marrink, H.J. Risselada, S. Yefimov, D.P. Tieleman, and A.H. de Vries. The MARTINI force field: Coarse grained model for biomolecular simulations. *J. Phys. Chem. B*, 111:7812–7824, 2007.

[57] L. Monticelli, S.K. Kandasamy, X. Periole, R.G. Larson, D.P. Tieleman, and S.J. Marrink. The MARTINI coarse-grained force field: Extension to proteins. *J. Chem. Theo. Comp.*, 4:819–834, 2008.

[58] S.J. Marrink, A.H. de Vries, and A.E. Mark. Coarse grained model for semi-quantitative lipid simulations. *J. Phys. Chem. B*, 108:750–760, 2004.

[59] R.H. Notter. Surface chemistry of pulmonary surfactant: The role of individual components. In B. Robertson, L.M.G. van Golde, and J.J. Batenburg, editors, *Pulmonary Surfactant*, pages 17–65. Elsevier Science Publishers, Amsterdam, The Netherlands, 1984.

[60] D.Y. Kwok, D. Vollhardt, R. Miller, D. Li, and A.W. Neumann. Axisymmetric drop shape analysis as a film balance. *Colloids and Surfaces A: Physicochem. Eng. Aspects*, 88:51–58, 1994.

[61] F. Vilallonga. Surface chemistry of L-α-dipalmitoyl lecithin at the air-water interface. *Biochim. Biophys. Acta*, 163:290–300, 1968.

[62] JM Crane, G. Putz, and S.B. Hall. Persistence of phase coexistence in disaturated phosphatidylcholine monolayers at high surface pressure. *Biophys. J.*, 77:3134–3143, 1999.

[63] H. Yun, Y.W. Choi, N.J. Kim, and D. Sohn. Physicochemical properties of phosphatidylcholine (PC) monolayers with different alkyl chains, at the air/water interface. *Bull. Korean Chem. Soc.*, 24:377–383, 2003.

[64] M.C. Phillips and D. Chapman. Monolayer characteristics of saturated 1,2-diacyl phosphatidylcholines (lecithins) and phosphatidylethanolamines at the air-water interface. *Biochim. Biophys. Acta*, 163:301–313, 1968.

[65] D.D. Baldyga and R.A. Dluhy. On the use of deuterated phospholipids for infrared spectroscopic studies of monomolecular films: a thermodynamic analysis of single and binary component phospholipid monolayers. *Chem. Phys. Lipids*, 96:81–97, 1998.

[66] B. Tummers. `http://www.datathief.org`, 2005.

[67] H.J.C. Berendsen, J.P.M. Postma, W.F. van Gunsteren, A. Dinola, and J. R. Hawk. Molecular-dynamics with coupling to an external bath. *J. Chem. Phys.*, 81:3684–3690, 1984.

[68] E. Lindahl, B. Hess, and D. van der Spoel. GROMACS 3.0: a package for molecular simulation and trajectory analysis. *J. Mol. Mod.*, 7:306–317, 2001.

[69] H.J.C. Berendsen, D. van der Spoel, and R. van Drunen. GROMACS - a message-passing parallel molecular-dynamics implementation. *Comp. Phys. Commun.*, 91:43–56, 1995.

[70] D. van der Spoel, E. Lindahl, B. Hess, A. R. van Buuren, E. Apol, P. J. Meulenhoff, D. P. Tieleman, A. L. T. M. Sijbers, K. A. Feenstra, R. van Drunen, and H. J. C. Berendsen. `http://www.gromacs.org`, 2005.

[71] R.C. Weast, editor. *Handbook of Chemistry and Physics. A Ready-Reference Book of Chemical and Physical Data*. CRC Press, Boca Raton, FL, 61st edition, 1981.

[72] V.V.Zakharov, E.N. Brodskaya, and A. Laakonen. Surface properties of water clusters: A molecular dynamics study. *Mol. Phys.*, 95:203–209, 1998.

[73] C. Vega and E. de Miguel. Surface tension of the most popular models of water by using the test-area simulation method. *J. Chem. Phys.*, 126(154707), 2007.

[74] H. Leontiadou, A.E. Mark, and S.J. Marrink. Molecular dynamics simulations of hydrophilic pores in lipid bilayers. *Biophys. J.*, 86:2156–2164, 2004.

[75] S.W. Chiu, M. Clark, V. Balaji, S. Subramaniam, H.L. Scott, and E. Jakobsson. Incorporation of surface tension into molecular dynamics simulation of an interface: A fluid phase lipid bilayer membrane. *Biophys. J.*, 69:1230–1245, 1995.

[76] J.J. López Cascales, T.F. Otero, A.J. Fernández Romero, and L. Camacho. Phase transition of a DPPC bilayer induced by an external surface pressure: From bilayer to monolayer behavior. A molecular dynamics study. *Langmuir*, 22:5818–5824, 2006.

[77] P.S. Adhangale and D.P. Gaver III. Equation of state for a coarse-grained DPPC monolayer at the air/water interface. *Mol. Phys.*, 104:3011–3019, 2006.

[78] Y. Zhang, S.E. Feller, B.R. Brooks, and R.W. Pastor. Computer simulation of liquid/liquid interfaces. I. Theory and application to octane water. *J. Chem. Phys.*, 103:10252–10266, 1995.

[79] S.J. Marrink. University of Groningen. Groningen Biomolecular Sciences and Biotechnology Institute. MARTINI: Biomolecular forcefield for coarse grained simulations. `http://md.chem.rug.nl/~marrink/coarsegrain.html`, 2008.

[80] S.J. Marrink and A.E. Mark. Effect of undulations on surface tension in simulated bilayers. *J. Phys. Chem. B*, 105:6122–6127, 2001.

[81] D.P. Tieleman. University of Calgary. Department of Biological Sciences. `http://moose.bio.ucalgary.ca/download.html`, 2002.

[82] B. Hess, H. Bekker, H.J.C. Berendsen, and G.E.M. Fraaije. LINCS: A linear constraint solver for molecular simulations. *J. Comp. Chem.*, 18:1463–1472, 1997.

[83] U. Essman, L. Perera, M.L. Berkowitz, T. Darden, H. Lee, and L.G. Pedersen. A smooth particle mesh ewald method. *J. Chem. Phys.*, 103:8577–8593, 1995.

[84] A.H. de Vries, I. Chandrasekhar, W.F. van Gunsteren, and P.H. Hünenberger. Molecular dynamics simulations of phospholipid bilayers: Influence of artificial periodicity, system size, and simulation time. *J. Phys. Chem. B*, 109:11643–11652, 2005.

[85] R.M. Venable, A. Skibinsky, and R.W. Pastor. Constant surface tension molecular dynamics simulations of lipid bilayers with trehalose. *Mol. Simul.*, 32:849–855, 2006.

[86] R.B.Gennis. *Biomembranes: Molecular Structure and Function.* Springer-Verlag, New York, 1989.

[87] H. Möhwald. Phospholipid and phospholipid-protein monolayers at the air/water interface. *Annu. Rev. Phys. Chem.*, 41:441–476, 1990.

[88] G. Ma and H.C. Allen. DPPC Langmuir monolayer at the air-water interface: Probing the tail and headgroups by vibrational sum frequency generation spectroscopy. *Langmuir*, 22:5341–5349, 2006.

[89] H. Hauser, I. Pascher, R.H. Pearson, and S. Sundell. Preferred conformation and molecular packing of phosphatidylethanolamine and phosphatidylcholine. *Biochim. Biophys. Acta*, 650:21–51, 1981.

[90] M. Pasenkiewicz-Gierula, Y. Takaoka, H. Miyagawa, K. Kitamura, and A. Kusumi. Charge pairing of headgroups in phosphatidylcholine membranes: a molecular dynamics simulation study. *Biophys. J.*, 76:1228–1240, 1999.

[91] M Lösche, E. Sackmann, and H. Möhwald. A fluorescence microscopic study concerning the phase-diagram of phospholipids. *Ber. Bunsenges. Phys. Chem.*, 87:848–852, 1983.

[92] S.O. Nielsen, C.F. Lopez, P.B. Moore, J.C. Shelly, and M.L. Klein. Molecular dynamics investigations of lipid Langmuir monolayers using a coarse-grain model. *J. Phys. Chem. B*, 107:13911–13917, 2003.

[93] M.L. Longo, A.M. Bisagno, J.A. Zasadzinski, R. Bruni, and AJ Waring. A function of lung surfactant protein SP-B. *Science*, 261:453–456, 1993.

[94] J.W. Munden and J. Swarbrick. Effect of spreading solvent on monolayer characteristics of dipalmitoyl lecithin. *J. Colloid Interface Sci.*, 42:657–659, 1973.

[95] B. Robertson and L.M.G. van Golde. Postscript: Surfactant research; Current concepts and perspectives for the future. In B. Robertson, L.M.G. van Golde, and J.J. Batenburg, editors, *Pulmonary Surfactant*, pages 549–564. Elsevier Science Publishers, Amsterdam, The Netherlands, 1984.

[96] R.H. Notter, R. Taubold, and R.D. Mavis. Hysteresis in saturated phospholipid films and its potential relevance for lung surfactant function in vivo. *Exp. Lung Res.*, 3:109–127, 1982.

[97] A. Jyoti, R.M. Prokop, J. Li, D. Vollhardt, D.Y. Kwok, R. Miller, H. Möhwald, and A.W. Neumann. An investigation of the compression rate dependence on the surface pressure-surface area isotherm for a dipalmitoyl phosphatidylcholine monolayer at the air/water interface. *Colloids and Surfaces A: Physicochem. Eng. Aspects*, 116:173–180, 1996.

[98] S.A. Tabak, R.H. Notter, J.S. Ultman, and S.M. Dinh. Relaxation effects in the surface pressure behavior of dipalmitoyl lecithin. *J. Colloid and Interface Sci.*, 60:117–125, 1977.

[99] K. Nag, C. Boland, N. Rich, and K.M. Keough. Epifluorescence microscopic observation of monolayers of dipalmitoylphosphatidylcholine: Dependence of domain size on compression rates. *Biochim. Biophys. Acta*, 1068:157–160, 1991.

[100] R.D. Hunt, M.L. Mitchell, and R.A. Dluhy. The interfacial structure of phospholipids monolayer films: An infrared reflectance study. *J. Mol. Struct.*, 214:93–109, 1989.

[101] V.L. Shapovalov. Interaction of DPPC monolayer at air-water interface with hydrophobic ions. *Thin Solid Films*, 327:599–602, 1998.

[102] S.Y. Zaitsev, V.P. Vereschetin, V.P. Zubov, W. Zeiss, and D. Möbius. Ionic selectivity of valinomycin in the dipalmitoylphosphatidylcholine monolayers. *Thin Solid Films*, 285:667–670, 1996.

[103] L. Wiegart, B. Struth, M. Tolan, and P. Terech. Thermodynamic and structural properties of phospholipid Langmuir monolayers on hydrosol surfaces. *Langmuir*, 21:7349–7357, 2005.

[104] H. Liu, R.Z. Lu, J.G. Turcotte, and R.H. Notter. Dynamic interfacial properties of surface-excess films of phospholipids and phosphonolipid analogs. 1. Effects of pH. *J. Colloid Interface Sci.*, 167:378–390, 1994.

[105] K. Gong, S.S. Feng, M.L. Go, and P.H. Soew. Effects of pH on the stability and compressibility of DPPC/cholesterol monolayers at the air-water interface. *Colloids and Surfaces A: Physicochem. Eng. Aspects*, 207:113–125, 2002.

[106] H. Liu, J.G. Turcotte, and R.H. Notter. Thermotropic behavior of structurally-related phospholipids and phosphonolipid analogs of lung surfactant glycerophospholipids. *Langmuir*, 11:101–107, 1995.

[107] S.A. Tabak and R.H. Notter. Modified technique for dynamic surface pressure and relaxation measurements at the air-water interface. *Rev. Sci. Instrum.*, 48:1196–1201, 1977.

[108] S. Schürch, H. Bachofen, J. Goerke, and F. Possmayer. A captive bubble method reproduces the in situ behavior of lung surfactant monolayers. *J. Appl. Physiol.*, 67:2389–2396, 1989.

[109] J.B. Li, R. Miller, D. Vollhardt, G. Weidemann, and H. Möhwald. Isotherms of phospholipid monolayers measured by the pendant drop technique. *Colloid Polym. Sci.*, 274:995–999, 1996.

[110] J.F. Nagle. Theory of lipid monolayer and bilayer phase transitions: Effect of headgroup interactions. *J. Membr. Biol.*, 27:233–250, 1976.

[111] R.H. Notter. *Lung Surfactants: Basic Science and Clinical Applications*. Marcel Dekker, New York, 2000.

[112] R.E. Barrow and B.A. Hills. Critical-assessment of the Wilhelmy method in studying lung surfactants. *J. Physiol. London*, 295:217–227, 1979.

[113] G. Enhorning. Pulsating bubble technique for evaluating pulmonary surfactant. *Appl. Physiol. Respir. Environ. Exerc. Physiol.*, 43:198–203, 1977.

[114] S. Schürch, H. Bachofen, J. Goerke, and F. Green. Surface properties of rat pulmonary surfactant studied with the captive bubble method: Adsorption, hysteresis and stability. *Biochim. Biophys. Acta*, 1103:127–136, 1992.

[115] J. Goerke and J. Gonzales. Temperature dependence of dipalmitoyl phosphatidylcholine monolayer stability. *Appl. Physiol. Respir. Environ. Exerc. Physiol.*, 51:1108–1114, 1981.

[116] G. Putz, J. Goerke, S. Schürch, and J.A. Clements. Evaluation of pressure-driven captive bubble surfactometer. *J. Appl. Physiol.*, 76:1417–1424, 1994.

[117] G. Putz, J. Goerke, H.W. Taeusch, and J.A. Clements. Comparison of captive and pulsating bubble surfactometers with use of lung surfactants. *J. Appl. Physiol.*, 76:1425–1431, 1994.

[118] R.H. Notter and P.E. Morrow. Pulmonary surfactant: A surface chemistry viewpoint. *Ann. Biomed. Eng.*, 3:119–159, 1975.

[119] J.C. Watkins. The surface properties of pure phospholipids in relation to those of lung extracts. *Biochim. Biophys. Acta*, 152:293–306, 1968.

[120] K.J. Klopfer and T.K. Vanderlick. Isotherms of dipalmitoylphosphatidylcholine (DPPC) monolayers: Features revealed and features obscured. *J. Colloid Interface Sci.*, 182:220–229, 1996.

[121] N. Wüstneck, R. Wüstneck, V.B. Fainerman, U. Pison, and R. Miller. Influence of over-compressed spread L-dipalmitoyl phosphatidylcholine films and the influence of solvent vapour in the gas phase on π/A isotherms measured by using the captive bubble technique. *Colloids and Surfaces A: Physicochem. Eng. Aspects*, 164:267–278, 2000.

[122] R.C. Ahuja and D. Möbius. Photophysical properties of a pyrene-labeled phospholipid in matrix monolayers at the gas/water interface. *Langmuir*, 8:1136–1144, 1992.

[123] F. Bordi, F.D. Luca, C. Cametti, A. Naglieri, R. Misasi, and M. Sorice. Interactions of mono- and di-sialogangliosides with phospholipids in mixed monolayers at the air-water interface. *Colloids and Surfaces B: Biointerfaces*, 13:135–142, 1999.

[124] G.P. Borissevitch, M. Tabak, and O.N. Oliveira. Interaction of dipyridamole with lipids in mixed Langmuir monolayers. *Biochim. Biophys. Acta*, 1278:12–18, 1996.

[125] L. Dubreil, V. Vié, S. Beaufils, D. Marion, and A. Renault. Aggregation of puroindoline in phospholipid monolayers spread at the air-liquid interface. *Biophys. J.*, 85:2650–2660, 2003.

[126] J. Miñones Jr., J.M. Rodríguez Patino, O. Conde, C. Carrera, and R. Seoane. The effect of polar groups on structural characteristics of phospholipids monolayers spread at the air-water interface. *Colloids and Surfaces A: Physicochem. Eng. Aspects*, 203:273–286, 2002.

[127] M.I. Sández, A. Suárez, and A. Gil. Surface pressure-area isotherms and fluorescent behavior of phospholipids containing labeled pyrene. *J. Colloid Interface Sci.*, 250:128–133, 2002.

[128] A.D. Williams, J.M. Wilkin, and R.A. Dluhy. An investigation of miscibility in monolayer films of phosphocholine-phosphoglycerol binary mixtures. *Colloids and Surfaces A: Physicochem. Eng. Aspects*, 102:231–245, 1995.

[129] P. Dynarowicz-Latka, V. Rosilio, P. Boullanger, P. Fontaine, M. Goldmann, and A. Baszkin. Influence of a neoglycolipid and its PEO-lipid moiety on the organization of phospholipids monolayers. *Langmuir*, 21:11941–11948, 2005.

[130] F.R. Rana, A.J. Mautone, and R.A. Dluhy. Surface chemistry of binary mixtures of phospholipids in monolayers. Infrared studies of surface composition at varying surface pressures in a pulmonary surfactant model system. *Biochemistry*, 32:3169–3177, 1993.

[131] J.P. Slotte and P. Mattjus. Visualization of lateral phases in cholesterol and phosphatidylcholine monolayers at the air-water interface - A comparative study with two different reporter molecules. *Biochim. Biophys. Acta*, 1254:22–29, 1995.

[132] S. Taneva, T. McEachren, J. Stewart, and K.M.W. Keough. Pulmonary surfactant protein SP-A with phospholipids in spread monolayers at the air-water interface. *Biochemistry*, 34:10279–10289, 1995.

[133] M. Gladston and D.O. Shah. Surface properties and hysteresis of dipalmitoyllecithin in relation to the alveolar lining layer. *Biochim. Biophys. Acta*, 137:255–263, 1967.

[134] Y. Kanintronkul, T. Srikhirin, C. Angsuthanasombat, and T. Kerdcharoen. Insertion behavior of the Bacillus thuringiensis Cry4Ba insecticidal protein into lipid monolayers. *Arch. Biochem. Biophys*, 442:180–186, 2005.

[135] Y.L. Lee, J.Y. Lin, and C.H. Chang. Thermodynamic characteristics and Langmuir-Blodgett deposition behavior of mixed DPPA/DPPC monolayers at air/liquid interfaces. *J. Colloid and Interface Sci.*, 296:647–654, 2006.

[136] H. Nakahara, S. Nakamura, H. Kawasaki, and O. Shibata. Properties of two-component Langmuir monolayer of single chain perfluorinated carboxylic acids with dipalmitoylphosphatidylcholine (DPPC). *Colloids and Surfaces B: Biointerfaces*, 41:285–298, 2005.

[137] Y. Shen, Y. Tang, A. Xie, J. Zhu, S. Li, and Y. Zhang. Studies on the behaviors of dipalmitoylphosphatidylcholine and bilirubin in mixed monolayer at the air/water interface. *Appl. Surf. Sci.*, 252:5861–5867, 2006.

[138] S.A. Maskarinec, J. Hannig, R.C. Lee, and K.Y.C. Lee. Direct observation of poloxamer 188 insertion into lipid monolayers. *Biophys. J.*, 82:1453–1459, 2002.

[139] M. Kodama, O. Shibata, S. Nakamura, S. Lee, and G. Sugihara. A monolayer study on three binary mixed systems of dipalmitoyl phosphatidyl choline with cholesterol, cholestanol, and stigmasterol. *Colloids and Surfaces B: Biointerfaces*, 33:211–226, 2004.

[140] P. Vitovic, D.P. Nikolelis, and T. Hianik. Study of calix[4]resorcinarene-dopamine complexation in mixed phospholipid monolayers formed at the air-water interface. *Biochim. Biophys. Acta*, 1758:1852–1861, 2006.

[141] Z. Kozarac, B. Cosovic, D. Möbius, and M. Dobric. Interaction of polysaccharides with lipid monolayers. *J. Colloid Interface Sci.*, 226:210–217, 2000.

[142] F. Ronzon, B. Desbat, J.P. Chauvet, and B. Roux. Behavior of a GPI-anchored protein in phospholipid monolayers at the air-water interface. *Biochim. Biophys. Acta*, 1560:1–13, 2002.

[143] Y. Su, L. Qingzhong, L. Chen, and Z. Yu. Condensation effect of cholesterol, stigmasterol, and sitosterol on dipalmitoylphosphatidylcholine in molecular monolayers. *Colloids and Surfaces A: Physicochem. Eng. Aspects*, 293:123–129, 2007.

[144] K. Hoda, H. Kawasaki, N. Yoshino, C.H. Chang, Y. Morikawa, G. Sugihara, and O. Shibata. Mode of interaction of two fluorinated-hydrogenated hybrid amphiphiles with dipalmitoylphosphatidylcholine (DPPC) at the air-water interface. *Colloids and Surfaces B: Biointerfaces*, 53:37–50, 2006.

[145] S. Schürch, F. Possmayer, S. Cheng, and A.M. Cockshutt. Pulmonary SP-A enhances adsorption and appears to induce surface sorting of lipid extract surfactant. *Am. J. Physiol.*, 263:L210–L218, 1992.

[146] C. Anézo, A.H. de Vries, H.D. Höltje, D.P. Tieleman, and S.J. Marrink. Methodological issues in lipid bilayer simulations. *J. Phys. Chem. B*, 107:9424–9433, 2003.

[147] E. Lindahl and O. Edholm. Mesoscopic undulations and thickness fluctuations in lipid bilayers from molecular dynamics simulations. *Biophys. J.*, 79:426–433, 2000.

[148] J. Wohlert and O. Edholm. The range and shielding of dipole-dipole interactions in phospholipid bilayers. *Biophys. J.*, 87:2433–2445, 2004.

[149] F. Castro-Román, R.W. Benz, S.H. White, and D.J. Tobias. Investigation of finite system-size effects in molecular dynamics simulations of lipid bilayers. *J. Phys. Chem. B*, 110:24157–24164, 2006.

[150] D.P. Kharakoz and E.A. Shlyapnikova. Thermodynamics and kinetics of the early steps of solid-state nucleation in the fluid lipid bilayer. *J. Phys. Chem. B*, 104:10368–10378, 2000.

[151] J. Erbes, A. Gabke, G. Rapp, and R. Winter. Kinetics of phase transformations between lyotropic mesophases of different topology: a time-resolved synchrotron x-ray diffraction study using the pressure-jump relaxation technique. *Phys. Chem. Chem. Phys.*, 2:151–162, 2000.

[152] B.A. Holm, Z. Wang, E.A. Egan, and R.H. Notter. Content of dipalmitoyl phosphatidylcholine in lung surfactant: Ramifications for surface activity. *Pediatr. Res.*, 39:805–811, 1996.

[153] J.J. Batenburg and H.P. Haagsman. The lipids of pulmonary surfactant: Dynamics and interactions with proteins. *Prog. Lipid Res.*, 37:235–276, 1998.

[154] T. Curstedt, H. Jörnvall, B. Robertson, T. Bergman, and P. Berggren. Two hydrophobic low-molecular-mass protein fractions of pulmonary surfactant: Characterization and biophysical activity. *Eur. J. Biochem.*, 168:255–262, 1987.

[155] T. Curstedt, J. Johansson, P. Persson, A. Eklund, B. Robertson, B. Löwenadler, and H. Jörnvall. Hydrophobic surfactant-associated polypeptides: SP-C is a lipopeptide with two palmitoylated cysteine residues, whereas SP-B lacks covalently linked fatty acyl groups. *Proc. Natl. Acad. Sci. U.S.A.*, 87:2984–2989, 1990.

[156] J. Pérez-Gil. Lipid-protein interactions of hydrophobic surfactant proteins SP-B and SP-C in lung surfactant assembly and dynamics. *Pediatr. Pathol. Mol. Med.*, 20:445–469, 2001.

[157] S. Schürch, R. Qanbar, H. Bachofen, and F. Possmayer. The surface-associated surfactant reservoir in the alveolar lining. *Biol. Neonate*, 67 (Suppl 1):61–76, 1995.

[158] M.M. Lipp, K.Y.C. Lee, J.A. Zasadzinski, and A.J. Waring. Phase and morphology changes in lipid monolayers induced by SP-B protein and its amino-terminal peptide. *Science*, 273:1196–1199, 1996.

[159] M.M. Lipp, K.Y.C. Lee, D.Y. Takamoto, J.A. Zasadzinski, and A.J. Waring. Coexistence of buckled and flat monolayers. *Phys. Rev. Lett.*, 81:1650–1653, 1998.

[160] K.Y.C. Lee, M.M. Lipp, J.A. Zasadzinski, and A.J. Waring. Effects of lung surfactant specific protein SP-B and model SP-B peptide on lipid monolayers at the air-water interface. *Colloids and Surfaces A: Physicochem. Eng. Aspects*, 128:225–242, 1997.

[161] J. Ding, D.Y. Takamoto, A. von Nahmen, M.M. Lipp, K.Y.C. Lee, A.J. Waring, and J.A. Zasadzinski. Effects of lung surfactant proteins, SP-B and SP-C, and palmitic acid on monolayer stability. *Biophys. J*, 80:2262–2272, 2001.

[162] R.V. Diemel, M.M. Snel, A.J. Waring, F.J. Walther, L.M. van Golde, G. Putz, H.P. Haagsman, and J.J. Batenburg. Multilayer formation upon compression of surfactant monolayers depends on protein concentration as well as lipid composition. an atomic force microscopy study. *J. Biol. Chem.*, 277:21179–21188, 2002.

[163] D.Y. Takamoto, M.M. Lipp, A. von Nahmen, K.Y.C. Lee, A.J. Waring, and J.A. Zasadzinski. Interaction of lung surfactant proteins with anionic phospholipids. *Biophys. J.*, 81:153–169, 2001.

[164] W.R. Schief, M. Antia, B.M. Discher, S.B. Hall, and V. Vogel. Liquid-crystalline collapse of pulmonary surfactant monolayers. *Biophys. J.*, 84:3792–3806, 2003.

[165] J. Ding, I. Doudevski, H.E. Warriner, T. Alig, and J.A. Zasadzinski. Nanostructure changes in lung surfactant monolayers induced by interactions between palmitoyloleoylphosphatidylglycerol and surfactant protein B. *Langmuir*, 19:1539–1550, 2003.

[166] S. Krol, M. Ross, M. Sieber, S. Kunneke, H.J. Galla, and A. Janshoff. Formation of three-dimensional protein-lipid aggregates in monolayer films induced by surfactant protein B. *Biophys. J.*, 79:904–918, 2000.

[167] S. Krol, A. Janshoff, M. Ross, and H.J. Galla. Structure and function of surfactant protein B and C in lipid monolayers: A scanning force microscopy study. *Phys. Chem. Chem. Phys.*, 79:904–918, 2000.

[168] M. Amrein, A. von Nahmen, and M. Sieber. A scanning force- and fluorescence light microscopy study of the structure and function of a model pulmonary surfactant. *Eur. Biophys. J.*, 26:349–357, 1997.

[169] A. von Nahmen, M. Schenk, M. Sieber, and M. Amrein. The structure of a model pulmonary surfactant as revealed by scanning force microscopy. *Biophys. J.*, 72:463–469, 1997.

[170] A. Kramer, A. Wintergalen, M. Sieber, H.J. Galla, M. Amrein, and R. Guckenberger. Distribution of the surfactant-associated protein C within a lung surfactant model film investigated by near-field optical microscopy. *Biophys. J.*, 78:458–465, 2000.

[171] P.N. Nakorn, M.C. Meyer, C.R. Flach, R. Mendelsohn, and H.J. Galla. Surfactant protein C and lung function: New insights into the role of α-helical length and palmitoylation. *Eur. Biophys. J.*, 36:477–489, 2007.

[172] H.J. Galla, N. Bourdos, A. von Nahmen, M. Amrein, and M. Sieber. The role of pulmonary surfactant protein C during the breathing cycle. *Thin Solid Films*, 327-329:632–635, 1998.

[173] R. Sibug-Aga and R.C. Dunn. High-resolution studies of lung surfactant collapse. *Photochem. Photobiol.*, 80:471–476, 2004.

[174] L. Wang, P. Cai, H.J. Galla, H. He, C.R. Flach, and R. Mendelsohn. Monolayer-multilayer transitions in a lung surfactant model: IR reflection–absorption spectroscopy and atomic force microscopy. *Eur. Biophys. J.*, 34:243–254, 2005.

[175] N. Bourdos, F. Kollmer, A. Benninghoven, M. Ross, M. Sieber, and H.J. Galla. Analysis of lung surfactant model systems with time-of-flight secondary ion mass spectrometry. *Biophys. J.*, 79:357–369, 2000.

[176] C. Alonso, T. Alig, J. Yoon, F. Bringezu, H. Warriner, and J.A. Zasadzinski. More than a monolayer: Relating lung surfactant structure and mechanics to composition. *Biophys. J.*, 87:4188–4202, 2004.

[177] K. Nag, J. Pérez-Gil, M.L. Ruano, L.A. Worthman, J. Stewart, C. Casals, and K.M.W. Keough. Phase transitions in films of lung surfactant at the air-water interface. *Biophys. J.*, 74:2983–2995, 1998.

[178] A.D. Bangham. Lung surfactant: How it does and does not work. *Lung*, 165:17–25, 1987.

[179] J.A. Clements. Functions of the alveolar lining. *Am. Rev. Respir. Dis.*, 115:67–71, 1977.

[180] A.D. Bangham, C.J. Morley, and M.C. Phillips. The physical properties of an effective lung surfactant. *Biochim. Biophys. Acta*, 573:552–556, 1979.

[181] S.H. Yu and F. Possmayer. Reconstitution of surfactant activity by using the 6 kDa apoprotein associated with pulmonary surfactant. *Biochem. J.*, 236:85–89, 1986.

[182] A. Takahashi and T. Fujiwara. Proteolipid in bovine lung surfactant: Its role in surfactant function. *Biochem. Biophys. Res. Commun.*, 135(2):527–532, 1986.

[183] A. Post, A.V. Nahmen, M. Schmitt, J. Ruths, H. Riegler, M. Sieber, and H.J. Galla. Pulmonary surfactant protein C containing lipid films at the air-water interface as a model for the surface of lung alveoli. *Mol. Membrane Biol.*, 12:93–99, 1995.

[184] S.H. Yu and F. Possmayer. Lipid compositional analysis of pulmonary surfactant monolayers and monolayer-associated reservoirs. *J. Lipid Res.*, 44:621–629, 2003.

[185] B. Piknova, W.R. Schief, V. Vogel, B.M. Discher, and S.B. Hall. Discrepancy between phase behavior of lung surfactant phospholipids and the classical model of surfactant function. *Biophys. J.*, 81:2172–2180, 2001.

[186] E.C. Smith, J.M. Crane, T.G. Laderas, and S.B. Hall. Metastability of a supercompressed fluid monolayer. *Biophys. J.*, 85:3048–3057, 2003.

[187] J. Pérez-Gil. Molecular interactions in pulmonary surfactant films. *Biol. Neonate*, 81 (Suppl 1)(6–15), 2002.

[188] B. Piknova, V. Schram, and S.B. Hall. Pulmonary surfactant: Phase behavior and function. *Curr. Opin. Struct. Biol.*, 12:487–494, 2002.

[189] F. Lhert, W. Yan, S.C. Biswas, and S.B. Hall. Effects of hydrophobic surfactant proteins on collapse of pulmonary surfactant monolayers. *Biophys. J.*, 93:4237–4243, 2007.

[190] K.Y.C. Lee. Collapse mechanisms of Langmuir monolayers. *Annu. Rev. Phys. Chem.*, 59:771–791, 2008.

[191] J.A. Zasadzinski, J. Ding, H.E. Warriner, F. Bringezu, and A.J. Waring. The physics and physiology of lung surfactants. *Curr. Opin. Colloid Interface Sci.*, 6:506–513, 2001.

[192] S.B. Hall S. Rugonyi, S.C. Biswas. The biophysical function of pulmonary surfactant. *Respir. Physiol. Neurobiol.*, 163:244–255, 2008.

[193] G.T. Barnes and I.R. Gentle. *Interfacial Science: An Introduction.* Oxford University Press, New York, 2005.

[194] H. Lee, S.K. Kandasamy, and R.G. Larson. Molecular dynamics simulations of the anchoring and tilting of the lung-surfactant peptide SP-B1-25 in palmitic acid monolayers. *Biophys. J.*, 89:3807–3821, 2005.

[195] J.A. Freites, Y. Choi, and D.J. Tobias. Molecular dynamics simulations of pulmonary surfactant protein B peptide in a lipid monolayer. *Biophys. J.*, 84:2169–2180, 2003.

[196] C.D. Lorenz and A. Travesset. Atomistic simulations of Langmuir monolayer collapse. *Langmuir*, 22:10016–10024, 2006.

[197] L.M. Gordon, K.Y.C. Lee, M.M. Lipp, J.A. Zasadzinski, F.J. Walther, M.A. Sherman, and A.J. Waring. Conformational mapping of the N-terminal segment of surfactant protein B in lipid using C-13-enhanced fourier transform infrared spectroscopy. *J. Pept. Res.*, 55:330–347, 2000.

[198] J. Johansson, T. Szyperski, T. Curstedt, and K. Wüthrich. The NMR structure of the pulmonary surfactant-associated polypeptide SP-C in an apolar solvent contains a valyl-rich α-helix. *Biochemistry*, 33:6015–6023, 1994.

[199] E.R. May, D.I. Kopelevich, and A. Narang. Coarse-grained molecular dynamics simulations of phase transitions in mixed lipid systems containing LPA, DOPA, and DOPE lipids. *Biophys. J.*, 94:878–890, 2008.

[200] S.J. Marrink and A.E. Mark. Molecular view of hexagonal phase formation in phospholipid membranes. *Biophys. J.*, 87:3894–3900, 2004.

[201] M.R. Morrow, J. Sterward, S. Taneva, A. Dico, and K.M.W. Keough. Perturbation of DPPC bilayers by high concentrations of pulmonary surfactant protein SP-B. *Eur. Biophys. J.*, 33:285–290, 2004.

[202] D. van der Spoel, E. Lindahl, B. Hess, G. Groenhof, A.E. Mark, and H.J.C. Berendsen. GROMACS: Fast, flexible, and free. *J. Comp. Chem.*, 26(1701-1718), 2005.

[203] M.R. Morrow, J. Pérez-Gil, G. Simatos, C. Boland, J. Stewart, D. Absolom, V. Sarin, and K.M.W. Keough. Pulmonary surfactant-associated protein SP-B has little effect on acyl chains in dipalmitoylphosphatidylcholine dispersions. *Biochemistry*, 32:4397–4402, 1993.

[204] A. Gericke, C.R. Flach, and R. Mendelsohn. Structure and orientation of lung surfactant SP-C and L-α-Dipalmitoylphosphatidylcholine in aqueous monolayers. *Biophys. J.*, 73:492–499, 1997.

[205] E. Egberts, S.J. Marrink, and H.J.C. Berendsen. Molecular dynamics simulation of a phospholipid membrane. *Eur. Biophys. J.*, 22:423–436, 1994.

[206] A. Gopal and K.Y.C. Lee. Morphology and collapse transitions in binary phospholipid monolayers. *J. Phys. Chem. B*, 2001:10348–10354, 105.

[207] C. Ybert, W.X. Lu, G. Möller, and C.M. Knobler. Collapse of a monolayer by three mechanisms. *J. Phys. Chem. B*, 106:2004–2008, 2002.

[208] K. Nag, S.G. Taneva, J. Pérez-Gil, A. Cruz, and K.M.W. Keough. Combinations of fluorescently labeled pulmonary surfactant proteins SP-B and SP-C in phospholipid films. *Biophys. J.*, 72:2638–2650, 1997.

[209] A. Cruz, L. Vázquez, M. Vélez, and J. Pérez-Gil. Effect of pulmonary surfactant protein SP-B on the micro- and nanostructure of phospholipid films. *Biophys. J.*, 86:308–320, 2004.

[210] D. Follows, F. Tiberg, R.K. Thomas, and M. Larsson. Multilayers at the surface of solutions of exogenous lung surfactant: Direct observation by neutron reflection. *Biochim. Biophys. Acta*, 1768:228–235, 2007.

[211] D. Knebel, M. Sieber, R. Reichelt, H.J. Galla, and M. Amrein. Scanning force microscopy at the air-water interface of an air bubble coated with pulmonary surfactant. *Biophys. J.*, 82:474–480, 2002.

[212] S.H. Yu and F. Possmayer. Effect of pulmonary surfactant protein SP-A and neutral lipid on accretion and organization of dipalmitoylphosphatidylcholine in surface films. *J. Lipid Res.*, 37:1278–1288, 1996.

[213] L. Pocivavsek, B. Leahy, N. Holten-Andersen, B. Lin, K.Y.C. Lee, and E. Cerda. Geometric tools for complex interfaces: From lung surfactant to the mussel byssus. *Soft Matter*, 5:1963–1968, 2009.

[214] L. Pocivavsek, R. Dellsy, A. Kern, S. Johnson, B. Lin, K.Y.C. Lee, and E. Cerda. Stress and fold localization in thin elastic membranes. *Science*, 320:912–916, 2008.

[215] R.A. Ridsdale, N. Palaniyar, F. Possmayer, and G. Harauz. The formation of folds and vesicles by dipalmitoylphosphatidylcholine monolayers spread in excess. *J. Membrane Biol.*, 180:21–32, 2001.

[216] P. Tchoreloff, A. Gulik, B. Denizot, J.E. Proust, and F. Puisieux. A structural study of interfacial phospholipid and lung surfactant layers by transmission electron microscopy after Blodgett sampling: Influence of surface pressure and temperature. *Chem. Phys. Lipids*, 59:151–165, 1991.

[217] Y.P. Yang and R.Y. Tsay. Morphology of compressed dipalmitoyl phosphatidylcholine monolayers investigated by atomic force microscopy. *J. Lumin.*, 127:186–191, 2007.

[218] W.R. Schief, L. Touryan, S.B. Hall, and V. Vogel. Nanoscale topographic instabilities of a phospholipid monolayer. *J. Phys. Chem. B*, 104:7388–7393, 2000.

[219] G. Ma and H.C. Allen. New insights into lung surfactant monolayers using vibrational sum frequency generation spectroscopy. *Photochem. Photobiol.*, 82:1517–1529, 2006.

[220] E.J. Cabré, J. Malmström, D. Sutherland, J. Pérez-Gil, and D.E. Otzen. Surfactant protein SP-B strongly modifies surface collapse of phospholipid vesicles: Insights from a quartz crystal microbalance with dissipation. *Biophys. J.*, 97:768–776, 2009.

[221] R. Qanbar, S. Cheng, F. Possmayer, and S. Schürch. Role of the palmitoylation of surfactant-associated protein C in surfactant film formation and stability. *Am. J. Physiol.*, 217:L572–L580, 1996.

[222] F. Bringezu, J.Q. Ding, G. Brezesinski, and J.A. Zasadzinski. Changes in model lung surfactant monolayers induced by palmitic acid. *Langmuir*, 17:4641–4648, 2001.

[223] H. Diamant, T.A. Witten, C. Ege, A. Gopal, and K.Y.C. Lee. Topography and instability of monolayers near domain boundaries. *Phys. Rev. E.*, 63(061602), 2001.

[224] A.G. Serrano, M. Ryan, T.E. Weaver, and J. Pérez-Gil. Critical structure-function determinants within the N-terminal region of pulmonary surfactant protein SP-B. *Biophys. J.*, 90:238–249, 2006.

[225] R. Chang, N. Shlomo, and F.R. Poulain. Analysis of binding and membrane destabilization of phospholipid membranes by surfactant apoprotein B. *Biochim. Biophys. Acta*, 1371:254–264, 1998.

[226] E.J.A. Veldhuizen, A.J. Waring, F.J. Walther, J.J. Batenburg, L.M.G. van Golde, and H.P. Haggsman. Dimeric N-terminal segment of human surfactant protein B (dSP-B1-25) has enhanced surface properties compared to monomeric SP-B1-25. *Biophys. J.*, 79:377–384, 2000.

[227] M.A. Ryan, X. Qi, A.G. Serrano, M. Ikegami, J. Pérez-Gil, J. Johansson, and T.E. Weaver. Mapping and analysis of the lytic and fusogenic domains of surfactant protein B. *Biochemistry*, 44:861–872, 2005.

[228] D.C. Beck, M. Ikegami, C.L. Na, S. Zaltash, J. Johansson, J.A. Whitsett, and T.E. Weaver. The role of homodimers in surfactant protein B function in vivo. *J. Biol. Chem.*, 275(5):3365–3370, 2000.

[229] B.J. Reynwar, G. Illya, V.A. Harmandaris, M.M. Müller, K. Kremer, and M. Deserno. Aggregation and vesiculation of membrane proteins by curvature-mediated interactions. *Nature*, 447:461–464, 2007.

[230] G. Mao, J. Desai, C.R. Flach, and R. Mendelsohn. Structural characterization of the monolayer-multilayer transition in a pulmonary surfactant model: IR studies of films transferred at continuously varying surface pressures. *Langmuir*, 24:2025–2034, 2008.

[231] S. Zaltash, M. Palmblad, T. Curstedt, J. Johansson, and B. Persson. Pulmonary surfactant protein B: A structural model and functional analogue. *Biochim. Biophys. Acta*, 1466:179–186, 2000.

[232] U. Klenz, M. Saleem, M.C. Meyer, and H.J. Galla. Influence of lipid saturation grade and headgroup charge. *Biophys. J.*, 95:699–709, 2008.

[233] M. Ross, S. Krol, A. Janshoff, and H.J. Galla. Kinetics of phospholipid insertion into monolayers containing the lung surfactant proteins SP-B or SP-C. *Eur. Biophys. J.*, 31:52–61, 2002.

[234] V. Schram and S.B. Hall. Thermodynamic effects of the hydrophobic surfactant proteins on the early adsorption of pulmonary surfactant. *Biophys. J.*, 81:1536–1546, 2001.

[235] S.B. Hall R.W. Walters, R.R. Jenq. Distinct steps in the adsorption of pulmonary surfactant to an air–liquid interface. *Biophys. J.*, 78:257–266, 2000.

[236] A. Cruz, L.A. Worthman, A.G. Serrano, C. Casals, K.M.W. Keough, and J. Pérez-Gil. Microstructure and dynamic surface properties of surfactant protein SP-B/dipalmitoylphosphatidylcholine interfacial films spread from lipid-protein bilayers. *Eur. Biophys. J.*, 29:204–213, 2000.

[237] W. Yan, S.C. Biswas, T.G. Laderas, and S.B. Hall. The melting of pulmonary surfactant monolayers. *J. Appl. Physiol.*, 102:1739–1745, 2007.

[238] H.S. Shieh, L.G. Hoard, and C.E. Nordman. The structure of cholesterol. *Acta Cryst.*, B37:1538–1543, 1981.

[239] J.R. Shewchuk. Delaunay refinement algorithms for triangular mesh generation. *Computational Geometry: Theory and Applications*, 22:21–74, 2002.

[240] O.G. Mouritsen, J.H. Ipsen, and M.J. Zuckermann. Lateral density fluctuations in the chain-melting phase transition of lipid monolayers. *J. Colloid Interface Sci.*, 129:32–40, 1988.

[241] P. Krüger, M. Schalke, Z. Wang, R.H. Notter, R.A. Dluhy, and M. Lösche. Effect of hydrophobic surfactant peptides SP-B and SP-C on binary phospholipid monolayers. I. Fluorescence and dark-field microscopy. *Biophys. J.*, 77:903–914, 1999.

[242] S.G. Taneva and K.M.W. Keough. Dynamic surface properties of pulmonary surfactant proteins SP-B and SP-C and their mixtures with dipalmitoylphosphatidylcholine. *Biochemistry*, 33:14660–14670, 1994.

[243] R.H. Notter, S.A. Tabak, S. Holcomb, and R.D. Mavis. Post-collapse dynamic surface pressure relaxation of binary surface films containing dipalmitoyl phosphatidylcholine. *J. Colloid Interface Sci.*, 74:370–377, 1980.

[244] A. Müller. A further x-ray investigation of long chain compounds (n-hydrocarbon). *Proc. Roy. Soc. London, Ser. A*, 120:437–459, 1928.

[245] N.K. Adam. *The Physics and Chemistry of Surfaces*, page 55. Oxford Press, London, 3rd edition, 1941.

[246] K.M.W. Keough. Physical chemistry of pulmonary surfactant in the terminal air spaces. In B. Robertson, L.M.G. van Golde, and J.J. Batenburg, editors, *Pulmonary Surfactant: From Molecular Biology to Clinical Practice*, pages 109–164. Elsevier Science Publishers, Amsterdam, The Netherlands, 1992.

[247] R. Wüstneck, N. Wüstneck, D.O. Grigoriev, U. Pison, and R. Miller. Stress relaxation behavior of dipalmitoyl phosphatidylcholine monolayers spread on the surface of a pendant drop. *Colloids and Surfaces B: Biointerfaces*, 15:275–288, 1999.

[248] K. Kjaer, J. Als-Nielsen, C.A. Helm, L.A. Laxhuber, and H. Möhwald. Ordering in lipid monolayers studied by synchrotron x-ray diffraction and fluorescence microscopy. *Phys. Rev. Lett.*, 58:2224–2228, 1987.

[249] K.B. Chen, C.H. Chang, Y.M. Yang, and J.R. Maa. Monolayer collapse behavior of dipalmitoyl phosphatidylcholine with normal long-chain alcohols at the air-water interface. *Colloids and Surfaces A: Physicochem. Eng. Aspects*, 216:45–53, 2003.

[250] J.A. Clements and D.F. Tierney. Handbook of physiology. In *Respiration*, volume 2 section 3, page 1567. American Physiological Society, Washington DC, 1964.

[251] C.A. Helm and H. Möhwald. Equilibrium and nonequilibrium features determining supperlattices in phospholipids monolayers. *J. Phys. Chem.*, 92:1262–1266, 1988.

[252] T. Luty, C.J. Eckhardt, and J. Lefebvre. Langmuir monolayers as disordered solids: Disorder and elastic fluctuations in mesophases. *J. Chem. Phys.*, 111:10321–10329, 1999.

[253] J.W. Munden and J. Swarbrick. Time dependent surface behavior of dipalmitoyllecithin and lung alveolar surfactant monolayers. *Biochim. Biophys. Acta*, 291:344–350, 1973.

[254] T.H. Chou and C.H. Chang. Thermodynamic behavior and relaxation processes of mixed DPPC/cholesterol monolayers at the air/water interface. *Colloids and Surfaces B: Biointerfaces*, 17:71–79, 2000.

[255] R. Wüstneck, N. Wüstneck, and U. Pison. Surface dilatational behavior of pulmonary surfactant components spread on the surface of a captive bubble. 3. Dipalmitoyl phosphatidylcholine, surfactant protein C, and surfactant protein B. *Langmuir*, 19:7521–7527, 2003.

[256] X. Bi, C.R. Flach, J. Pérez-Gil, I. Plasencia, D. Andreu, E. Oliveira, and R. Mendelsohn. Secondary structure and lipid interactions of the N-terminal segment of pulmonary surfactant SP-C in Langmuir films: IR reflection-adsorption spectroscopy and surface pressure studies. *Biochemistry*, 41:8385–8395, 2002.

[257] S. Schürch, J. Goerke, and J.A. Clements. Direct determination of volume- and time- dependence of alveolar surface tension in excised lungs. *Proc. Nat. Acad. Sci. U.S.A.*, 75:3417–3421, 1978.

[258] G.L. Gaines Jr. *Insoluble Monolayers at the Liquid-Gas Interface*. Interscience-Wiley, New York, 1966.

[259] J.N. Hildebran, J. Goerke, and J.A. Clements. Pulmonary surface film stability and composition. *J. Appl. Physiol. Respir. Environ. Exerc. Physiol.*, 47:604–611, 1979.

[260] P. Baglioni, G. Cestelli, L. Dei, and G. Gabrielli. Monolayers of cholesterol at water air interface - mechanism of collapse. *J. Colloid Interface Sci.*, 104:143–150, 1985.

[261] R.D. Smith and J.C. Berg. Collapse of surfactant monolayers at the air-water-interface. *J. Colloid Interface Sci.*, 74:273–286, 1980.

[262] I. Langmuir. The constitution and fundamental properties of solids and liquids. II. Liquids. *J. Am. Chem. Soc.*, 39:1848–1906, 1917.

[263] R.H. Notter, S.A. Tabak, and R.D. Mavis. Surface properties of binary mixtures of some pulmonary surfactant components. *J. Lipid Res.*, 21:10–22, 1980.

[264] S.B. Hall, M.S. Bermel, Y.T. Ko, H.J. Palmer, G. Enhorning, and R.H. Notter. Approximations in the measurement of surface tension on the oscillating bubble surfactometer. *J. Appl. Physiol.*, 75:468–477, 1993.

[265] J. Goerke and S. Schürch. Mechanical properties of the alveolar surface. In R.G. Crystal, J.B. West, P.J. Barnes, and E.R. Weibel, editors, *The Lung: Scientific Foundations*, pages 1169–1176. Lippincott-Raven Publishers, Philadelphia, 2nd edition, 1977.

[266] A. Jyoti, R.M. Prokop, and A.W. Neumann. Manifestation of the liquid-expanded/liquid-condensed phase transition of a dipalmitoylphosphatidylcholine monolayer at the air-water interface. *Colloids and Surfaces B: Biointerfaces*, 8:115–124, 1997.

[267] R. Wüstneck, N. Wüstneck, D. Vollhardt, R. Miller, and U. Pison. The influence of spreading solvent traces in the atmosphere on surface tension measurements by using a micro-film balance and the captive bubble method. *Mat. Sci. Eng. C - Bio. S.*, 8-9:57–64, 1999.

[268] H.A. Wege, J.A. Holgado-Terriza, M.J. Gálvez-Ruiz, and M.A. Cabrerizo-Vílchez. Development of a new Langmuir-type pendant-drop film balance. *Colloids and Surfaces B: Biointerfaces*, 12:339–349, 1999.

[269] A. Miller and H. Möhwald. Diffusion limited growth of crystalline domains in phospholipid monolayers. *J. Chem. Phys.*, 86:4258–4265, 1987.

[270] E.M. Scarpelli and A.J. Mautone. The surfactant system and pulmonary mechanics. In B. Robertson, L.M.G. Van Golde, and J.J. Batenburg, editors, *Pulmonary Surfactant*, pages 119–170. Elsevier Science Publishers, Amsterdam, The Netherlands, 1984.

[271] D. Papahadjopoulos. Surface properties of acidic phospholipids: Interaction of monolayers and hydrated liquid crystals with uni- and bi-valent metal ions. *Biochim. Biophys. Acta*, 163:240–254, 1968.

[272] D.O. Shah and J.H. Schulman. Binding of metal ions to monolayers of lecithins plasmalogen cardiolipin and dicetyl phosphate. *J. Lipid Res.*, 6:341–349, 1965.

[273] H. Akutsu and J. Seelig. Interaction of metal ions with phosphatidylcholine bilayer membranes. *Biochemistry*, 20:7366–7373, 1981.

[274] S.A. Simon, L.J. Lis, J.W. Kauffman, and R.C. Macdonald. A calorimetric and monolayer investigation of the influence of ions on the thermodynamic properties of phosphatidylcholine. *Biochim. Biophys. Acta*, 375:317–326, 1975.

[275] M.S. Aston, T.M. Herrington, and T.F. Tadros. Interfacial properties of mixtures of lecithin with a block copolymer surfactant at the water/air and water/oil interface. *Colloid Polym. Sci.*, 273:444–452, 1995.

[276] M. Ross, C. Steinem, H.J. Galla, and A. Janshoff. Visualization of chemical and physical properties of calcium-induced domains in DPPC/DPPS Langmuir-Blodgett layers. *Langmuir*, 17:2437–2445, 2001.

[277] A. Aroti, E. Leontidis, E. Maltseva, and G. Brezesinski. Effects of Hofmeister anions on DPPC Langmuir monolayers at the air-water interface. *J. Phys. Chem. B*, 108:15238–15245, 2004.

[278] J.N. Sachs and T.B. Woolf. Understanding the Hofmeister effect in interactions between chaotropic anions and lipid bilayers: Molecular dynamics simulations. *J. Am. Chem. Soc.*, 125:8742–8743, 2003.

[279] A. Bredlow, H.J. Galla, and L.D. Bergelson. Influence of fluorescent lipid probes on the packing of their environment. A monolayer study. *Chem. Phys. Lipids*, 62:293–301, 1992.